GEOMETRICAL ACCURACY IMPROVEMENT IN FLEXIBLE ROLL FORMING PROCESS BY MEANS OF LOCAL HEATING

A thesis submitted
in fulfillment of the requirements for the degree of
Doctor por Mondragon Unibertsitatea

JON LARRAÑAGA AMILIBIA

Supervised by Dr. Lander Galdos Errasti

Mondragon, May 11th, 2011

Mondragon Goi Eskola Politeknikoa,
Department of Mechanical and Industrial Production,
Mondragon Unibertsitatea

Preface

Declaration

I hereby declare that this thesis is the result of my own work and that, to the best of my knowledge and belief, no part of this dissertation has previously been submitted for any similar qualification or degree.

Jon Larrañaga
(March 2011)

Copyright and reproduction

This thesis is copyright of Jon Larrañaga, 2011.

I authorize Mondragon Unibertsitatea to reproduce this thesis, in part or in whole, at the request of other institutions or individuals for the purpose of academic research.

Laburpena

Ibilgailuen pisua gutxitzeko joera garbia izan da azken hamarkadan, ingurugiroarekiko legediak eta arrazoi ekonomikoak bultzatuta. Helburu horrek ibilgailuen egitura nagusien ikerkuntza bi norantza nagusitan bideratu du. Batetik, material arinen azterketan eta garapenean, eta bestetik, material berri horiek eraldatzeko prozesu berritzaleen ikerkuntzan. Alde batetik, erresistentzia espezifiko handiko materialeen erabilerak ibilgailuen pisuaren jaitsiera eta ezaugarri estrukturalen hobekuntza ekarri du. Halere, material hauek oso konformabilitate baxua eta errekuperazio elastiko handia dutenez, zaila egiten da geometrikoki forma egokia duten profilak ekoiztea. Arrazoi horiek guztiak direla eta, ekonomikoa den eta kontsumitzaileari egokituriko fabrikazio prozesu berrien garapena beharrezkoa egiten da.

Ingurumari honetan, eta eskakizun guzti horiei erantzuna emateko, profilaketa arruntaren abantaila guztiak eta sekzio aldakorreko profilak sortzeko aukera uztartzen dituen prozesu berria sortu da, profilaketa aldakorra. Halere, profilaketa aldakorra oraindik garapen prozesuan izanik, prozesua berarenak diren akats geometriko bereziak konpontzeko beharra dago. Horregaitik, doktorego tesi honetan, akats geometriko horiek gutxitzeko helburuarekin, termikoki lagunduriko profilaketa aldakorra izeneko irtenbide termiko-mekanikoa proposatzen eta ikertzen da. Hiru ikerketa lerro nagusi jarraitu dira helburu hori lortzeko asmotan.

Ikerkuntza lan honen lehenengo atalean, erresistentzi altuko hiru altzairuren (MS1200, CP800 eta DP600) eta altzairu arrunt baten (DC01) karakterizazio mekanikoa burutu da, trakzio saiakuntza kausiestatikoak burutuz. Material horiek doktoradutza tesian zehar garatu diren eredu matematikoak egiaztatzeko erabili dira. Bestalde, CP800 altzairua, termikoki lagundutako profilaketa aldakorreko esperimentazioa burutzeko aukeratua izanik, tenperatura altuetan ere mekanikoki karakterizatu da. Tenperaturak mikroegituran duen eragina eta eman daitezkeen deformazio mekanismoak aztertzeko asmotan, tenperatura altuetan entseatutako probetak mikroskopio optikoaz eta X-izpien difrakzioaz aztertu dira.

Bigarrengo atalean, profilaketa arruntaren eta termikoki lagundutako profilaketa aldakorraren eredu matematikoak garatu eta egiaztatu dira. Eredu matematikoen emaitzak helburu horretarako sortu den profilatzeko makina arrunt batetan buruturiko entsegu esperimentalen emaitzekin aldaratu dira. Bestalde, entsegu hauek profilaketa prozesuan materialaren gogortasunak nola eragiten duen aztertzeko ere balio izan dute.

Azkenik, termikoki lagunduriko profilaketa aldakorreko entsegu esperimentalak burutu dira, Proform Europear proiektuan zehar garatutako profilaketa aldakorreko makinan. Lortutako emaitzek akats geometrikoen hobekuntza adierazgarri bat erakusten dute, sekzio aldakorreko perfila termikoki lagundua izan denean.

Abstract

In the last decade the tendency to reduce vehicle weight due to rising fuel prices and environmental requirements, have pushed two main trends of research in the field of vehicle structure manufacturing. On the one hand, the development of new high strength steels allowed to reduce weight and increase the structural performance of vehicles. However, these materials exhibit low formability and high springback effect at room temperature, making difficult to form high strength steel accurate parts. For all these reasons it is necessary to develop flexible and consumer-oriented manufacturing processes in order to allow the manufacturing of accurate parts in an economic way.

In this context, the flexible roll forming process was developed, which combines all the advantages of conventional roll forming, allowing to manufacture continuously, profiles with variable cross section along its longitudinal direction. However, the flexible roll forming process is still under development and characteristic geometrical error of the process must be solved. Therefore, the current dissertation proposes and studies the reduction of geometrical errors created during the manufacture of flexible profiles using a thermo-mechanical process called heat-assisted flexible roll forming. Three have been the main fields of research conducted for this purpose.

In the first section of the present dissertation, the quasi-static mechanical behavior of three ultra high strength steel sheets (MS1200, CP800 and DP600) and a soft steel sheets (DC01) are characterized by means of uniaxial tensile tests. These materials are used to validate the numerical models developed during the thesis. On the other hand, the CP800 material, selected to perform heat-assisted flexible roll forming experiments, is mechanically characterized at high temperatures. In order to determine the microstructural changes that take place and identify possible deformation mechanisms at high temperatures, the microstructure of the specimens tested at high temperature are analyzed by optical microscopy and X-ray diffraction methods.

In the second section, numerical models of the conventional roll forming process and heat assisted flexible roll forming process are developed. Numerical models are used to develop and optimize the heat assisted flexible roll forming process. However, in order to check the reliability of the models, conventional roll forming trials results are compared with numerical results.

In the last section, heat assisted flexible roll forming experiments are carried out using the flexible roll forming machine developed within the European Proform project. The results show a significant decrease of the web warping when the flexible profile is heat assisted.

Resumen

En la última década la tendencia a reducir el peso de los vehículos debido al encarecimiento de los combustibles y a los requerimientos medioambientales han marcado dos principales vías de investigación en el campo de la fabricación de estructuras para vehículos. Por un lado, el desarrollo de nuevos aceros de alta resistencia ha permitido la reducción del peso y el aumento de las prestaciones estructurales de los vehículos. Sin embargo, estos materiales presentan una baja conformabilidad y una gran recuperación elástica a temperatura ambiente, dificultando el conformado de piezas de acero de alta resistencia geométricamente precisas. Por todo ello, se hace necesario el desarrollo de procesos de fabricación flexibles y orientados al consumidor que permitan el conformado de piezas geométricamente precisas de una forma económica.

En este contexto, se ha desarrollado el perfilado flexible o de sección variable, donde se combinan todas las ventajas del perfilado convencional, permitiendo la fabricación de forma contínua de perfiles con secciones cambiantes a lo largo de su dirección longitudinal. Sin embargo, al ser un proceso de fabricación todavía en proceso de desarrollo, existen errores geométricos característicos del proceso que deben ser resueltos. Por todo ello, en la presente teśis se propone y estudia la disminución de los errores geométricos creados durante la fabricación de perfiles flexibles mediante un proceso termo-mecánico, llamado perfilado flexible asistido térmicamente. Han sido tres las principales vías de investigación llevadas a cabo para para conseguir este objetivo:

En un primer apartado, se ha caracterizado el comportamiento mecánico de tres tipos chapas de acero de ultra alta resistencia (MS1200, CP800 y DP600) y chapas de acero de embutición convencional (DC01), mediante ensayos de tracción uniaxial cuasi-estáticos. Estos materiales, han sido empleados para validar los modelos numéricos desarrollados durante la tesis doctoral. Por otro lado, el material CP800, elegido para realizar ensayos de perfilado flexible asistido térmicamente, se ha caracterizado mecánicamente a altas temperaturas. Con el objetivo de determinar los cambios microestructurales e identificar los mecanismos de deformación a altas temperaturas, se han analizado las microestruc-

turas de las probetas ensayadas mediante microscopia óptica y difracción de rayos X.

En un segundo apartado, se han desarrollado y validado modelos de simulación numérica del proceso de perfilado convencional y perfilado flexible asistido térmicamente. Los resultados de los modelos numéricos han sido contrastados mediante ensayos experimentales realizados en una perfiladora convencional desarrollada con este objetivo. Por otro lado, los ensayos de perfilado convencional han servido para determinar la influencia de la resistencia del material en los diferentes parámetros de proceso analizados. Los resultados de la simulación del proceso de perfilado asistido termicamente han servido para optimizar el proceso y la estrategia de calentamiento utilizada.

En el último apartado, se han realizado ensayos experimentales de perfilado asistido térmicamente, en la perfiladora flexible desarrollada en el seno del proyecto Europeo Proform. Los resultados obtenidos, muestran una significativa disminución del error en la base del perfil, cuando el perfil flexible ha sido asistido térmicamente.

Contents

Preface i

Laburpena iii

Abstract v

Resumen vii

Contents ix

Simbols and abreviations xv

List of figures xviii

List of tables xxvi

1 Introduction 1

1.1 Motivation and background 1
1.2 Scope of the present thesis 3
1.3 Structure of the present thesis 4

2 Roll forming technology 7

2.1 Introduction 8
2.2 Conventional roll forming 8
    2.2.1 Definition and background 8
    2.2.2 Sheet deformation and geometrical errors in roll forming 11
2.3 Flexible roll forming 13
    2.3.1 Definition and background 13
    2.3.2 Sheet deformation and geometrical errors in flexible roll forming 14
2.4 Heat assisted roll forming 18
2.5 Heat assisted flexible roll forming 21
2.6 Conclusions 22

3 Material Characterization 23
- 3.1 Introduction . . . 24
- 3.2 Advanced high strength steels . . . 24
  - 3.2.1 Dual Phase (DP) . . . 26
  - 3.2.2 TRansformation Induced Plasticity (TRIP) . . . 26
  - 3.2.3 Complex Phase (CP) . . . 26
  - 3.2.4 Martensitic (MS) . . . 26
- 3.3 Quasi-static tensile test at room temperature . . . 27
  - 3.3.1 Experimental procedure . . . 28
    - Longitudinal and transversal strain measurement . . . 28
    - Strain anisotropy calculation, Lankford coefficient (r-value) . . . 30
  - 3.3.2 Experimental results . . . 31
    - MS1200 . . . 31
    - CP800 . . . 32
    - DP600 . . . 33
    - DC01 . . . 34
- 3.4 Quasi-static tensile tests at high temperature . . . 35
  - 3.4.1 Experimental procedures . . . 35
    - Mechanical properties characterization . . . 35
    - Calculation of the work hardening coefficient (n) . . . 36
    - Optical micrographs . . . 36
    - X - ray diffraction measurements . . . 37
  - 3.4.2 Experimental results . . . 37
    - Effect of the employed specimen geometry . . . 37
    - Effect of the temperature . . . 39
    - Effect of the strain rate . . . 41
    - Effect of the tensile test at high temperature in the microstructure 41
  - 3.4.3 Mechanical behavior and microstructure evolution relation . . . 43
- 3.5 Conclusions . . . 45

4 Numerical modeling of roll forming processes 47
- 4.1 Introduction and numerical background of roll forming . . . 48
  - 4.1.1 Background in numerical modeling of roll forming process . . . 48
  - 4.1.2 Literature review of finite element models of roll forming process 51
    - Body discretization . . . 51
    - Material property modeling . . . 52
    - Boundary conditions . . . 52

Finite element formulation 53
Finite element commercial codes 53
4.2 Conventional roll forming numerical modeling 54
4.2.1 Mechanical analysis 54
Body discretization 55
Material property modeling 57
Boundary conditions 61
4.2.2 Results of the conventional roll forming numerical model 64
Profile geometry 64
Longitudinal and transversal strains 64
Forming loads and torques 65
Effect of material strength 66
4.2.3 Validation of the conventional roll forming model 68
Profile geometry 69
Longitudinal and transversal strains 70
Forming loads and torques 71
4.3 Heat assisted flexible roll forming numerical modeling 72
4.3.1 Coupled thermo-mechanical analysis 72
Body discretization 74
Material property modeling 75
Boundary conditions 78
4.3.2 Results of the heat assisted flexible roll forming numerical model 80
Profile geometry 80
Longitudinal web warping definition 80
Strain distribution within the workpiece and heating strategy . . 81
Heat distribution 82
Effect of the temperature in the longitudinal web warping 84
Effect of the temperature on the profile cross section 85
Effect of the heated zone in the longitudinal web warping 86
Effect of the heated zone on the profile cross section 87
4.3.3 Validation of the heat assisted flexible roll forming model 88
4.4 Conclusions 91

5 Experimental tests **93**
5.1 Introduction 94
5.2 Conventional roll forming experiments 94
5.2.1 Objectives of the experimentation 94

5.2.2 Experimental procedure . . . 95
Conventional roll forming prototype . . . 95
Profile geometry and forming sequence . . . 96
Force and torque measurement . . . 97
Longitudinal and transversal strain measurements . . . 98
5.2.3 Experimental results of conventional roll forming test . . . 98
Profile geometry . . . 98
Effect of the material strength in the longitudinal and transversal cross sections . . . 99
Effect of the material strength on the longitudinal and transverse strains . . . 101
Effect of the material strength on the forming forces and torques 103
5.3 Heat assisted flexible roll forming experiments . . . 104
5.3.1 Objectives of the experimentation . . . 104
5.3.2 Experimental procedure . . . 104
Proform flexible roll forming prototype . . . 104
Profile geometry and forming sequence . . . 106
Heating method and set-up . . . 106
Temperature measurement by means of calorimetry . . . 108
Emissivity measurement experimental procedure . . . 112
5.3.3 Experimental results of heat assisted flexible roll forming test . . 114
Emissivity experimental results . . . 114
Heating experiment results . . . 114
Profile geometry . . . 117
Effect of the temperature in the longitudinal web warping . . . 118
Effect of the temperature on the profile cross section . . . 120
5.3.4 Final properties of heat assisted flexible profiles . . . 121
Microstructural analysis of heat assisted areas . . . 122
Tensile test of the heat affected area . . . 123
Bending tests . . . 124
Torsion tests . . . 125
5.4 Conclusions . . . 127

6 Conclusions and future work **129**
6.1 Concluding remarks . . . 129
6.2 Future work . . . 133

7 Published work and other submissions **135**

Acknowledgement **137**

References **139**

References **139**

Appendix A **152**

Appendix B **156**

Appendix C **158**

Simbols and abreviations

Notations

a_1, a_2, a_3, a_4, a_5, a_6	Material experimental constant for Hill's criteria
A	Contact area between two solids
A_{heat}	Heating area
b_i^0	Body force tensor
b_i	Body force
c	Speed of the light in vacuum
$\mathrm{C_{Bolt}}$	Constant of proportionality, Boltzmann constant
C_{p}	Specific heat
E	Young modulus
$E_{i,j}$	Green-Lagrange strain tensor
F_{t}, F_{n}	Friction force and normal force
F_{heat}	Heat flux
$\mathbf{F}_{\mathrm{ext}}$	External force matrix
G	Shear modulus
h	Plank's constant
h_{conv}	Film coefficient
k_{th}	Thermal conductivity coefficient
h_{cond}	Thermal conductance coefficient
K	Hardening coefficient
K_{Hol}	Hollomon model hardening coefficient
$\mathbf{K}$	Rigidity matrix
L_0	Bend line length
L	Helix shape flange edge length
M_{b}	Radiated total energy of a black body
n	Work hardening coefficient
n_{Hol}	Hollomon model work hardening coefficient
r	Lankford coefficient
S	Surface

R_λ	Emitted radiative flux
S_λ	Acquired signal spectrum of radiation flux
$S_{i,j}$	Second Piola-Kirchhoff stress tensor
t_i^0	Traction vector
t_i	Surface traction
t	Time
T	Temperature
$\dot{q}$	Heat generated
Q	Quantity of heat transferred
$\dot{Q}$	Heat transfer rate
$\mathbf{u}$	Displacement vector
U	Internal thermal energy
V	Volume
$\dot{W}$	Work transfer rate
Y_s	Yield Stress
Y_{τ_xy}, Y_{τ_yz}, Y_{τ_xz}	Yield stress in shear with respect to the axes of anisotropy
Y_{σ_0}, $Y_{\sigma_{45}}$, $Y_{\sigma_{90}}$	Yield stress in 0°, 45°and 90°
Y_{σ_L}, Y_{σ_W}, Y_{σ_T}	Yield stress in longitudinal, transversal and thickness direction
Y_{σ_av}	Averaged yield stress
Y_{σ_x}, Y_{σ_y}, Y_{σ_z}	Yield stress in the axes of anisotropy

Greek letters

α	Ferrite, martesite, bainite or cementite phases, bcc orientation
α_th	Thermal diffusivity
α_λ	Absorptivity
β	Cross sectional angle
β_1, β_2, β_3, β_4	Cross sectional angles of flexible profile
δ	Reversible displacement threshold
Δh	Web warping error
Δh_Bow	Longitudinal bow error
ε	Strain
ε_λ	Emissivity
ε_f	Elongation at failure
ε_c, ε_s	Compression and stretch strain
$\varepsilon_\mathrm{true}$	True strain

ε_{L}, ε_{W},ε_{T}	Strain in longitudinal, width and thickness direction
$\varepsilon_{\mathrm{eps}}$	Effective plastic strain
$\dot{\varepsilon}$	Strain rate
γ	Austenite phase, fcc orientation
η_i	Virtual displacements
λ	Wavelength
μ	Friction coefficient
ν	Poisson's ratio
θ	Angle between the radiation source and the receptor
ρ	Material density
ρ_λ	Reflectivity
σ	Stress
σ_{true}	True stress
σ_{uts}	Ultimate tensile strength
σ_{Hol}	Hollomon model stress
σ_{ik}	Cauchy stress tensor
ς	Standard deviation
τ_λ	Transmissivity

Abreviations

AHSS	Advanced High Strength Steels
BW	Body-in-White
CP	Complex Phase steel
DC	Mild steel
DP	Dual Phase steel
bcc	Body-centered cubic lattice structure
fcc	Face-centered cubic lattice structure
MS	Martensitic Steel
NURBS	Non-uniform rational B-splines
PM	Partially Martensitic Steel
TRIP	Transformation Induced Plasticity Steels
UTS	Ultimate Tensile Strength
ULSAB	Ultra Light Steel Auto Body
XRD	X-ray Diffraction

List of figures

1.1 Body-in-white of the Porsche Cayenne formed with different materials [Wor10]. 1

1.2 The main objective of the present thesis is develop and analyze the heat assisted flexible roll forming process, this main objective is faced in three different interrelated fields: The material characterization, the numerical modeling and the experimental work. 3

2.1 Roll forming process diagram for an U profile [Swe03]. 9

2.2 Typical roll forming workshop composed by an accumulator-uncoiler, the forming machine and a cut-off press [Hal05]. 9

2.3 Additional operations can be introduced in the same line [Swe03]. 10

2.4 (L) Helix shaped edge and (L_0) the bend line have different lengths. . . 11

2.5 Redundant deformations during the roll forming process [Hal05]. 12

2.6 Typical errors in roll forming [Hal83a]. 12

2.7 (a) Profiles with variable cross sections [Ona05] and (b) continuous production of flexible profiles [Gro03]. 13

2.8 (a) Position of the forming rolls during the forming of flexible part zone [Gro03] and (b) 3D model of the flexible roll forming stand [Lar10a]. . . 14

2.9 (a) Compressed-stretched zones of the transition zone of flexible U profile in width and (b) pre-cut sheet of the flexible U profile. 15

2.10 (a) Compressed-stretched zones of the transition zone of flexible in depth U profile and (b) pre-cut sheet of the flexible U profile. 15

2.11 Typical failure modes in flexible roll forming. (a) Flange wrinkling and (b) Web warping (Δh) [Lar10a]. 16

2.12 Blank holder systems proposed by different authors, (a) [Gro09] and (b) [Lar10a]. 17

2.13 Temperature dependent material flow. 19

2.14 Heat assisted roll forming lines: (a) Chair of Manufacturing Technology of the University of Erlanger-Nuremberg [Pit04] and (b) Dalarna University [Lin09b]. 20
2.15 Heat assisted flexible roll forming process. 21

3.1 Schematic microstructures of different AHSS [Ada06]. 25
3.2 Cooling strategies during the fabrication of different AHSS [Ada06]. . . 25
3.3 Microstructures of a) MS1200, b) CP800, c) DP600 and d) DC01 steels. MS1200, DP600 and DC01 steels were etched with nital 5% agent and CP800 using Klemm's agent. Sample preparation procedure is explained in section §3.4.1. 27
3.4 Geometry of the specimen employed at room temperature tensile tests. . 28
3.5 Longitudinal and transversal strain measurement. 29
3.6 (a) Transversal strain (ε_{T}) vs longitudinal strain (ε_{L}) and (b) Lankford coefficient (r) vs longitudinal strain (ε_{L}) of a tensile test performed with DC01 material. 30
3.7 Mechanical properties of MS1200 steel. The summary of the results can be seen in Table A.1 of appendix A. 31
3.8 Mechanical properties of CP800 steel. The summary of the results can be seen in Table A.2 of appendix A. 32
3.9 Mechanical properties of DP600 steel. The summary of the results can be seen in Table A.3 of appendix A. 33
3.10 Mechanical properties of DC01 steel. The summary of the results can be seen in Table A.4 of appendix A. 34
3.11 Geometry of the specimen employed in high temperature tensile tests [Per96]. 36
3.12 Engineering stress - engineering strain curves with different specimens. . 38
3.13 True stress - effective plastic strain curves at different temperatures and at 0.01 s^{-1}. The summary of the results can be seen in Table A.5 of appendix B. 39
3.14 True stress - effective plastic strain curves at different temperatures and at 0.1 s^{-1}. The summary of the results can be seen in Table A.6 of appendix A. 39
3.15 Mechanical properties of CP800 steel at different temperatures. The summary of the results can be seen in Table A.5 and Table A.6 of appendix A. 40

3.16 Microstructure of different specimens: a) As received material, b) room temperature, c) 300°C and d) 700°C, etched with Klemm's agent. 41
3.17 Diffractograms of specimens tested at different temperatures. 42
3.18 Microstructure of the specimen tested at 700°C etched with nital 5%. . 43

4.1 Modelization of an element strip isolated from a roll forming pass with a single active bend [Pan94]. 49
4.2 Discretization of the sheet metal in elements [Hal05]. 50
4.3 Body definition in roll forming numerical models. Rolls were defined as undeformable rigid bodies and the sheet metal was defined by solid elements. Fine mesh was used in bending zones and where the load forces and torques were calculated. 56
4.4 Axes of anisotropy for the specimen at 0° rolling direction. 58
4.5 (a) Comparison of true stress-strain curve and true stress - effective plastic strain curve and (b) comparison of effective plastic strain curve and the Hollomon's material laws. 59
4.6 Comparison between experimental results and Hollomon's laws. 61
4.7 (a) Coulomb model of friction and (b) Coulomb bilinear model of friction aproach [MSCa]. 62
4.8 Profile calculated using DC01 material properties. The cross section angle (β), the longitudinal bow Δh_{Bow} and longitudinal and transversal strains are extracted from the numerical model. 64
4.9 Calculated longitudinal and transversal strain during the roll forming. . 65
4.10 (a) Forming forces and (b) forming torques calculated using CP800 material properties. 65
4.11 Calculated (a) longitudinal section and (b) transversal sections depending on the formed materials. 66
4.12 Calculated (a) longitudinal bow and (b) profile angle values depending on the formed materials. 67
4.13 Calculated (a) longitudinal and transversal peak strain and (b) longitudinal and transversal residual plastic strain values depending on the formed materials. 67
4.14 Calculated (a) forming load and (b) forming torque values depending on the formed materials. 68
4.15 Comparison of calculated and experimental (a) longitudinal bow and (b) profile angle (β) values depending on the formed materials. 69

4.16 Comparison of the numerical and experimental (a) longitudinal and transversal peak strains and (b) longitudinal and transversal plastic residual strain values depending on the formed materials. 70
4.17 Comparison of the numerical and experimental (a) forming loads and (b) torque values depending on the formed materials. 71
4.18 Interaction between the mechanical and thermal fields. 72
4.19 Comparison between experimental results and Hollomon's laws at 10^{-2} s^{-1} strain rates. The summary of the results can be seen in Table B.1 of Appendix B. 76
4.20 Comparison between experimental results and Hollomon's laws at 10^{-1} s^{-1} strain rates. The summary of the results can be seen in Table B.2 of Appendix B. 76
4.21 Temperature dependent data of the heat conductivity (k_{th}) and of the specific heat capacity (C_{p}) are taken from [Mil02], coefficients of the thermal expansion (α) and elastic modulus (E) are taken from [Pit05]. 77
4.22 Flow chart of the FLUX subroutine. 79
4.23 The longitudinal and transversal cross sections and different heated zones of the profile. 80
4.24 The height deviation of a real flexible roll formed profile at room temperature along the longitudinal direction. 81
4.25 Calculated longitudinal strain distribution on the profile after forming at room temperature. 82
4.26 Calculated temperature distribution during the forming of flexible profile at 400°C. 83
4.27 Calculated temperature evolution from heating to forming zone. 83
4.28 The height deviation of the numerical flexible roll formed profiles within the longitudinal direction for different temperatures. 84
4.29 Calculated values of the total web warping and relative web warping depending on the process temperature. 85
4.30 Calculated (a) slim and (b) wide cross sections at room and 600°C temperature. 85
4.31 Calculated angles β_1, β_2, β_3 and β_4 of the (a) slim and (b) wide section depending temperature. 86
4.32 Calculated height deviations of the flexible roll formed profiles within the longitudinal direction for different heated zones. 87
4.33 Values of calculated total web warping and relative web warping depending on the heating condition. 87

4.34 Values of total web warping and relative web warping depending on the heating condition. 88

4.35 Comparison of numerical and experimental (a) total warping and (b) relative web warping depending on the temperature. 89

4.36 Comparison between experimental and numerical values of β_1, β_2, β_3 and β_4 of the slim and wide sections depending on the process temperature. 90

5.1 (a) Conventional roll forming prototype design and (b) conventional roll forming prototype. 95

5.2 (a) Selected U profile for the study and (b) rolls used to roll form the profile. 96

5.3 (a) Kristler 91071A load cells and (b) Burster 8645-E torque sensor used to measure the forming load and torques during experimentation. 97

5.4 Measured longitudinal and transversal cross sections at 500 mm, 1000 mm and 1500 mm from the edge of the profile. 98

5.5 Profiles fabricated with different materials show different longitudinal bow deffect. 99

5.6 Longitudinal bow of profiles fabricated with different materials. 100

5.7 (a) Measured and (b) experimental transversal cross sections. 100

5.8 (a) Longitudinal bow and (b) measured angle depending on the material strength. The average and standard deviation values of the measured longitudinal bow and angles are summarized in Table C.1 of appendix C. 101

5.9 Longitudinal and transversal strains of the edge of the profile for different materials. 102

5.10 Longitudinal and transversal (a) peak strains and (b) residual plastic strain values depending on the material. The average values are summarized in Table C.2. 102

5.11 Measured (a) forming forces and (b) forming torques during the forming of CP800 material profile. 103

5.12 (a) Forming loads and (b) torques depending on the formed materials. The average and standard deviation values of the measured forming loads and torques are summarized in Table C.3 of appendix C. 103

5.13 (a) Laser trimming unit and (b) flexible roll forming stand with static blank holder and conventional stand. 105

5.14 (a) Forming sequence of the Proform profile and (b) one side flexible forming stand. 105

5.15 Geometry of selected profile for heat assisted flexible roll forming experimentation. 106
5.16 Inductive heating device installed in the Proform machine. 107
5.17 Thermal radiation spectrum comprises part of ultra violet, visible and infrared radiation portion. 109
5.18 (a) Spectral radiance of a black body at different temperatures and (b) comparison between the emissive power of different body types at 1000°C. 110
5.19 (a) Emissivity values of used black paint depending on the wavelength and temperature and (b) emissivity values at different temperatures at 3.9 μm wavelength. 114
5.20 Thermal image of the controlled surfaces in the profile. 115
5.21 (a) and (b) not homogeneous temperature distribution in the profile, (c) zones in transition remains without heating and (d) at highest temperatures the black paint is removed in certain zones. 115
5.22 Temperature distribution during the heating process at different temperatures and the temperature evolution along the profile. 116
5.23 Measured longitudinal section and cross sections in the flexible roll forming profile. 117
5.24 Flexible profiles formed at room temperature and at 600°C. 118
5.25 Longitudinal sections of flexible profiles at different temperatures. 119
5.26 (a) Total web warping and relative web warping depending on the process temperature and (b) web buckling. The average and standard deviation values are summarized in Table C.4 of Appendix C. 119
5.27 (a) Slim and (b) wide cross sections, of profiles flexible roll formed at room and 600°C temperature. 120
5.28 Evolution of the different angles depending on the process temperature at the slim (a) and wide part (b). The average and standard deviation values are of the angles of the slim and wide sections are summarized respectively in Table C.5 and Table C.6 of Appendix C. 121
5.29 Tensile tests specimen and microstructural analysis samples. 121
5.30 Microstructures of the heat assisted zones of profiles formed at (a) 300°C, (b) 400°C, (c) 500°C and (d) 600°C. The extracted samples were etched using Klemm's agent. Information regarding the sample preparation is explained in section §3.4.1. 122
5.31 Engineering strain - stress curves of samples extracted from heat assisted flexible profiles at different temperatures. 123
5.32 (a) Closed profile and (b) Zwick 1474 bending test machine. 124

5.33 Results of the bending tests performed with profiles formed at different temperatures. 125
5.34 Closed (a) profile and (b) Schenck torsion test machine used to perform the torsion tests. 126
5.35 Results of the torsion tests performed with profiles formed at different temperatures. 126

List of tables

3.1 Properties of CP800 depending of the specimen type. 38

4.1 Values used for Hill's yield criteria. 59
4.2 Values used for Hollomon's material model 61

A.1 Summary of tensile test results of MS1200 at room temperature. 153
A.2 Summary of tensile test results of CP800 at room temperature. 154
A.3 Summary of tensile test results of DP600 at room temperature. 154
A.4 Summary of tensile test results of DC01 at room temperature. 155
A.5 Mechanical properties of CP800 steel depending on temperature at 0.01 s^{-1}. 155
A.6 Mechanical properties of CP800 steel depending on temperature at 0.1 s^{-1}.155
B.1 Values of the Hollomon law hardening coefficient (K_{Holl}) and strain hardening exponent (n_{Holl}) at high temperature and at 0.01 s^{-1}. 157
B.2 Values of the hardening coefficient (K_{Holl}) and is the strain hardening exponent (n_{Holl}) at high temperature and at 0.1 s^{-1}. 157
C.1 Experimental values of the measured angles and longitudinal bow. . . . 159
C.2 Experimental values of the peak strain and final residual strain in longitudinal and transversal direction. 159
C.3 Experimental values of the measured load and torques for different materials. 159
C.4 Experimental values of the measured web warping and relative web warping for different temperatures. 160
C.5 Experimental values of the measured β_1, β_2, β_3 and β_4 angles in the slim section for different temperatures. 160
C.6 Experimental values of the measured β_1, β_2, β_3 and β_4 angles in the wide section for different temperatures. 160

CHAPTER 1

Introduction

Scientia ac labore

“ By means of knowledge and hard work ”

1.1 Motivation and background

Interest in high strength steels in the automotive industry has increased in recent years due to environmental and economical restrictions. The lightening of automobiles is directly related to the fuel consumption saving and the decrease of CO_2 generation [Sen01]. In this context, several researches have been carried out in order to reduce the weight of the Body-in-White (BW) of cars, which constitutes approximately 25% of the total car weight and is responsible for passenger safety [Eng01]. In order to achieve the lightening of the BW, the ULSAB project (Ultra Light Steel Auto Body) was conducted in 1994 [Sen01], where the main objective was to reduce the body weight, without compromising passenger safety and without any additional cost, using high strength steel materials. This project succeeded in a weight reduction of 25% using a large number of high strength steel sheets and sophisticated forming and welding technologies such as stamping, hydroforming, tailored blanking, laser welding [Sen01; Eng01]. The BW of the Porsche Cayenne car composed of different high strength steels parts can be seen in Figure 1.1 [MV09].

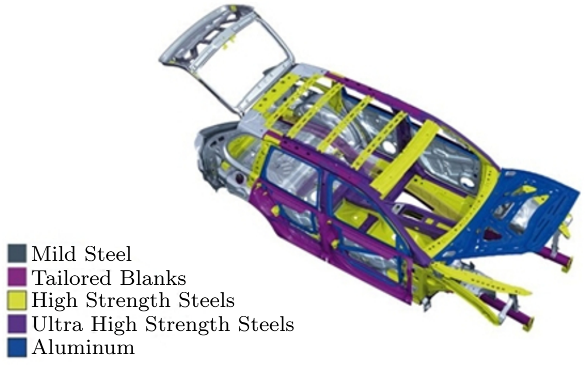

Figure 1.1: Body-in-white of the Porsche Cayenne formed with different materials [Wor10].

In recent years a new family of high strength steels characterized by fine grain and multi-phase microstructure has been developed in order to fulfill the aforementioned requirements [Gei04; Ber08]. However, these new Advanced High Strength Steels (AHSS) have shown limited formability and high springback and high forces and high amount of energy are needed to form those materials [Kle03**?**]. For all these reasons, it is necessary to develop flexible and consumer-oriented manufacturing processes in order to allow the manufacturing of accurate parts in an economic way using high strength steels.

The forming limits of high strength steels can be raised increasing the temperature of the forming process [Gei04]. However, an overall heating of the workpiece can cause inconvenients like high temperature corrosion or a very difficult handling [Lie02]. Heating of the whole workpiece in an oven is not necessary in the case of several forming processes such as bending or roll forming processes, since the deformation takes place only in restricted regions of the volume of the work piece. A selective heating can be performed in these processes to increase locally the formability in those zones [Sch04].

Roll forming technology is one of the most competitive forming process for the production of profiles. However, roll forming process is limited to the production of profiles with a constant cross section geometry lengthwise. Further on, bifurcations have to be manufactured by other high cost forming processes such as stamping or hydroforming and often cause welding operations [Gro03]. As a result, and despite to the significant advantages of the conventional roll forming process, it is not possible to manufacture customer-modifiable products by conventional roll forming process [Gro03].

The flexible roll forming process was developed by several researchers [Ort01; Gro03; Ona04; Ona05; Lin09c], which combines all the advantages of conventional roll forming process allowing to manufacture continuously profiles with variable cross section along its longitudinal direction. However, the flexible roll forming process is still under development and characteristic geometrical errors of the process, the wrinkling of the flange and the web warping, must to be solved. Moreover all geometrical deviations are enhanced when advanced high strength materials are used [Lar08a].

1.2 Scope of the present thesis

The main objective of the present dissertation is to develop and analyze the heat assisted flexible roll forming process in order to increase the quality of advanced high strength steel flexible roll formed profiles. For that purpose, this thesis covers both theoretical and experimental work and faces the investigation in three main interrelated fields: Material characterization, numerical modeling and experimental work (Figure 1.2):

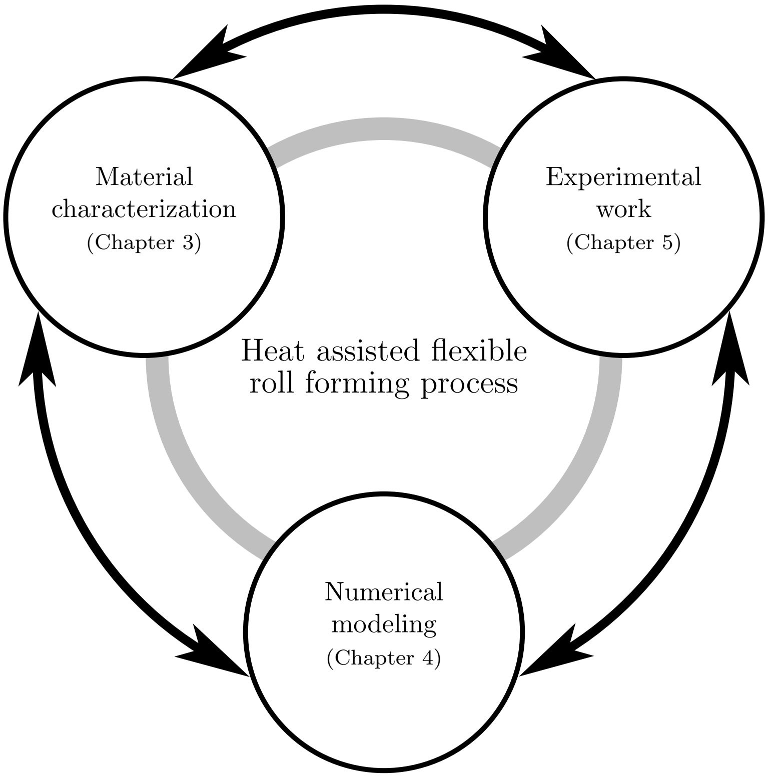
Material characterization
(Chapter 3)
Experimental work
(Chapter 5)
Heat assisted flexible roll forming process
Numerical modeling
(Chapter 4)

Figure 1.2: The main objective of the present thesis is develop and analyze the heat assisted flexible roll forming process, this main objective is faced in three different interrelated fields: The material characterization, the numerical modeling and the experimental work.

Material mechanical characterization, it is necessary in order select the appropriate forming conditions for the used material. During the forming process design, it is essential to understand the behavior of the material at different loading conditions. Additionally, the material characterization is interesting in order to provide the numerical simulations with material data at different strain rate and temperature conditions. Thus, the first objective of the present thesis is: the mechanical characterization of materials that will be used during the thesis at same using conditions as the experimentation of the heat assisted flexible roll forming process.

Numerical modeling, it is important in the development and optimization stage of the forming process, not only to save time and costs related with traditional trial and error process, but also in order to study and understand the failure mechanism of the heat assisted flexible roll forming process itself. Thus, the second objective of the present thesis is: the development of reliable numerical model of roll forming process and heat assisted flexible roll forming process.

Experimental work, it is essential in order to prove the proposed hypotheses and statements during the development of the heat assisted flexible roll forming process. Thus, the third objective of the present thesis is: the development of the heat assisted flexible roll forming experimental test in order to increase the accuracy of the formed profiles.

1.3 Structure of the present thesis

The current thesis comprises 7 chapters including the introduction and it is structured in the following way:

Chapter 2

Due to the novelty of the flexible roll forming and heat assisted roll forming process, it is considered interesting to summarize the newest trends of roll forming technology at the beginning of the document. Thus, Chapter 2 is dedicated to the review of the state of the art in roll forming processes.

On the other hand, the specific state of the art regarding the other areas analyzed in this dissertation is divided in each of the chapters. The background analysis performed in the beginning of the chapters helps to introduce the specific research to overcome among them.

Chapter 3

The mechanical characterization work performed during the thesis is compiled in Chapter 3. In the first part of chapter, the quasi-static mechanical behavior of three ultra high strength steels (MS1200, CP800 and DP600) and a mild steel sheets (DC01) is studied at three different strain rates. The anisotropy of the materials is also studied performing tensile tests at 0°, 45° and 90° regarding the rolling direction. The Lankford coefficient (r-value) depending on the strain level is also calculated for the samples tested at 10^{-3} s^{-1} strain rate.

In the second part of Chapter 3, the tensile behavior of CP800 steel is shown for a wide range of temperatures. This steel is selected to perform heat assisted flexible roll forming tests. Results from room temperature up to 700°C and at different strain rates are presented. Finally, microstructural analysis and X-ray diffraction measurements (XRD) of specimens tested at high temperature are performed and related with the deformation mechanisms.

Chapter 4

The numerical modeling work performed during the thesis is summarized in Chapter 4. In the first part of the chapter, the development of the numerical model for the simulation of conventional roll forming processes is explained. Numerical and experimental results are compared in order to identify the strengths and weaknesses of the numerical model. Additionally, the influence of each modeling parameter is discussed and the need for further improvements is analyzed.

In the second part of chapter, the development of the numerical model for the simulation of heat assisted flexible roll forming processes is explained. The effect of the temperature and the heating zone in the total and relative web warping is analyzed numerically in order to optimize the heat assisted flexible roll forming process.

Chapter 5

The experimental work performed during the thesis is summarized in Chapter 5. The chapter is divided in two parts. In the first part of the chapter, conventional roll forming experimental work is explained in order to validate the numerical models. Experimental measurements of the longitudinal and transversal strains, forming load and torques and the final geometry of the profiles are shown. Additionally, the behavior of the different conventional roll forming parameters is analyzed using different material strength.

In the second part of Chapter 5, heat assisted flexible roll forming experiments carried out with CP800 material are shown. The effect of the temperature in the web warping and in the different cross sections is analyzed. Finally, different experiments to account the effect of the temperature in the local and global properties of the profile are shown.

Chapter 6

In Chapter 6 a summary with the global conclusions is drawn. Some ideas opened for future research are also given.

Chapter 7

In Chapter 7 the scientific contributions are listed.

CHAPTER 2

Roll forming technology

Respice, adspice, prospice

“ Examine the past, examine the present, examine the future ”

Synopsis

Although, the roll forming technology was developed in the beginning of the 20th century, little research was performed until the last 10 years, when, new processes have been developed. However, the roll forming process offers a number of advantages, high production rate with low investment, compared with other processes such as stamping that make the process attractive for the fabrication of profile-shaped parts. The latest developments in the field of roll forming are the flexible roll forming and the heat assisted roll forming processes.

Flexible roll forming process allows the fabrication of different profiles with variable cross section lengthwise in a continuous way. The main objective of heat assisted roll forming is to increase the formability of roll formed high strength materials as well as to decrease the geometrical errors produced during the fabrication. In this chapter the main characteristics and limitations of roll forming processes are explained.

2.1 Introduction

The roll forming process is a very interesting process for the production of profile shaped parts because of its high production rate, low investment and efficient use of the material. However, the conventional roll forming process is limited to the production of profiles with constant cross section in longitudinal direction. Additional problems such as high springback effect and need of high forming forces, have to be solved when high strength materials are used. New variants of the roll forming process have appeared in the last decade in order to produce profiles with variables cross sections, and to solve the inaccuracies and formability limitations of high strength roll formed parts. The main objective of the present chapter is to describe the basic concepts and the latest developments of roll forming technology. The chapter is divided into three different parts.

The conventional roll forming technology is presented, and the main problems and limitations of the process are highlighted in the first part of the current chapter. Flexible roll forming process main geometrical errors such as profile wrinkling and web warping are analyzed and different solutions investigated by different authors are presented. Finally, new variants of the roll formed process, such as heat assisted roll forming process developed with the aim to increasing the formability and the accuracy of the roll formed parts are presented in the last part of the current chapter.

2.2 Conventional roll forming

2.2.1 Definition and background

According to DIN 8586 standard, roll forming is a type of bend forming with a rotating tool motion used to manufacture open and closed cold rolled sections. Roll forming passes in progressive stages by feeding a flat strip of metal through successive pairs of stands to obtain the desired profile.

The roll forming line generally includes an accumulator with an uncoiler, the forming machine with in general 20-50 forming stands, a straightener and a cutoff press. The accumulator permits continuous operation of the machine even during coil changeover. At the end of the line, the continuous profile section is cut to the desired length by the cutoff press [Gro03]. A roll forming process diagram can is shown in Figure 2.1 and an example of a roll forming machine can is shown in Figure 2.2.

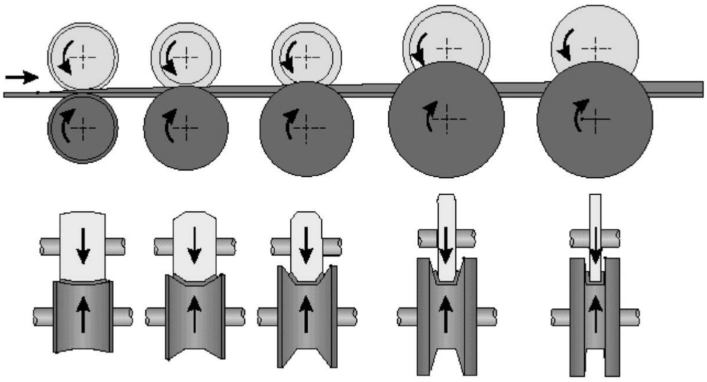

Figure 2.1: Roll forming process diagram for an U profile [Swe03].

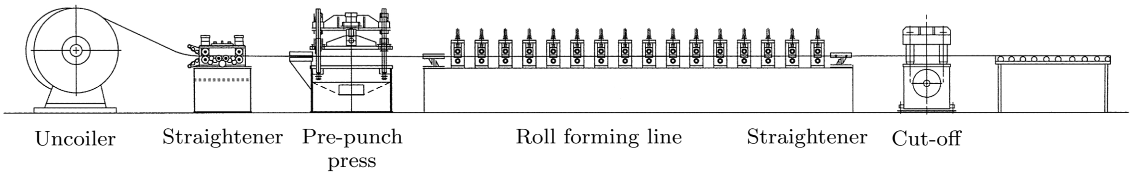

Figure 2.2: Typical roll forming workshop composed by an accumulator-uncoiler, the forming machine and a cut-off press [Hal05].

Compared with other forming processes, roll forming process offers the following advantages [Gro03]:

- High output per unit of time: Using the roll forming process high fabrication rates can be attained. Typical roll forming lines can produce profiles at 30-60 m/min [Gro03; Hal05] and even in some special applications at 160 m/min [Swe03].
- Low tool costs combined with long tool life: The tooling cost of the roll forming processes are smaller than the tooling cost of other forming processes like stamping. On the other hand, the rolls can be used for longer time without change or damage [Gro03; Abe08].
- Efficient use of material: The roll forming lines are optimized to avoid the scrap material. In a typical roll forming line less than 5% of the used steel is scrap material, coming this scrap from the piercing and from the cut-off process [Eng06].
- Although, the process of roll forming is limited to the production of profiles that have constant cross sections along the longitudinal axis, a virtually unlimited spectrum of geometries can be produced [Gro03; Hal05].
- Good surface finish can be attained [Gro03; Hal05].

- Permits processing almost all material types that can be formed by other processes. Steels, high strength steels, aluminium alloys, and other metallic materials such as copper, brass, tint, zinc, titanium, zirconium [Hal05] can be roll formed. Non-metallic materials such as rubber, thermoplastics, prepainted metallic materials, composite materials, can be roll formed also [Swe03; Dyk00].
- Roll forming process is a low sound emission technology [Gro03].
- The roll forming process allows the incorporation of secondary operations into the roll forming line avoiding additional steps [Gro03; Swe03]. Additional operations that can be added before, during or after the roll forming process are shown in Figure 2.3.

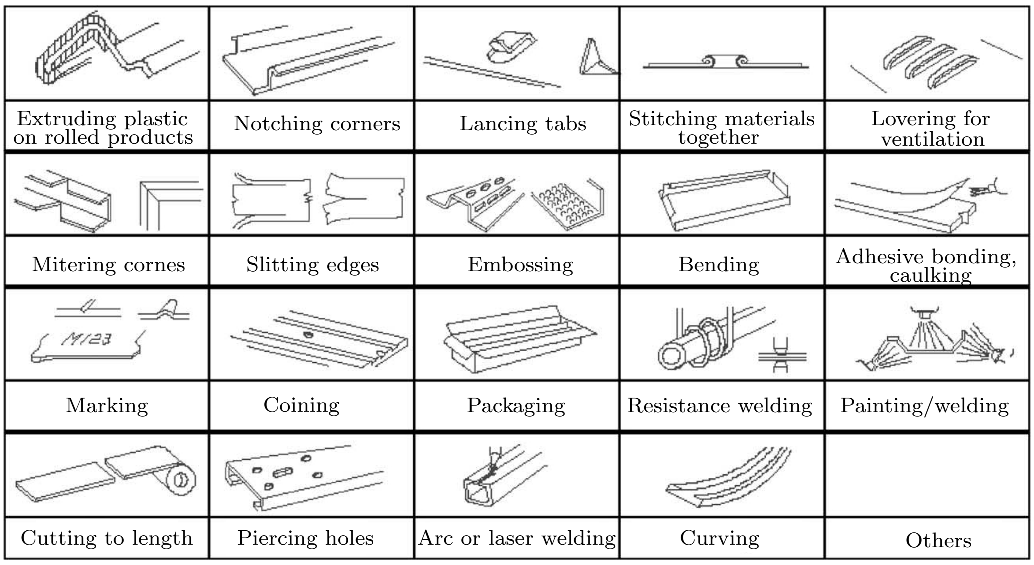
Extruding plastic on rolled products
Notching corners
Lancing tabs
Stitching materials together
Lovering for ventilation
Mitering cornes
Slitting edges
Embossing
Bending
Adhesive bonding, caulking
M123
Marking
Coining
Packaging
Resistance welding
Painting/welding
Cutting to length
Piercing holes
Arc or laser welding
Curving
Others

Figure 2.3: Additional operations can be introduced in the same line [Swe03].

Halmost divided in three different phases the short history of the roll forming process [Hal83b]:

- Development phase: during the first half of the 20th Century the roll forming process was developed.
- Expansion phase: from the second world war to the late 60s and into early 70s, roll forming technology spread widely; the number of lines in operation greatly increased and other operations such as piercing, curving and welding were added to the lines.

- Optimization and modernization phase: from the early 70s until the present day can be considered a time of qualitative change. The process was refined and improved. Additionally the new computer aided drawing methods and finite element simulations helped to improve and to understand of the process.

Nowadays, the roll forming process is used worldwide. The economical importance of roll forming is evident since 8% of the 700 million tons of steel produced annually worldwide is processed into cold-rolled sections by this method [Gro03]. During the last decade many researches have been performed in order to increase the process understanding and to form new materials such as advanced high strength steels, titanium and magnesium alloys. For this purpouse, new variants of the process such as flexible roll forming and heat assisted roll forming are being studied.

2.2.2 Sheet deformation and geometrical errors in roll forming

During the roll forming process the metal strip is formed feeding a flat strip of metal through successive pairs of rolls. The stresses and strains developed in the material through the roll forming process are complex, even in the case of a simple U channel. During the roll forming process the flat sheet metal is bended progressively, inducing transversal plastic strains in the sheet in the bending line. However, other undesired transversal and longitudinal strains occur during the roll forming process even during the roll forming of a simple U channel [Hal83a]. Considering the roll forming of a U channel, the edge travels in a helix, as shown in Figure 2.4.

As the length of the helix (L) is longer than the straight bend line (L_0), the edge and all parts between the edge and the bend line will be stretched during the forming. After the forming process and if the elastic limit of the material is not exceeded, the longitudinally stretched parts recover their initial length. Otherwise, geometrical errors appear in the final profile [Hal83a].

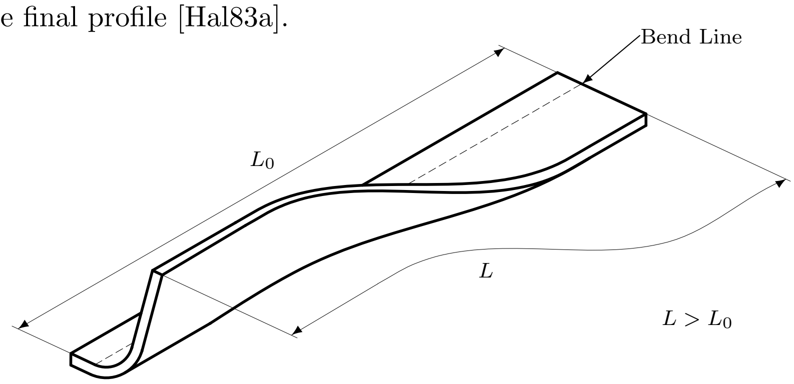

Figure 2.4: (L) Helix shaped edge and (L_0) the bend line have different lengths.

Kiuchi et al. [Hal05] investigated and identified the undesired deformations in the conventional roll forming process: longitudinal bending and bending back, longitudinal elongation and/or shrinkage, transversal elongation and/or shrinkage, shear in metal's plane and shear in the direction of the metal thickness. These redundant deformations superimposed on the transversal bending and induced the geometrical errors of the last parts. The redundant deformations investigated by Kiuchi et al. are shown in Figure 2.5.

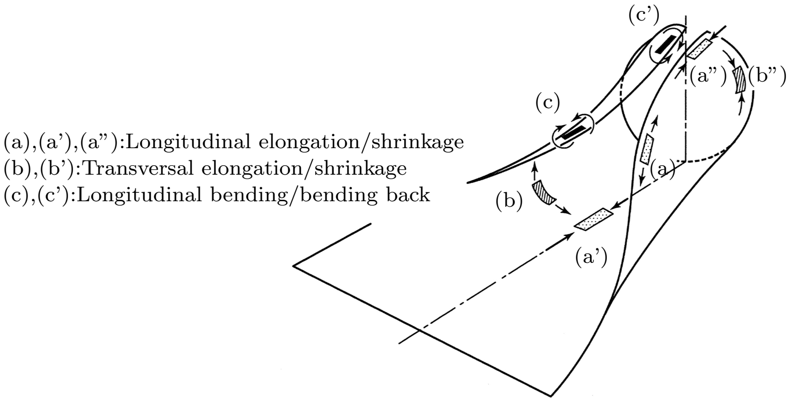
(c')
(a")
(b")
(c)
(a),(a'),(a"):Longitudinal elongation/shrinkage
(b),(b'):Transversal elongation/shrinkage
(c),(c'):Longitudinal bending/bending back
(a)
(b)
(a')

Figure 2.5: Redundant deformations during the roll forming process [Hal05].

However, the geometrical errors in the final parts can be avoided by adjusting different roll forming parameters: profile flower design, roll design, distance between stands, roll forming method, material selection etc. On the other hand, a straightener is used in conventional roll forming machines to correct the aforementioned geometrical deviations. After the last forming station and before the cut-off of the profile the profile is forced to pass through the straightener to compensate the stresses and redundant deformations produced during the roll forming operation [Hal05]. The main geometrical errors of roll formed parts are shown in Figure 2.6.

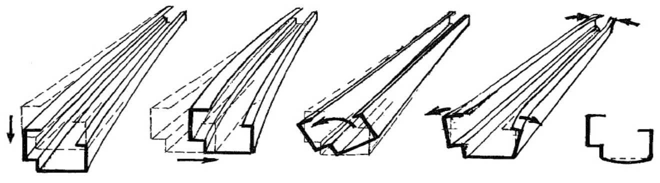

a) Longitudinal bow b) Camber c) Twist d) Flare e) Cross bow

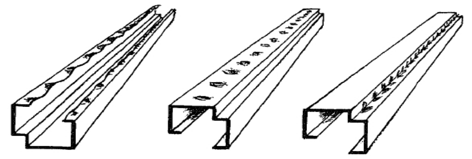

f) Wavy edges g) Wavy centre h) Herringbone effect

Figure 2.6: Typical errors in roll forming [Hal83a].

2.3 Flexible roll forming

2.3.1 Definition and background

It is shown in the precedent section that roll forming technology is one of the most competitive forming process for the production of profiles. However, the roll forming process is limited to the production of profiles with a constant cross section geometry length wise. Further on, bifurcations have to be manufactured by other high cost forming processes and often cause welding operations. As a result, and despite the significant economic and ecological advantages of the conventional roll forming process, the manufacture of customer-modifiable products by conventional roll forming often cannot be taken into consideration [Gro03].

Due to this limitation flexible roll forming was developed by several researchers [Ort01; Gro03; Ona04; Ona05; Lin09c], whereby the fabrication of profiles with variable cross sections along the profile length is possible in a continuous way. Ortic AB developed in 2001 a variable roll forming machine for the construction of 3D roof panels [Ort01]. The machine was used to fabricate conical, longitudinally curved and profiles with variable width in the longitudinal direction. For example, this technology made it possible to cover, the Budapest arena and many other buildings worldwide.

Other authors [Gro03; Ona04] saw the interest of the flexible roll forming technology for the fabrication of automobile parts and the first investigations started in order to develop the basics of the technology. Using the flexible roll forming process, profile shaped components with similar geometries can be fabricated only changing the machine parameters and without huge capital investments [Gro03]. An example of flexible roll formed profile and a continuous fabrication line can be seen in Figure 2.7.

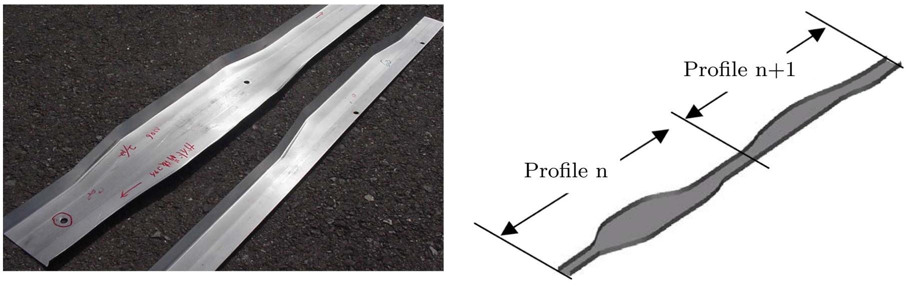

a) b)

Figure 2.7: (a) Profiles with variable cross sections [Ona05] and (b) continuous production of flexible profiles [Gro03].

A particular tooling system with movable forming rolls enables the fabrication of profiles flexible in width. For example, three selected positions of the forming rolls during the forming process are displayed in Figure 2.8 a. Since a perpendicular roll gap on the bend edge is essential for the forming of profiles in close tolerances, the tool movement needs to contain rotatory and translatory degrees of freedom. This can be realized by a cnc-controlled spindle driven kinematics (Figure 2.8 b) [Lar10a].

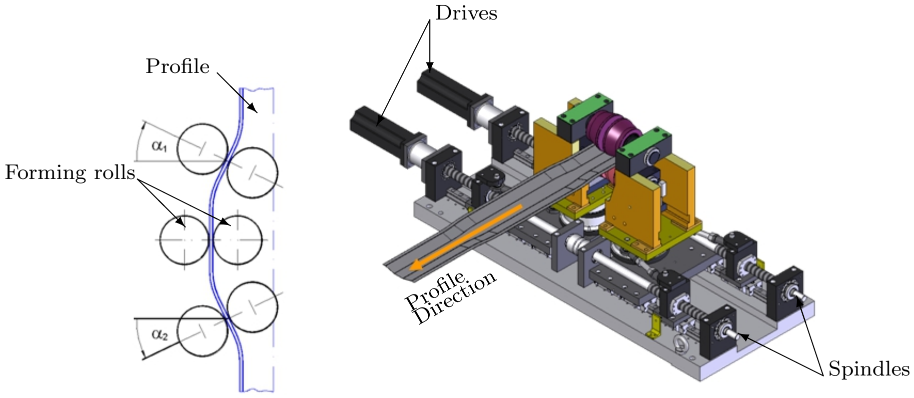

a) b)

Figure 2.8: (a) Position of the forming rolls during the forming of flexible part zone [Gro03] and (b) 3D model of the flexible roll forming stand [Lar10a].

However, two different types of flexible roll forming processes can be defined. Flexible roll forming in width direction and flexible roll forming in depth direction depending on the orientation of the cross sectional variation. Historically, flexible roll forming in width direction have been developed and investigated more than flexible roll forming in depth direction. However, different industries have shown interest for both variants and currently both flexible roll forming processes are being investigated.

2.3.2 Sheet deformation and geometrical errors in flexible roll forming

Contrary to conventional roll forming, flexible roll forming is not a pure bending process. In the transition zone, where the profile changes its cross section, longitudinal strains are necessary to obtain the intended profile geometry.

The fabrication of a flexible U profile variable in width is considered, the undeformed transition zone of the pre-cut sheet is shown in Figure 2.9 b. It is noted that in the initial stage the edge of the pre-cut sheet and the bend line have different lengths in curved zones, ($\overline{B''C''} > \overline{BC}$ and $\overline{D''E''} < \overline{DE}$). During the forming of the flexible profile, the material in $\overline{B''C''}$ is compressed and in $\overline{D''E''}$ is stretched in order to reach the desired profile geometry (Figure 2.9 a).

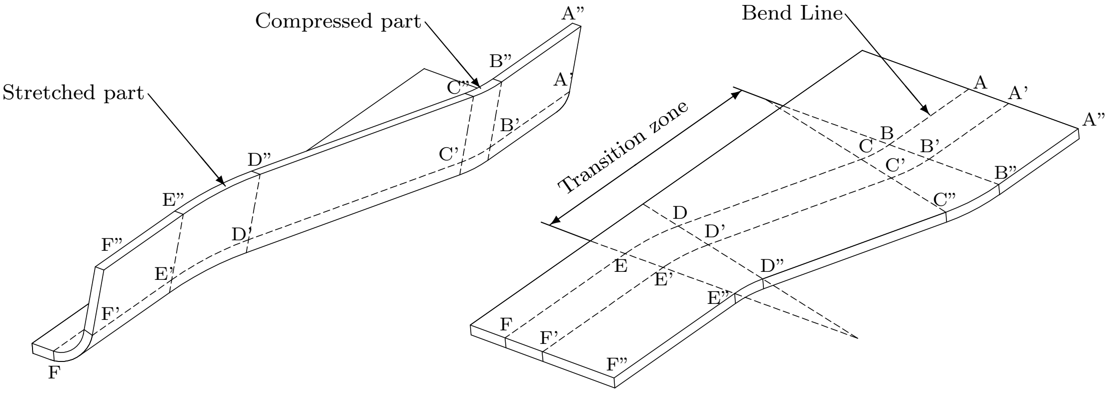
Compressed part
Stretched part
A"
B"
C"
A'
B'
C'
D"
E"
F"
D'
E'
F'
F
Bend Line
Transition zone
A
A'
A"
B
B'
B"
C
C'
C"
D
D'
D"
E
E'
E"
F
F'
F"

a) b)

Figure 2.9: (a) Compressed-stretched zones of the transition zone of flexible U profile in width and (b) pre-cut sheet of the flexible U profile.

Something similar occurs during the fabrication of flexible U profiles variable in depth (Figure 2.10). During the forming of the flexible profile, the material in $\overline{B''C''}$ is stretched and in $\overline{D''E''}$ is compressed in order to reach the desired profile geometry (Figure 2.10 a).

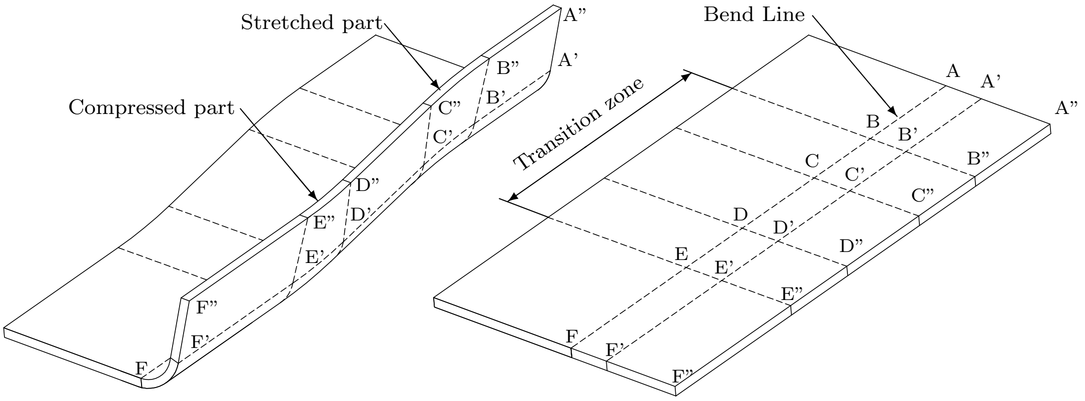
Stretched part
Compressed part
A"
A'
B"
B'
C"
C'
D"
D'
E"
E'
F"
F'
F
Bend Line
Transition zone
A
A'
A"
B
B'
B"
C
C'
C"
D
D'
D"
E
E'
E"
F
F'
F"

a) b)

Figure 2.10: (a) Compressed-stretched zones of the transition zone of flexible in depth U profile and (b) pre-cut sheet of the flexible U profile.

Following the aforementioned reasoning, the transition zone can be split into two areas for both cases. On the one hand the stretched zone, where the profile shape is concave and on the other, the convex compression zone. After the forming of the profile, if the edge and the bend line of the stretched and compressed zones have different lengths, geometrical deviations occur in the flexible roll formed part. Thus, longitudinal plastic deformations are necessaries in flexible roll forming process.

Typical geometrical errors in flexible roll formed parts are wrinkling of the flange and the web warping (Figure 2.11). The geometrical deviations are enhanced when advanced high strength materials are used due to the high springback effect of these steels [Lar08a].

The wrinkling is caused by the resulting longitudinal compression stresses during the forming. If compression stresses exceed a certain level the profile's flange bulges. Groche et al. [Gro10] investigated the appearance of wrinkles in the profile and developed a one-step-model to use in the design of flexible roll formed U-profiles free of wrinkles.

However, the latest investigations have shown that the web warping is the most challenging problem to be solved. The web warping is defined as the height deviation of the profile web from the entry of the transition zone to the exit (Figure 2.11 b).

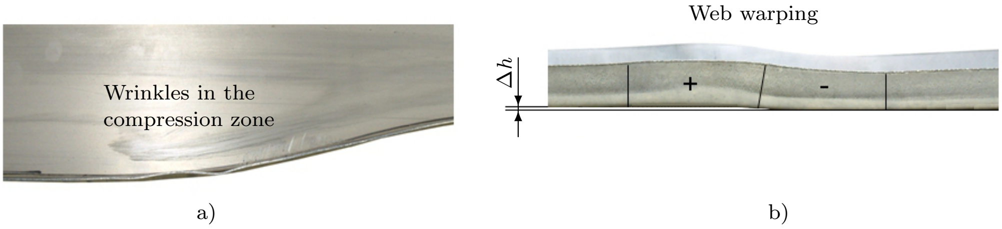

Figure 2.11: Typical failure modes in flexible roll forming. (a) Flange wrinkling and (b) Web warping (Δh) [Lar10a].

The web warping (Δh) is caused by the resulting insufficient longitudinal plastic strains in the flanges of the transition zone. If the plastic deformations are insufficient in transition, the sheet reacts to the stresses generated during the forming and changes its shape until a state of equilibrium is reached. This effect deforms the transition zone raising the compressed zone and lowering the stretched zone [Abe08].

New developments must be developed in order to solve accuracy problems of flexible roll forming profiles, due to conventional straighteners can not be used. Different authors have investigated the web warping and proposed different solutions.

Abee et al. [Abe08; Sed09; Abe09] demonstrated by means of numerical simulations the improvement of the geometrical accuracy of flexible U profiles using blank holders. The blank holders are a sort of special tooling system designed for avoiding the web warping during the flexible roll forming process. The correction of the the geometrical deviations is difficult only by the effect of the rolls and blank holders are used to avoid these geometrical inaccuracies. These blank holders can be positioned in before and after the flexible roll forming stands and support the profile web when the flange enters into the forming rolls. The development of efficient blank holders is the most challenging current issue. Two concepts of blank holder systems are shown in Figure 2.12 a and b.

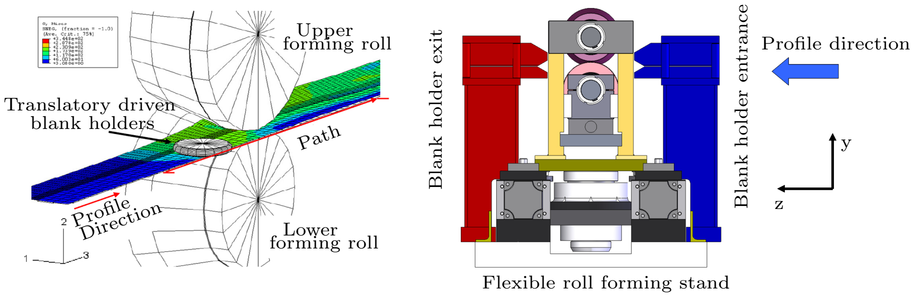

a) b)

Figure 2.12: Blank holder systems proposed by different authors, (a) [Gro09] and (b) [Lar10a].

Abee et al. [Abe08; Sed09] numerically studied a clamping blank holder system with translatory movement perpendicular to the profiling direction. The blank holder was used to clamp the web of the profile in those zones where web warping occurred and also guide the web of the profile between two stations. The clamping mechanism was switched off before entering into the next forming station and the blank holder moved back to their original position without contacting the sheet.

The Institute for production engineering and forming machines - PtU of the Technische Universität Darmstadt developed within the European project Proform [Eur10] a flexible roll forming prototype in order to study different blank holder systems and a special over bending flexible stand. The studied blank holder follow the bending line of the profile to support the profile's web as close to the forming zone as possible, allowing only the deformation of the part in the intended zone [Gro09]. Different contact systems between the sheet and the blank holder are being investigated: rolling contact, line contact and surface contact.

The idea of the over bending station was to reduce the web warping by an active intervention in the bending angle during the forming process. The bending angle was adjusted during the forming process in order to minimize the web warping. During the loading phase, the strains in the profile length direction were adjusted by increasing the bending angle in the transition zone. With this method the springback and the warping seemed to be reducible [Eur10].

Ona et al. [Ona10] proposed also an active solution in order to increase the longitudinal deformations in the flexible zone. The author proposed to roll different zones in the flange of the profile in order to increase the longitudinal strains and decrease the profile web warping. A decrease of about 50% was achieved in the web warping error when the longitudinal strains were increased by 5% by means of flange rolling.

Within the Proform project [Eur10] an industrial roll forming machine has been developed and constructed to form flexible hat profiles [Gut10; Lar10a]. The line consisted of 9 conventional stands, 8 flexible stands and static blank holders that supported the web of the profile. A conceptual design of one flexible roll forming stand can be seen in Figure 2.12 b. The geometrical accuracy of flexible profiles was improved using static blank holder [Gut10; Lar10a].

Lindgren et al. [Lin09c] presented a 3D flexible roll forming line constructed for research and prototyping of profiles with variable cross-section in both width and depth for the automotive industry. The flexible roll forming machine was composed by 6 flexible forming stands. Each flexible forming stand were designed with 4 degree of freedom (2 rotational and 2 translational) and cylindrical rolls were used in all stations without blank holders. The different passes were achieved by changing the relative position of the cylindrical rolls. Although little geometrical errors appeared during the experimentation, the author says that it is possible to produce 3D roll-formed profiles with close tolerances.

2.4 Heat assisted roll forming

High strength steels are being using more and more in order to decrease the weight of the vehicles even if these materials show a limited formability. The forming limits of high strength steels can be raised by increasing the temperature of the process [Gei04]. In Figure 2.13 a tensile test of a high strength steel material is considered at two different temperatures $T_1 < T_2$. Increasing the process temperature, the formability of the material increases ($\Delta\varepsilon$), the flow curve decreases ($\Delta\sigma$) and as a consequence the forming forces and the springback effect ($\varepsilon_{T_2} < \varepsilon_{T_1}$) decreases.

However, the effect of the temperature in the initial material must be considered and the differentiation between warm forming and hot forming can be made depending on the process temperature. Warm forming is considered as forming below the recrystallization temperature and the activation of additional sliding systems is found. Hot forming is considered as forming above the recrystallization temperature and additionally to the activation of more sliding systems more complex microstructural changes take place [Neu06].

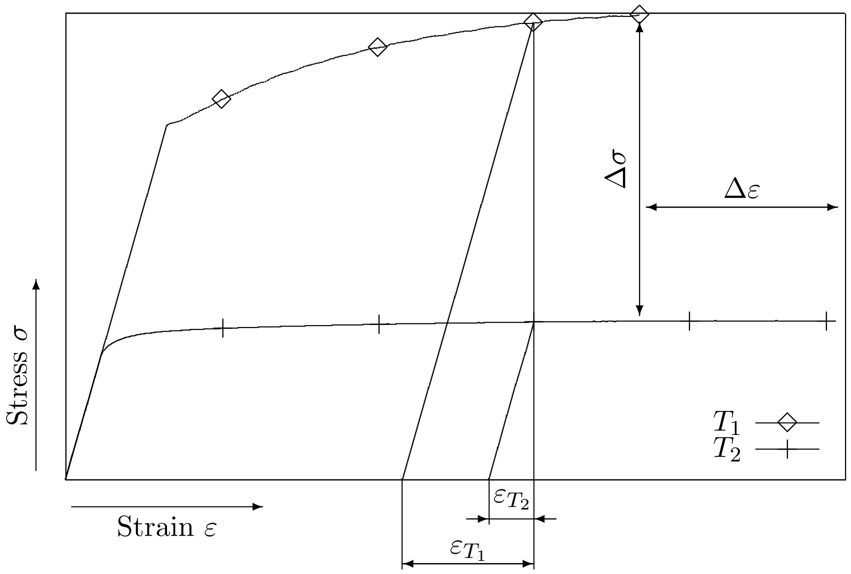

Figure 2.13: Temperature dependent material flow.

Heating the whole workpiece can cause inconvenients like high temperature corrosion or a very difficult handling [Lie02]. Heating the whole workpiece is not necessary in the case of several forming processes such as bending or roll forming since the deformation takes place only in restricted regions of the volume of the workpiece. A selective heating can be performed in these processes to increase locally the formability in those zones where the deformations take place. Additionally to the local formability increment, heating the workpiece locally saves energy and time compared to heating the whole workpiece [Sch04].

Although, some experiments of hot roll forming process were made in the late 1960s with titanium alloys [Hal05] only few investigations have been published. However, roll forming at high temperature is a potential new technology that can make it possible to form high strength profiles in an economical manner [Hal05]. The main objective of heat assisted roll forming is to increase the formability of roll formed materials as well as to decrease the geometrical deviations of the roll formed parts [Mer02; Lin09b].

Pitz et al. [Mer02; Pit04], presented a single-step roll forming machine (Figure 2.14 a) equipped with a diode laser. The machine was able to bend the workpiece up to 170°. The incremental bending was performed moving the workpiece forward and backward and changing the angle of forming roll between both movements. The laser was used to heat the bending area before the forming roll. Several experiments using a CP800 complex phase high strength steel were performed and the longitudinal and transversal bow of the heat assisted and non assisted parts were compared. The heat assisted parts showed 3 times less transverse bow and 5 times less longitudinal bow than cold roll formed profiles.

Lindgrend et al. [Lin09b] investigated a conventional heat assisted roll forming process, with the objective of increasing the formability of a HyTens 1600 stainless steel. In this case the initial metal sheets were heat treated out of the machine in order to change the microstructure of the material in the bending zone. The partial heating was performed using resistance heating wheels, Figure 2.14 b. Afterwards, the pretreated sheets were roll formed in a six stand roll forming machine (15°, 30°, 60°, 90°, 105°and 120°). The cold roll formed parts were roll formed until 30° without rupture and heat assisted parts until 120°.

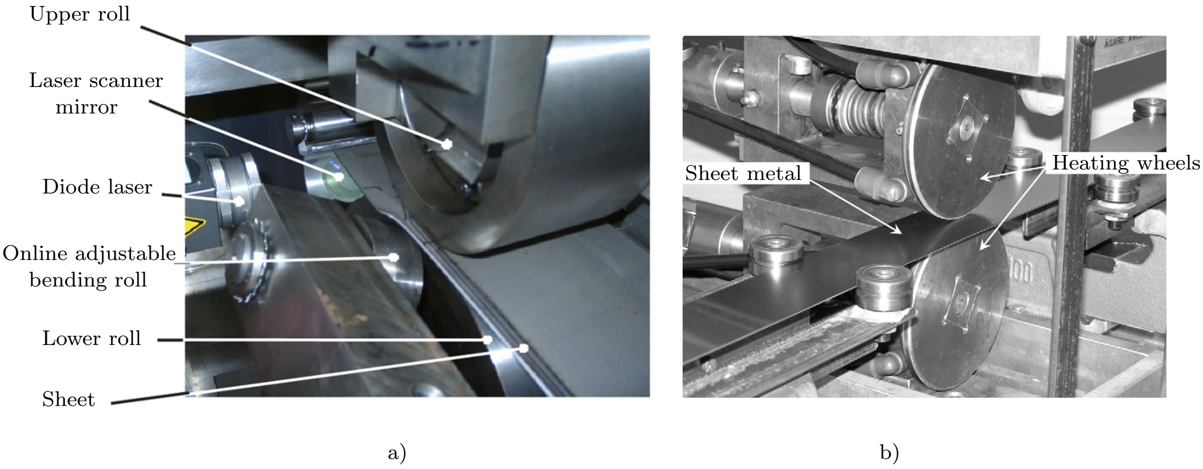

a)

b)

Figure 2.14: Heat assisted roll forming lines: (a) Chair of Manufacturing Technology of the University of Erlanger-Nuremberg [Pit04] and (b) Dalarna University [Lin09b].

2.5 Heat assisted flexible roll forming

Heat assistance have been used in conventional roll forming processes to increase the formability of high strength steels as well as to decrease the geometrical deformations of targeted profiles but never in the flexible roll forming processes.

The flexible roll forming process of a U profile is considered in Figure 2.15. It is shown in the precedent section that the curved zones of the transition zone will longitudinally stretch (ε_{s}) and compress (ε_{c}). The idea of heat assisted flexible roll forming is to use the temperature to increase the formability of those zones that have to be longitudinally deformed. The wrinkles in the flange and the web warping can be avoided if the longitudinal deformations reach the intended degree. The profile could be heated before the last forming station, and the last station could be used to calibrate the profile and compensate the residual stresses accumulated during the fabrication process.

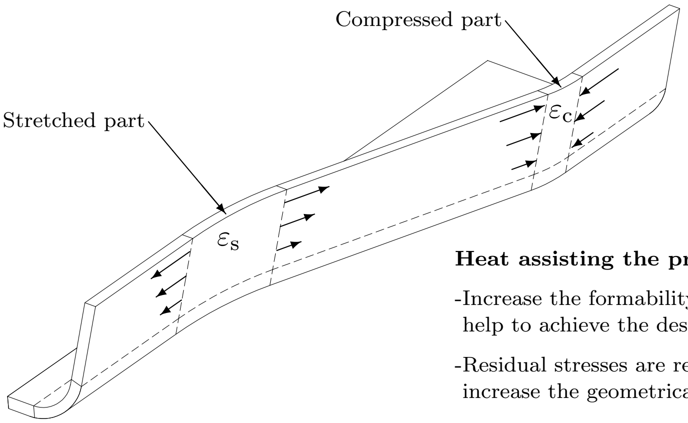

Heat assisting the profile:

-Increase the formability of the material and help to achieve the desired longitudinal deformation.

-Residual stresses are relaxed and thus increase the geometrical accuracy.

-Decrease the yield stress and thus decrease the forming forces.

Figure 2.15: Heat assisted flexible roll forming process.

The heat assistance could be introduced into the flexible roll forming process, keeping the process continuous. On the other hand, heat assistance can be applied together with any blank holder system that help enhancing the geometrical accuracy of the part. However, different process variants, material considerations and quality requirements must be analyzed in detail for each part in order to find the optimal heating strategy.

As it is explained in Chapter 1, the main objective of the present thesis is to study and develop a method to increase the geometrical accuracy of flexible roll formed parts by means of local heating. In the following chapters, the work made to achieve this general purpose is explained.

2.6 Conclusions

Conventional roll forming processes offer different technological, economical and environmental advantages that are used in many industries worldwide. However, conventional roll forming is limited to producing profiles with constant cross section.

Flexible roll forming offers the possibility to produce profiles with variable cross sections lengthwise but due to the complex compression-stretch stress distribution of the transition zones geometrical deviations occur. It is difficult to compensate those geometrical errors adjusting only the process parameters and additional tooling systems are being studied. However, those tooling systems do not completely solve the inaccuracy of the flexible profiles and more investigations are needed.

Heat assisted forming processes are used in order to increase the forming capabilities of limited formability materials, decrease the forming forces and increase the geometrical accuracy of final parts. Very few investigations have been made in the field of heat assisted roll forming process and never in the field of heat assisted flexible roll forming process. The basics of heat assisted flexible roll forming process are presented. This new technology can be used together with the aforementioned tooling systems to increase the geometrical accuracy of flexible profiles.

CHAPTER 3

Material Characterization

Scientia vincere tenebras

" Conquering darkness by science "

Synopsis

Interest in high strength steels in the automotive industry has increased in recent years due to ecological and economical reasons. In order to save the weight of vehicles, advanced high strength steels are being used. However these materials show limited formability and it is essential to analyze the mechanical properties and material behaviors under different conditions, in order to optimize and improve the forming processes of these steels. Therefore, in this chapter, three different high strength steels and a conventional mild steel are characterized at different quasi-static strain rates. The anisotropic behavior depending on the strain, is also analyzed.

Furthermore, the CP800 steel, selected to perform heat assisted flexible roll forming experimental tests, is characterized over a wide range of temperatures from room temperature up to 700°C and at two strain rates. Temperature and strain rate effects on macroscopic properties such as flow stress and elongation to fracture are discussed. Microstructure and X-ray diffraction analysis are also performed in order to analyze the possible deformation mechanisms at different conditions.

A paper based on the work described in this chapter has been submitted to the journal *Materials Characterization* [Lar11]

3.1 Introduction

The use of high strength steels have increased in the automotive industry in the recent years due to the lightening of automobile weight. However, these new Advanced High Strength Steels (AHSS) have shown a limited formability, high springback effect and high forces and energy are needed to form those materials [Kle03**?**]. For all these reasons, in order to correctly design the fabrication processes, it is necessary to characterize the mechanical behavior of these materials over a wide range of conditions.

The first part of the present chapter deals with the tensile characterization of three different AHSS, Martensitic MS1200, Complex Phase CP800 and Dual Phase DP600 high strength steels and also the characterization of a DC01 mild steel. Tensile deformation behavior of the different steels is characterized at three different strain rates. In order to consider the anisotropy of the mechanical properties, tensile tests are performed in 0°, 45° and 90° with respect to the rolling direction. The Lankford coefficients (r-values) depending on the strain level are calculated for the samples tested at 10^{-3} s^{-1} strain rate.

The second part of the present chapter deals with the tensile characterization at different temperatures of the CP800 steel. This steel is selected to perform the heat assisted flexible roll forming experiments. The tensile deformation behavior of CP800 sheet material is characterized over a wide range of temperatures, from room temperature up to 700°C and at 10^{-2} s^{-1} and 10^{-1} s^{-1} strain rates. Microstructural analysis and X-ray diffraction analysis (XRD) of specimens tested at high temperature are performed and related with the deformation mechanisms.

3.2 Advanced high strength steels

AHSS are characterized by an ultra fine multiphase microstructure, composed by ferrite, martensite, bainite, and/or retained austenite in quantities sufficient to produce unique mechanical properties [Int09; Ada06; Iml07]. The combination of different phases allows the fabrication of targeted steels with different hardness. Ferrite is very soft and easy to form, whereas martensite is extremely strong but only formable to a limited extent. The strength and formability of bainite lays between these two extremes. The transformation of retained austenite to martensite during the deformation increase the material strength, increase the work hardening rate and postpones the onset of necking [Iml07; Jac04]. The schematic microstructure of AHSS are shown in Figure 3.1.

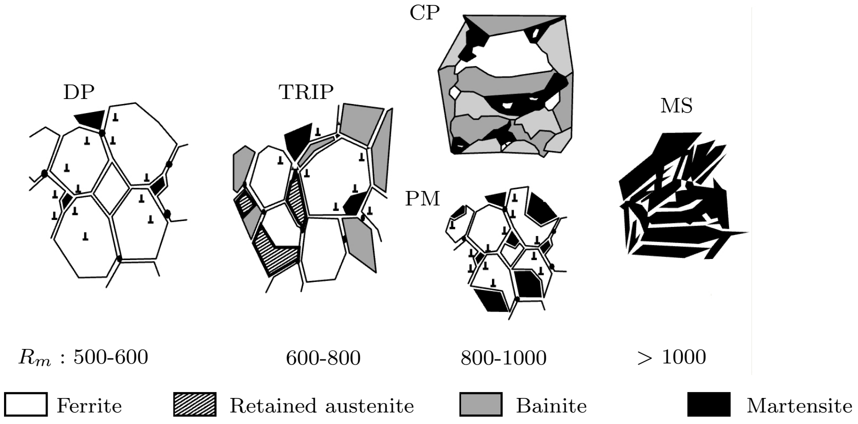
CP
DP
TRIP
MS
PM
R_m : 500-600
600-800
800-1000
> 1000
Ferrite
Retained austenite
Bainite
Martensite

Figure 3.1: Schematic microstructures of different AHSS [Ada06].

The latest studies in metallurgy in combination with the development of new steel fabrication processes, allow modifying the steel properties in a targeted manner and customizes them, obtaining the desired strength level [Iml07; Ada06]. All AHSS are produced by controlling the cooling rate from the austenite phase and following different cooling and rolling strategies at different temperatures [Iml07; Ada06]. The different fabrication processes that produce different types of AHSS are shown schematically in Figure 3.2.

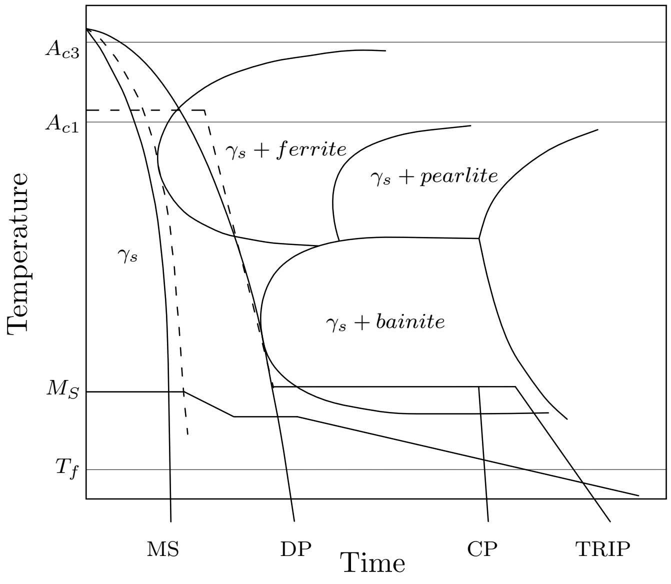
A_{c3}
A_{c1}
Temperature
M_S
T_f
$\gamma_s + ferrite$
$\gamma_s + pearlite$
γ_s
$\gamma_s + bainite$
MS
DP
CP
TRIP
Time

Figure 3.2: Cooling strategies during the fabrication of different AHSS [Ada06].

3.2.1 Dual Phase (DP)

The microstructure of Dual Phase (DP) steels consists of a ferrite matrix with dispersed martensite. The ductile phase in DP steels is the ferrite while increasing the volume fraction of the martensite, increases the strength of the material [Int09; Iml07; Sen01]. During the deformation of DP steels, the strain is concentrated in the soft ferrite phase first and provides a high initial work hardening rate increasing the formability of the material [Int09; Iml07; Sen01]. The DP steels show a low yield strength (Y_s), high Ultimate Tensile Strength (σ_uts), high work hardening rate (n) and relatively high elongation (ε_f) compared with other high strength and conventional steels [Int09; Gei08; Iml07].

3.2.2 TRansformation Induced Plasticity (TRIP)

The microstructure of TRansformation Induced Plasticity (TRIP) steels is composed by retained austenite (minimum of 5%), martensite and bainite in a matrix of ferrite [Int09; Jac04]. During the deformation process of TRIP steels, the retained austenite progressively transforms to martensite. This effect increases the work hardening rate, postpones the onset of necking and thus, increases the formability of the material [Jac04]. TRIP steels can therefore be engineered or tailored to provide excellent formability for manufacturing complex parts or to exhibit high work hardening during crash deformation, for provide excellent energy absorption [Int09].

3.2.3 Complex Phase (CP)

The microstructure of complex phase (CP) steels is characterized by an extremely fine grain size that contains small amounts of martensite, retained austenite and pearlite within the ferrite/bainite matrix [Int09; Iml07]. In comparison with other AHSS, CP steels show significantly higher yield strength for similar tensile strength and strain levels [Int09].

3.2.4 Martensitic (MS)

Martensitic (MS) steels are characterized by a martensitic matrix containing small amounts of ferrite and/or bainite [Int09]. Within the group of AHSS, MS steels show the highest yield strength and tensile strength with the lowest elongation [Int09; Spi04].

3.3 Quasi-static tensile test at room temperature

In the present thesis three commercial AHSS were characterized mechanically in order to compare the effect of the material strength in the roll forming experiments. The selected AHSS were: MS1200 sheet with 1.5 mm thickness, CP800 sheet with 1.2 mm thickness and DP600 with 1.5 mm thickness. In addition to AHSS steels, soft DC01 ductile steel sheets with 1.5 mm thickness was also characterized. The microstructures of selected AHSS are shown in Figure 3.3.

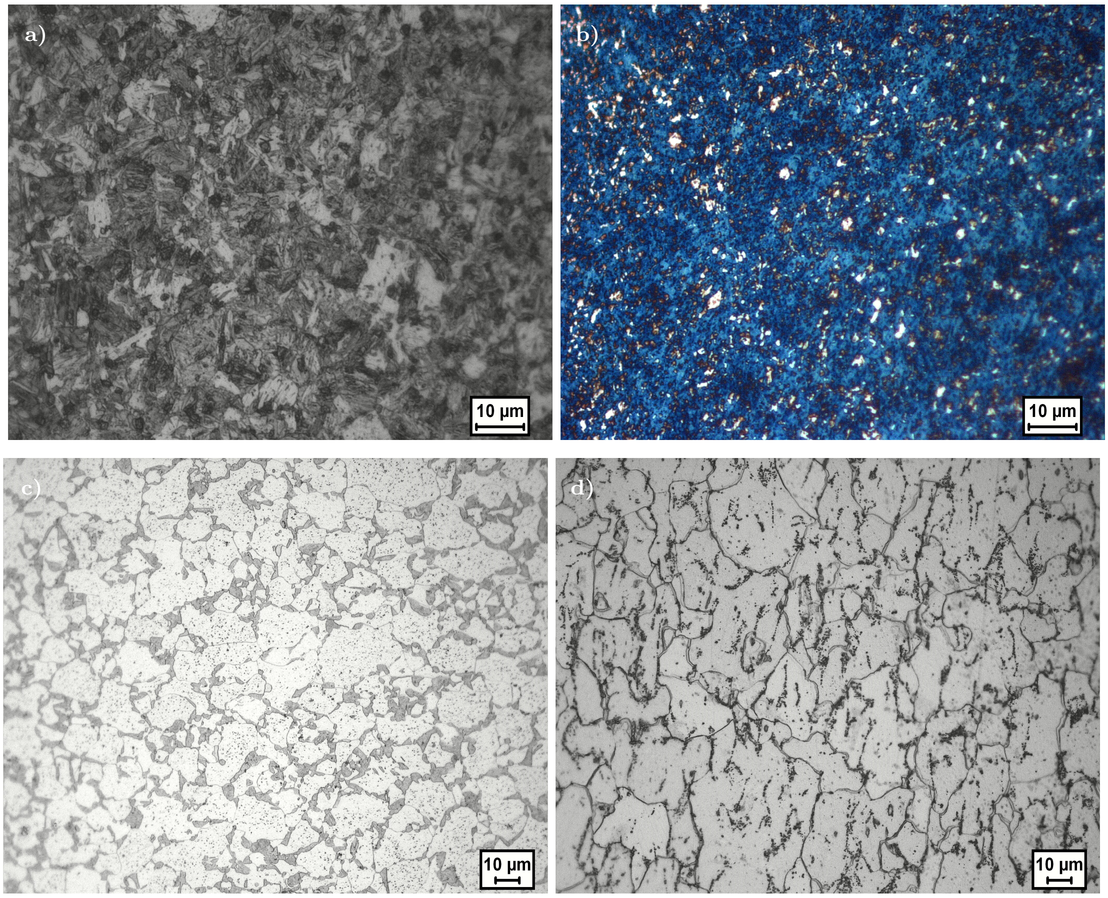

Figure 3.3: Microstructures of a) MS1200, b) CP800, c) DP600 and d) DC01 steels. MS1200, DP600 and DC01 steels were etched with nital 5% agent and CP800 using Klemm's agent. Sample preparation procedure is explained in section §3.4.1.

The selected MS1200 material shows a martenistic matrix with some ferritic islands, CP800 material is characterized by an ultra-fine microstructure composed of small amounts of martensite, retained austenite and pearlite within a ferritic matrix. DP600 microstructure is composed by ferritic matrix with martensitic islands and the selected DC01 material shows a ferritic microstructure with some perlite/cementite grains.

3.3.1 Experimental procedure

Quasi-static tensile tests at room temperature were carried out in the laboratories of Mondragon University using a conventional electro-mechanic drive INSTRON-4206 testing machine. Specimens were tested according to UNE-EN 100002-1 standard at strain rates of 10^{-3} s^{-1}, 10^{-2} s^{-1} and 10^{-1} s^{-1} and using specimens extracted in $0°, 45°$ and $90°$ regarding the rolling direction ($0°, 45°$ and $90°$ hereafter). Specimens were machined using a wire electric discharge machining machine type Robofil 100. The strain rates were selected to be as close as possible to the real roll forming conditions. Forces were measured using an Instron load cell of 100kN. The geometry of the specimens can be seen in Figure 3.4.

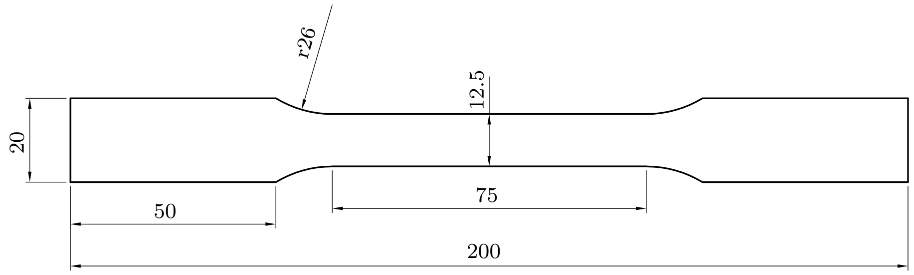

Figure 3.4: Geometry of the specimen employed at room temperature tensile tests.

Longitudinal and transversal strain measurement

The longitudinal displacements were measured using an Instron extensometer of 25 mm. This extensometer allowed the measurement of the displacements until the failure of the tested specimen. The limited elongation capability of the selected steels makes it difficult to measure accurately the transversal strain variation by a mechanical measuring system (e.g. micrometer). In order to solve this problem, strain gages glued in the transversal direction were used to measure the transversal strain. Additionally, using strain gages the anisotropic behavior of the steel can be analyzed depending on the deformation degree of the material [Mar02]. The transversal strain measurements were performed using high elongation strain measurement gages EP-08-250BG-120 type, from Vishay Micro-Measurement.

The strain gages installation consisted of cleaning the surface with acetone and grinding the surface at $0°, 45°$ and -45° using 120 grit SiC paper and then using 400 grit SiC paper. The adhesive used must be rigid enough to prevent gage relaxation and flexible enough to permit large deformations without cracking. The strain gages were glued in the middle of the specimen at 90° with regard to the rolling direction and using a 100%

solid epoxy system adhesive. The strain gages were then cured for 2 hours at 75°C [Vis09]. The strain measurement was carried out using a quarter Wheatstone bridge, and the data acquisition was carried out using equipment from National Instrument and using the LabVIEW software. The tensile test lay-out combining the extensometer and the strain gages can be seen in Figure 3.5.

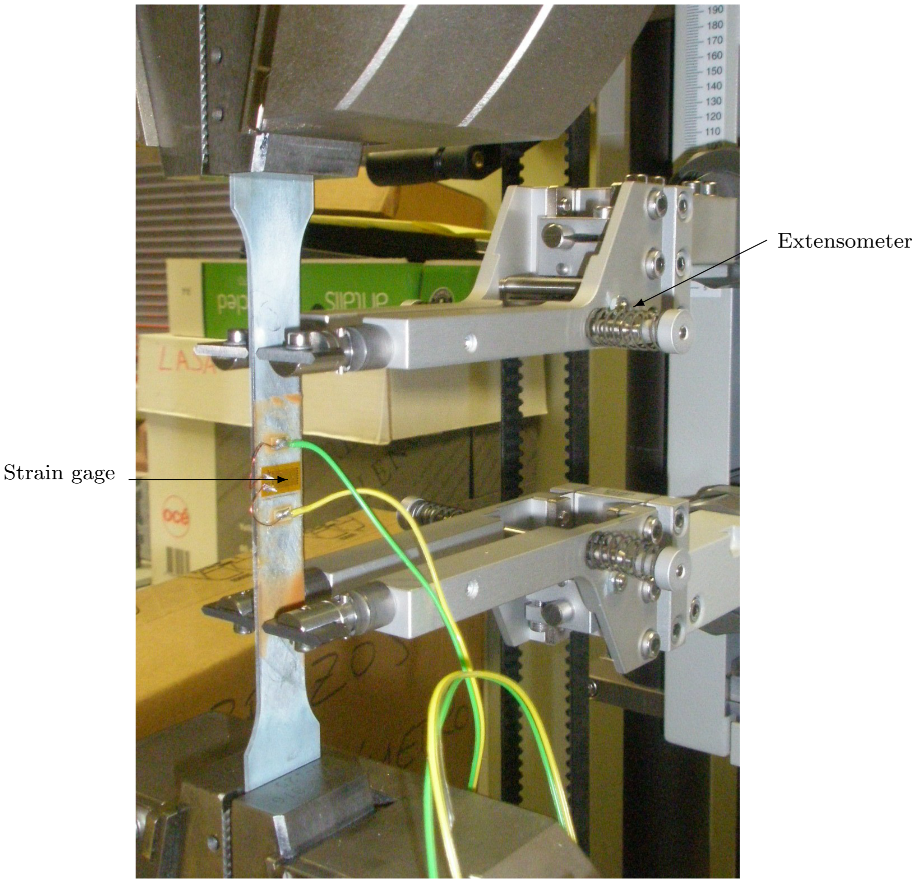

Figure 3.5: Longitudinal and transversal strain measurement.

Strain anisotropy calculation, Lankford coefficient (r-value)

The anisotropic Lankford coefficient (r-value), gives an idea of the strain anisotropy and it refers to the resistance of the sheet to thinning during uniaxial tension testing. The r-value is defined as:

$$r = \frac{\varepsilon_{\mathrm{W}}}{\varepsilon_{\mathrm{T}}} = \frac{\varepsilon_{\mathrm{W}}}{-\varepsilon_{\mathrm{L}} - \varepsilon_{\mathrm{W}}} \tag{3.1}$$

where W, T and L denote sample width, thickness and longitudinal directions respectively. The final expression is obtained invoking volume constancy and it is used in order to obtain more accurate r-value measurements due to small thickness variations.

$$\frac{\Delta V}{V} = \varepsilon_{\mathrm{W}} + \varepsilon_{\mathrm{T}} + \varepsilon_{\mathrm{L}} = 0 \tag{3.2}$$

Even though special care was taken during the strain gage installation, some of the strain gages failed prematurely. In these cases only the linear part of the longitudinal strain vs transversal strain curve was taken into account.

As example, the longitudinal strain vs transversal strain diagram, and the r-value vs longitudinal strain diagram of the tensile test performed with the DC01 material are shown respectively in Figure 3.6 a and b. It can be clearly seen that at $\varepsilon_{\mathrm{L}} \approx 0.08$ the strain gages failed before the specimen failure at $\varepsilon_{\mathrm{f}} \approx 0.31$. The strain gages failure was caused by the adhesive cracking.

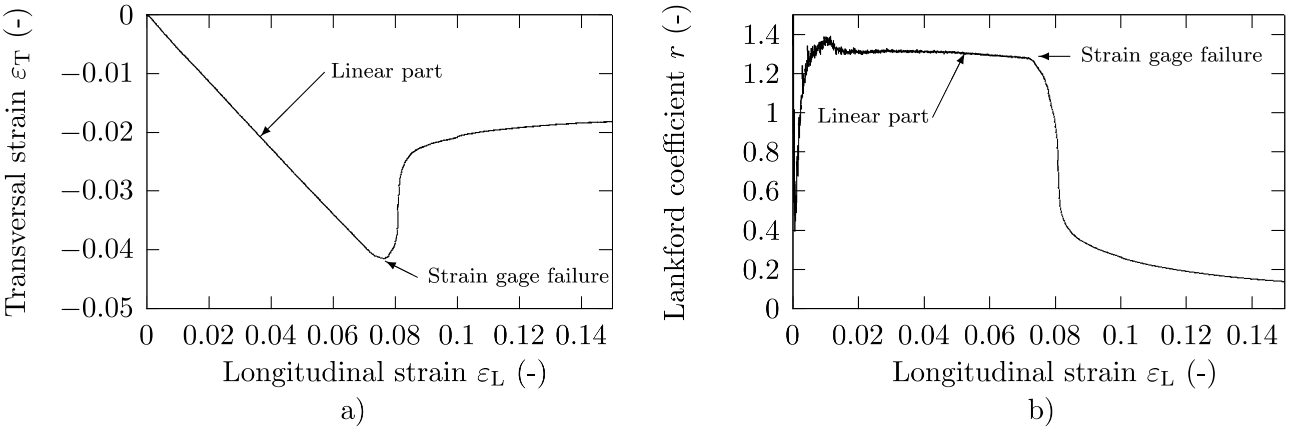

Figure 3.6: (a) Transversal strain (ε_{T}) vs longitudinal strain (ε_{L}) and (b) Lankford coefficient (r) vs longitudinal strain (ε_{L}) of a tensile test performed with DC01 material.

3.3.2 Experimental results

MS1200

The experimental results from the mechanical characterization of the MS1200 material are shown in Figure 3.7.

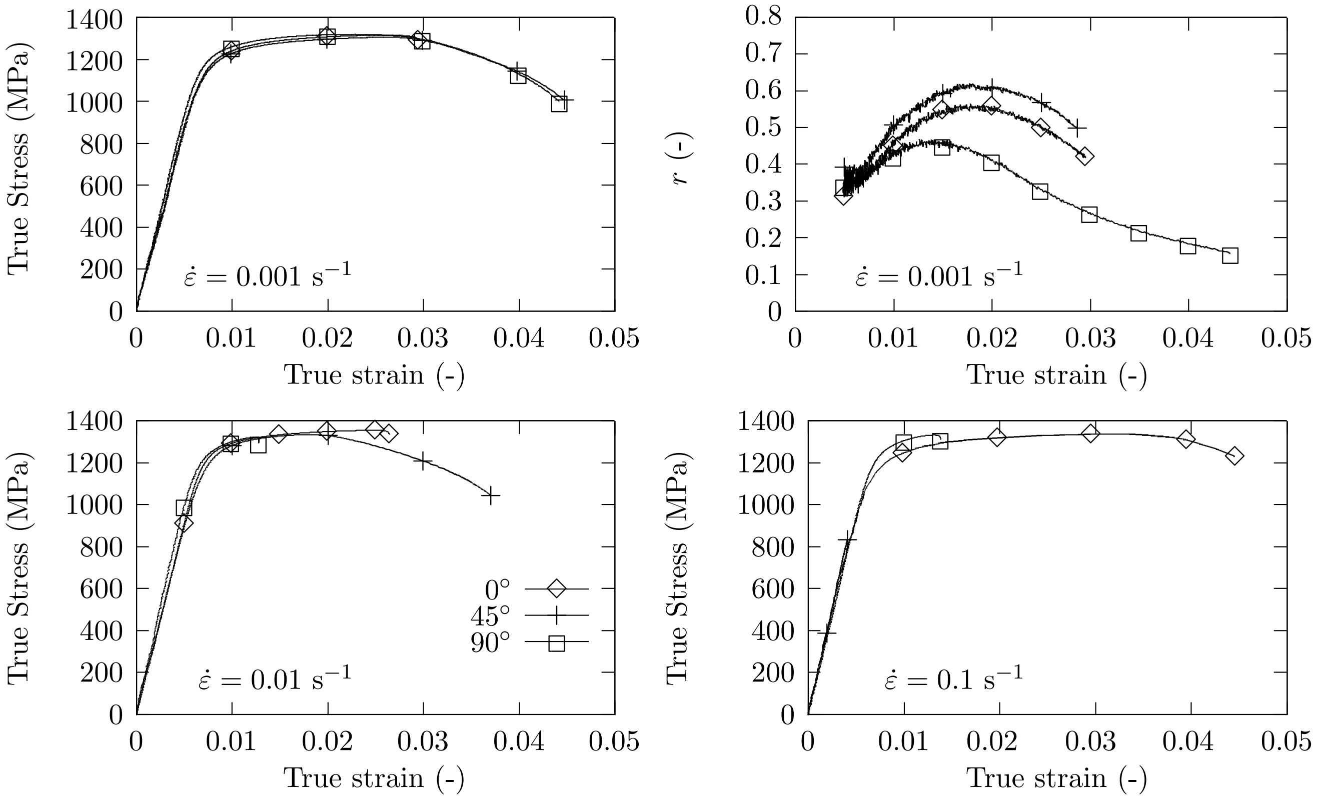

Figure 3.7: Mechanical properties of MS1200 steel. The summary of the results can be seen in Table A.1 of appendix A.

The tensile test results of MS1200 material shows very high Y_s ($\approx$ 1200 MPa) and σ_{uts} ($\approx$ 1350 MPa) combined with very limited ε_f ($\approx$ 0.04) as reported previously in [Int09; Spi04]. This high strength and reduced ε_f is attributed to the high martensite content of the MS1200 material (Figure 3.3 a).

The strain rate has little influence on the flow stress behavior of the MS1200 material. Similar values of Y_s, σ_{uts} and ε_f are obtained at the different strain rates. The loading direction also has little influence on the flow stress behavior of the MS1200 material in all the strain rate range. The only remarkable point is that the MS1200 material at 0° shows slightly higher Y_s and σ_{uts}, and slightly lower ε_f than at 45° and 90°. On the other hand, the MS1200 at 45° and at 10^{-1} s^{-1} strain rate shows a very limited ε_f. All the specimens tested at these conditions failed prematurely before achieving the plastic regime.

The upper right graph of Figure 3.7 shows the evolution of r-value with the strain level of samples tested at 10^{-3} s^{-1}. It is noted a very low r-value and it is strain dependent. The high strength, the low ε_f and the low r-value makes it very difficult to form parts with this material. On the other hand, due to the limited ε_f showed by the MS1200 it is difficult to see a clear tendency of the material under the strain rate and the rolling direction.

CP800

The experimental results from the mechanical characterization of the CP800 material are shown in Figure 3.8. The tensile test results of CP800 material shows a relatively high Y_s ($\approx$ 680 MPa) and σ_{uts} ($\approx$ 880 MPa) combined with considerable high ε_f ($\approx$ 0.15), as reported previously in [Int09; Gei08].

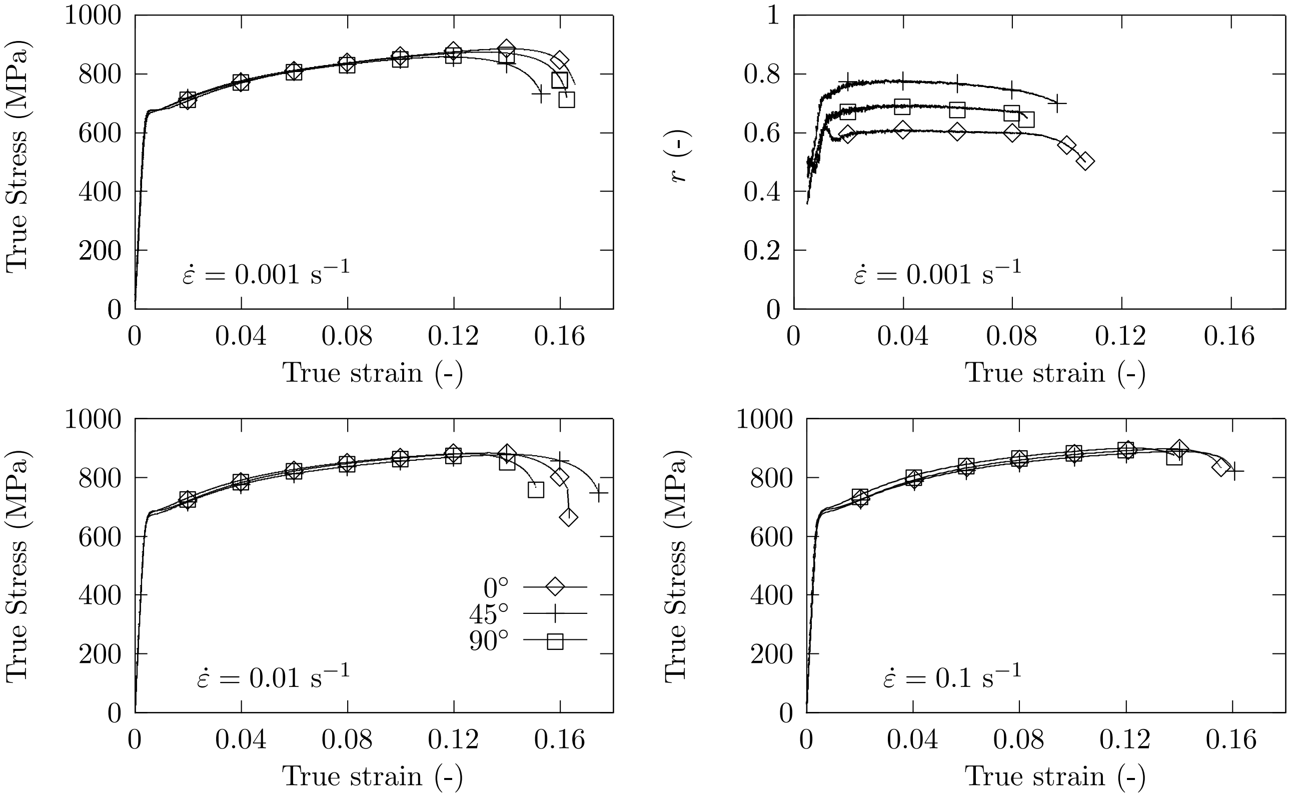

Figure 3.8: Mechanical properties of CP800 steel. The summary of the results can be seen in Table A.2 of appendix A.

Analyzing the effect of the strain rate on the CP800 material, it can be denoted that the Y_s and the σ_uts slightly increase while the ε_f remains invariable, when increasing the strain rate from 10^{-3} s^{-1} to 10^{-1} s^{-1}. It is generally known that in quasi-static regime, increasing the strain rate the flow stress of the material increases and the deformation capability decreases [Cur09a]. The loading direction has little influence on the flow stress behavior of the CP800 material in all the strain rate range. The only remarkable point is the CP800 material at 45° shows slightly lower Y_s and σ_uts, with similar ε_f than at 0° and 90° .

The upper right graph of Figure 3.8 shows the evolution of the r-value of the samples tested at 10^{-3} s^{-1} with the strain level. The CP800 steel shows a highest r-value at 45°.

DP600

The experimental results from the mechanical characterization of the DP600 material are shown in Figure 3.9.

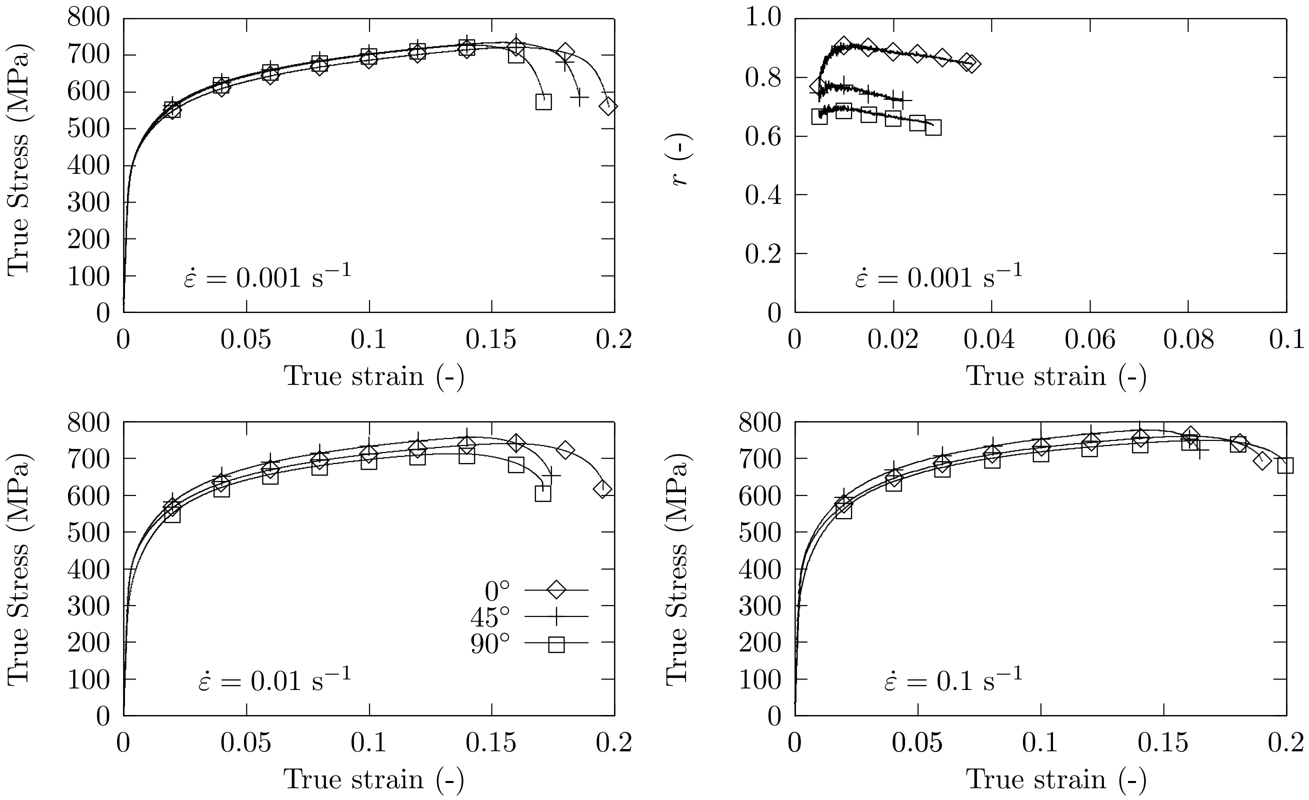

Figure 3.9: Mechanical properties of DP600 steel. The summary of the results can be seen in Table A.3 of appendix A.

The tensile test results of DP600 material shows a lowest Y_s ($\approx$ 410 MPa) and σ_uts ($\approx$ 740 MPa) combined with highest ε_f ($\approx$ 0.18) of the AHSS, as reported previously in [Int09; Gei08; Cur09b]. Analyzing the effect of the strain rate of the DP600 material, it can be seen that the Y_s and the σ_uts slightly increase while the ε_f decreases when increasing the strain rate from 10^{-3} s^{-1} to 10^{-1} s^{-1}, the same behavior of DP600 was reported in [Cur09b]. The influence of the rolling direction is more important in the DP600 steel than in the previous ones. The DP600 material at 45° shows a higher σ_uts and lower ε_f than at 0° and 90°.

The upper right graph of Figure 3.9 shows the evolution of the r-value of the samples tested at 10^{-3} s^{-1} depending on the strain level. It can also be seen that in this case the r-value is strain dependent, increasing the strain level the r-value decreases.

DC01

The experimental results from the mechanical characterization of the DC01 material are shown in Figure 3.10.

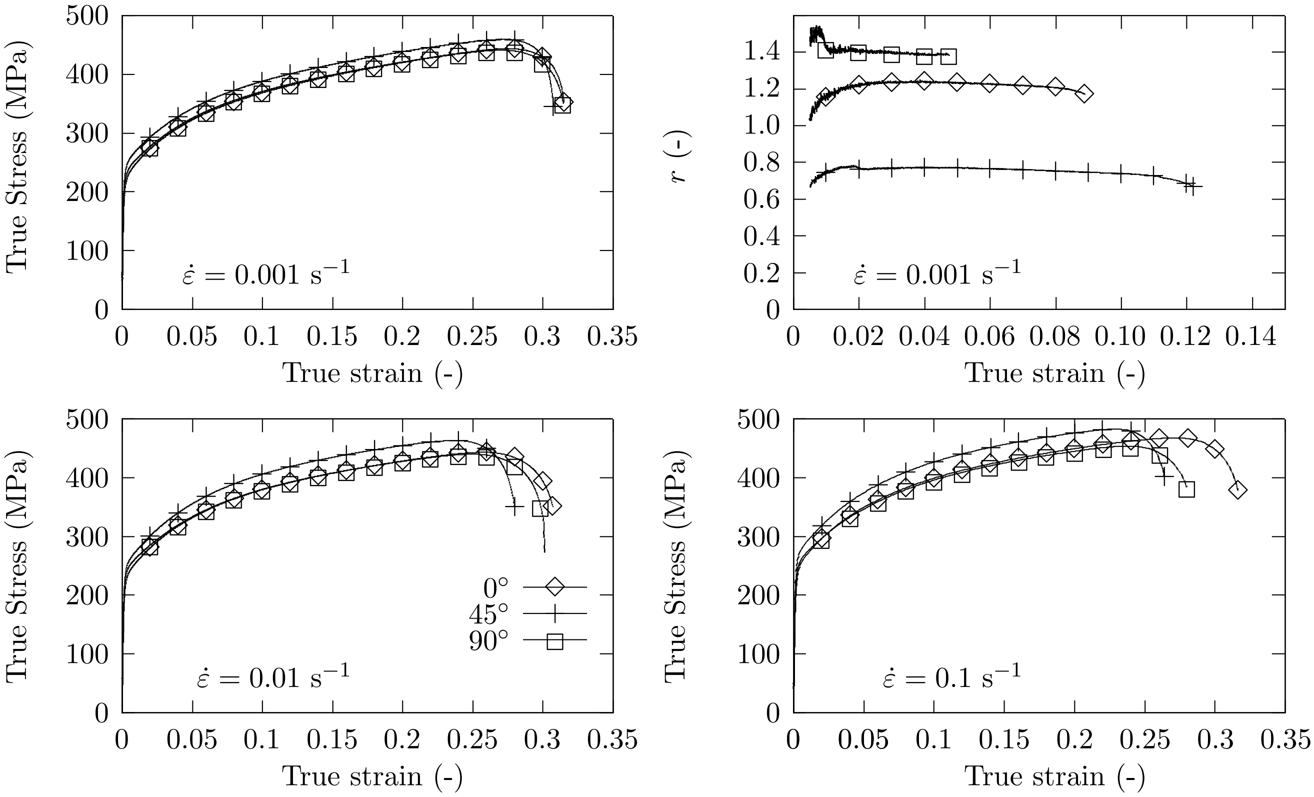

Figure 3.10: Mechanical properties of DC01 steel. The summary of the results can be seen in Table A.4 of appendix A.

Comparing the tensile test results of DC01 material with the tensile test results of other AHSS, the DC01 shows low Y_s ($\approx$ 230 MPa) and σ_uts ($\approx$ 445 MPa) combined with a high elongation ε_f ($\approx$ 0.3). Analyzing the effect of the strain rate of the DC01 material, it is shown that the Y_s and the σ_uts slightly increase while the elongation at fracture decreases when increasing the strain rate from 10^{-3} s^{-1} to 10^{-1} s^{-1} (table A.4 of appendix A). The influence of the rolling direction is remarcable in the DC01 material. As it was expected the DC01 material at 45° shows a higher Y_s and σ_uts and slightly lower ε_f than at 0° and 90°. This anisotropic behavior is common in mild steels.

The r-value of the DC01 is not strain dependent. On the other hand DC01 materials show a r-value higher than 1 at 0° and 90°. This is interesting since this material at these directions shows a resistance to thinning.

3.4 Quasi-static tensile tests at high temperature

The CP800 AHSS mechanically characterized in the precedent section was selected to perform the heat assisted roll forming tests, due to the good strain-stress relation and the good crashworthiness behavior showed by this material. On the other hand, CP800 is widely used in the construction of the BW of cars and different authors [Gei04; MV09] are currently investigating the enhancement of forming properties of CP800 steels by means of local heating.

3.4.1 Experimental procedures

Mechanical properties characterization

Quasi-static tensile tests at high temperature were carried out in the laboratories of CEntro Nacional de Investigaciones Metalúrgicas - CENIM using a conventional electromechanic drive testing machine INSTRON 1362 equipped with an elliptical quartz lamp heating furnace. During the test forces were measured using an INSTRON Mod. 2518-103 load cell. Tensile tests were performed at different temperatures (20°C, 100°C, 200°C, 300°C, 400°C, 500°C, 600°C and 700°C) and strain rates (10^{-2} s^{-1} and 10^{-1} s^{-1}). The specimens were extracted at 0° respect to the rolling direction and using a wire electric discharge machining machine type Robofil 100. For each test, specimens were heated at the nominal temperature for 5 minutes in order to guarantee temperature homogenization and minimize any temperature gradient. A thermocouple positioned on the surface of the specimens was used to measure the initial temperature of the sample. After the tensile tests, the specimens were cooled down in the air. A special specimen geometry was used due to the tensile test machine characteristics. This specimen geometry was chosen to concentrate the stresses into the calibrated zone during the tensile test and avoid the strain propagation out of calibrated zones. This specimen geometry was optimized in a previous work [Per96], with a 4 mm width and 6 mm gage length. The geometry of the specimen is shown in Figure 3.11.

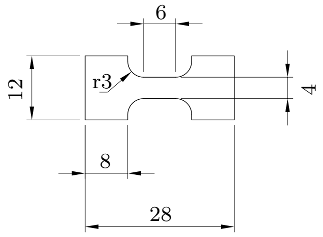

Figure 3.11: Geometry of the specimen employed in high temperature tensile tests [Per96].

Calculation of the work hardening coefficient (n)

The work hardening coefficient was calculated according to UNE 36-405-88 standard (Eq. 3.3). The coefficients were calculated between 0.05 strain and the strain corresponding to the ultimate tensile stress (σ_{uts}).

$$\sigma_{\mathrm{true}} = K\varepsilon_{\mathrm{true}}^{n} \tag{3.3}$$

where σ_{true} is the true stress, $\varepsilon_{\mathrm{true}}$ is the true strain, K the hardening coefficient and n is the strain hardening exponent.

Optical micrographs

Optical micrographs were obtained from the fracture zone of the deformed specimens in order to compare the deformation behavior of the material at different conditions. The sample preparation consists of embedding the sectioned specimens in resin, grinding them up to 4000 grit SiC paper and finally polishing with 1 μm diamond suspension.

After polishing, the specimens were chemically etched in order to be analyzed in an inverted optical microscope (Leica DM IRM) equipped with picture measurement software (Leica Qwin v3). The etchant used to reveal grain boundaries was Nital 5% for 3 s and the etchant used to identify different phases was Klemm's agent for 90 s [Dim06; Gir98; VV05]. Klemm's agent was composed by a mixture of 100 cm^3 stock solution (300 cm^3 H_2O + 1000 gr $Na_2S_2O_3 \cdot 5\ H_2O$) and 2 gr of reagent ($K_2S_2O_5$).

After etching with Klemm's agent, ferrite grains show mainly blue and bright-brown colors, retained austenite and untempered martensite are white, bainite and tempered martensite are brown and pearlite is black [Dim06; Gir98]. Using this etching procedure the different phases of the material and the microstructure change can be identified. However, it is difficult to make a distinction between the untempered martensite and retained austenite phases, because both phases are colored white.

X - ray diffraction measurements

In order to determine the presence of retained austenite in the different specimens, X-ray diffraction (XRD) measurements were also carried out. XRD method uses a known wavelength X-Ray to pass through the sample lattice and identify the crystal structure. As the austenite phase has a face-centered cubic (fcc) lattice structure and the martensite phase has a body-centered cubic (bcc) lattice structure, the XRD measurements gives a different pattern of peaks for each phase. Analyzing the intensity of each peak and comparing it with theoretical intensities, the percentage of each phase can also be determined [AST08]. Thus, XRD method allows the identification and the quantification of the amount of the retained austenite [AST08], whereas the bainite, ferrite and martensite can be distinguished by means of light optical microscopy and color etching [Pet07]. However, due to the small quantity of the austenite phase found in the material, in the present thesis the retained austenite content will only be considered qualitatively.

XRD measurements were performed in the laboratories of Azterlan Metallurgy Research Center, using a in a D8 ADVANCE Bruker diffractrometer equipped with a Kristalloex K760 generator, a vertical goniometer (Bragg-Brentano geometry), fixed gaps and an automated control. Bruker's DIFFRAC plus (r. 2000) software is used to control the diffractometer and ICDD's PDF2 data base to identify the different phases. The diffractograms were measured in the 40°-80° 2θ range. The measurements were carried out at 40kV and 30mA using a Cu tube with an associated wavelength 1.5418 Å ($\lambda_{\mathrm{Cu(k\alpha1)}}$=1.54060 Å and $\lambda_{\mathrm{Cu(k\alpha2)}}$=1.54439 Å).

3.4.2 Experimental results

Effect of the employed specimen geometry

As a consequence of employing not standardized specimen geometry, the mechanical response of high temperature specimen should be considered first and compared with the standard specimen at room temperature. The influence of the specimen geometry at quasi-static strain rate at room temperature is shown in Figure 3.12.

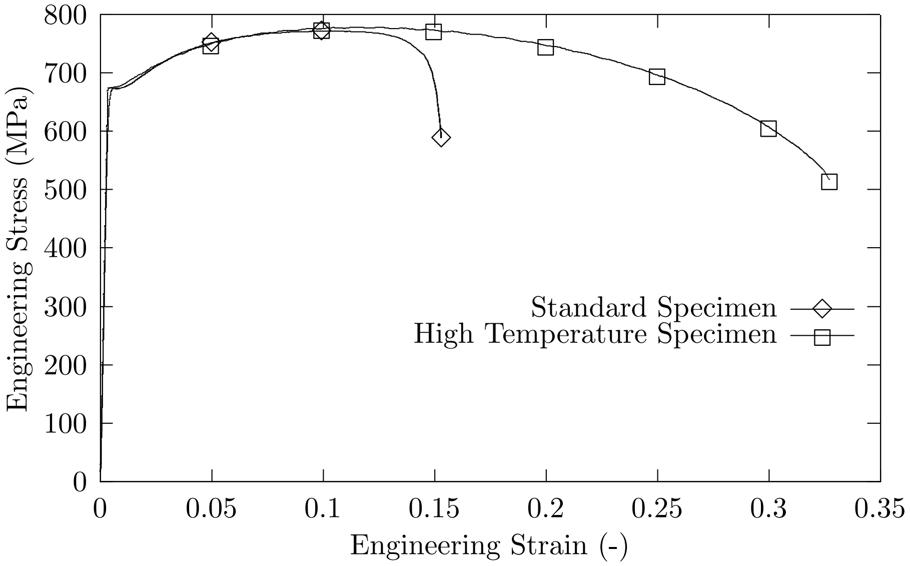

Figure 3.12: Engineering stress - engineering strain curves with different specimens.

Comparing the standard specimen with high temperature specimen, it can be observed that the flow stress is similar in both the cases until the σ_{uts} although as it was expected the maximum strain values (ε_{f}) differ. Therefore, in the current study, elongation values are compared only for the same specimen geometry. The comparison of the mechanical properties for both specimens are summarized in Table 3.1. It is noted that the variation of the Y_{s}, the σ_{uts} and work hardening (n) are insignificant, therefore, these values can be compared.

Table 3.1: Properties of CP800 depending of the specimen type.

Specimen	UNE	High Temperature
Y_{s} (MPa)	673.13	674.20
σ_{uts} (MPa)	853.08	882.18
ε_{f} (-)	0.14	0.33
n	0.107	0.119

Effect of the temperature

The effect of the temperature in CP800 high strength steel at 0.01 s^{-1} and 0.1 s^{-1} strain rate is analyzed. The true stress - effective plastic strain curves at different temperatures are shown in Figure 3.13 and Figure 3.14.

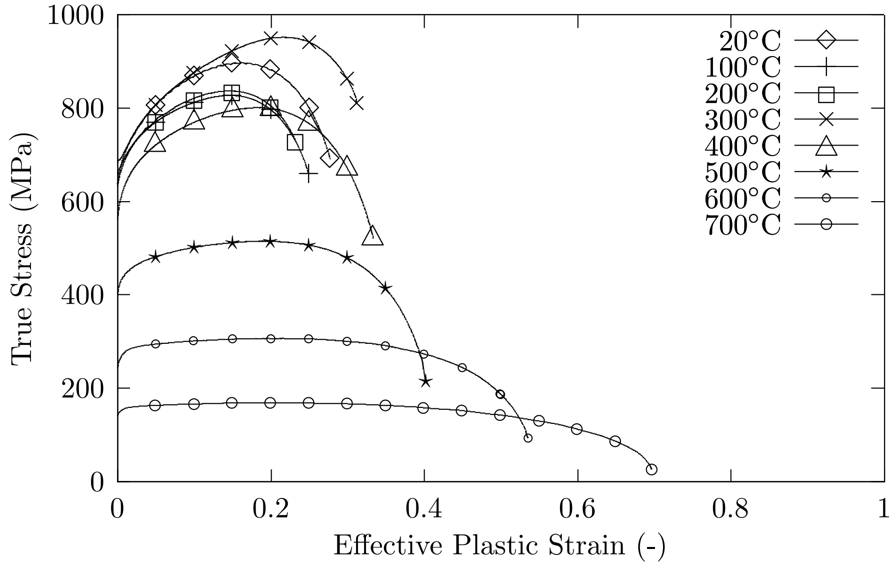

Figure 3.13: True stress - effective plastic strain curves at different temperatures and at 0.01 s^{-1}. The summary of the results can be seen in Table A.5 of appendix B.

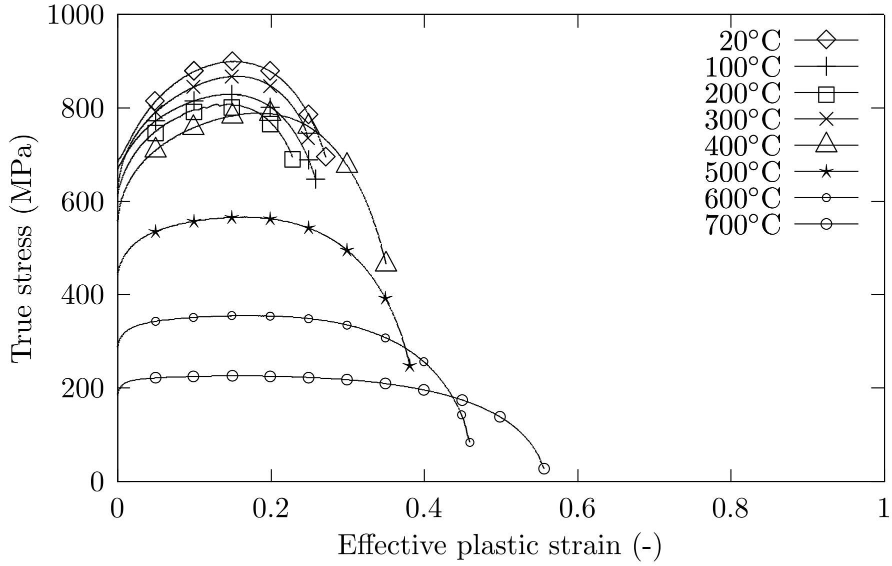

Figure 3.14: True stress - effective plastic strain curves at different temperatures and at 0.1 s^{-1}. The summary of the results can be seen in Table A.6 of appendix A.

Temperature dependent mechanical properties are shown in Figure 3.15.

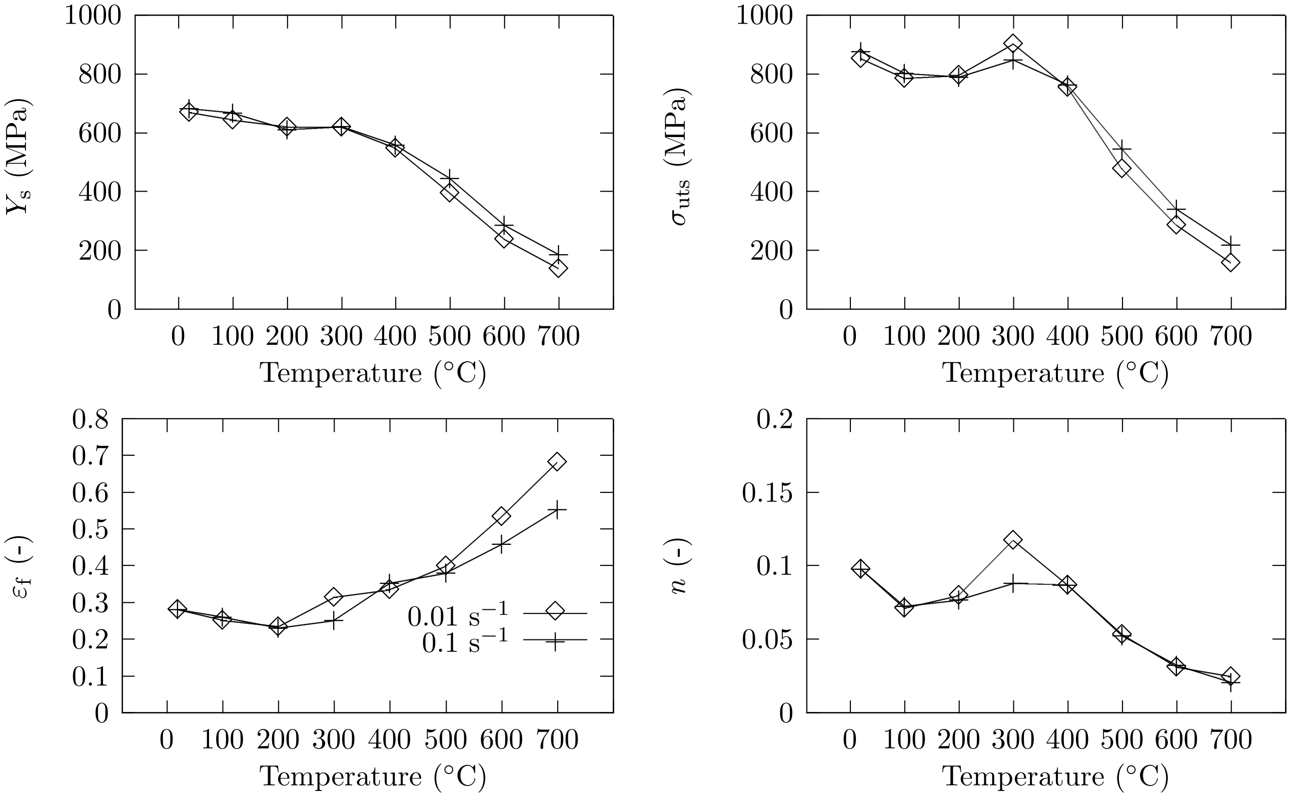

Figure 3.15: Mechanical properties of CP800 steel at different temperatures. The summary of the results can be seen in Table A.5 and Table A.6 of appendix A.

Comparing the flow curves at room temperature with the flow curves at 100°C and at 200°C, the Y_s, the σ_{uts}, the ε_{f} and n decrease slightly under both strain rates. At temperatures lower than 300°C the ductility of the CP800 decreases, showing a reduction of the ε_{f}.At 300°C the σ_{uts}, the n and the ε_{f} slightly increase while the Y_s decreases. A similar effect of increasing the flow stress of the CP800 at 300°C has already been reported by Geiger et al. [Gei04] and will be discussed later with the microstructure analysis, in section §3.4.3.

On the other hand, a clear softening behavior is outlined for temperatures higher than 400°C, decreasing the Y_s and σ_{uts} of the specimens and increasing the ε_{f}. At 700°C, the yield stress, the σ_{uts} and the n decrease considerably and the ε_{f} increases 139% compared with the specimen at room temperature.

Effect of the strain rate

The effect of increasing strain rate from 10^{-2} s^{-1} to 10^{-1} s^{-1} has little influence in the flow behavior of the CP800 material at temperatures below 400°C. Similar values of Y_s and σ_uts are obtained for both strain rates at this temperature range. However, at the higher temperatures (500°C, 600°C and 700°C) the difference in Y_s, σ_uts and ε_f increases, as expected. It is generally known that the effect of strain rate is accentuated, when the temperature is increased [Bla87].

Effect of the tensile test at high temperature in the microstructure

Optical micrographs of the fracture zone of specimens tested at different temperatures and at 10^{-2} s^{-1} strain rate are shown in Figure 3.16 and Figure 3.18. XRD results of the same specimens are shown in Figure 3.17.

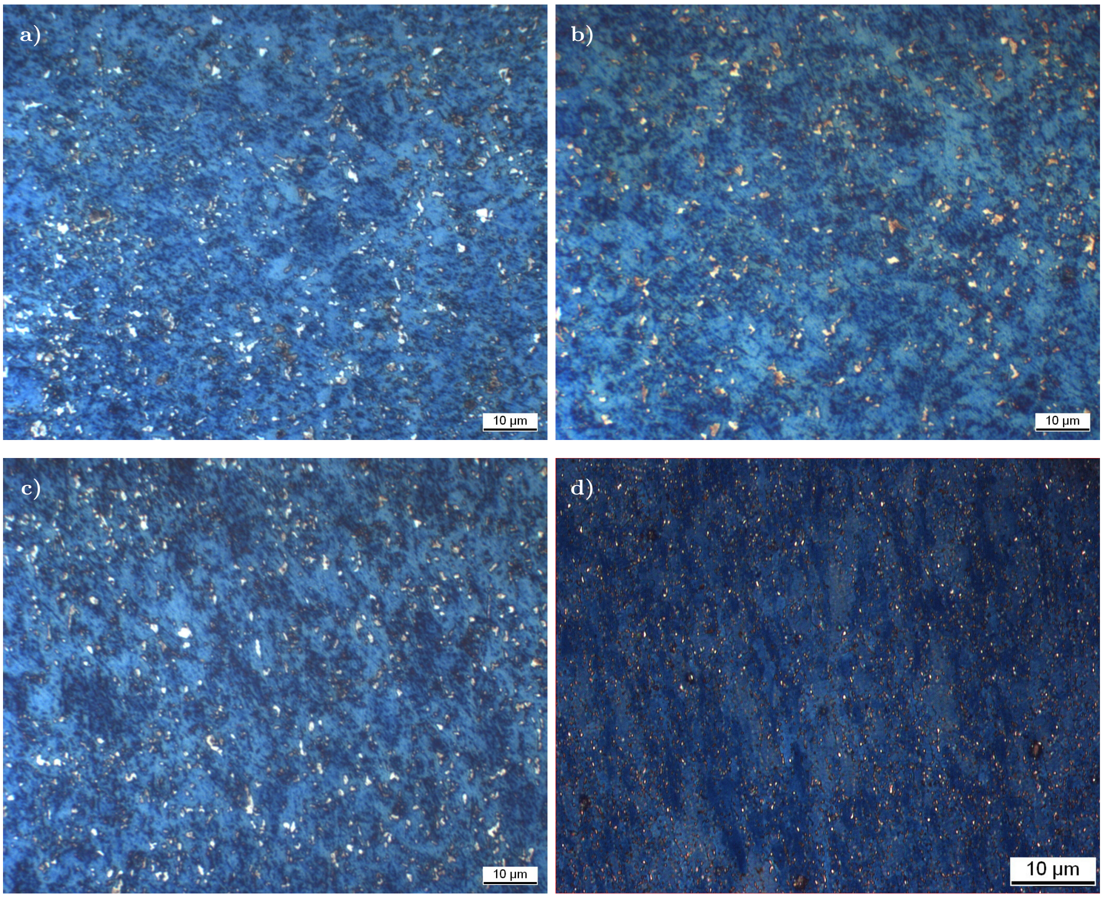

Figure 3.16: Microstructure of different specimens: a) As received material, b) room temperature, c) 300°C and d) 700°C, etched with Klemm's agent.

The microstructure of the as-received material (Figure 3.16 a) shows an extremely fine microstructure, with well dispersed bainite, martensite and retained austenite phases, within the ferritic matrix as previously reported by other authors [Gei04]. The XRD measurement of the as received material (Figure 3.17) clearly shows (110)α and (200)α peaks corresponding to ferrite, martensite and bainite phases. Moreover the (220)γ peak corresponding to metastable retained austenite is also observed (while (111)γ and (200)γ peaks are not observable). Thus, the initial material has a small amount of textured austenite.

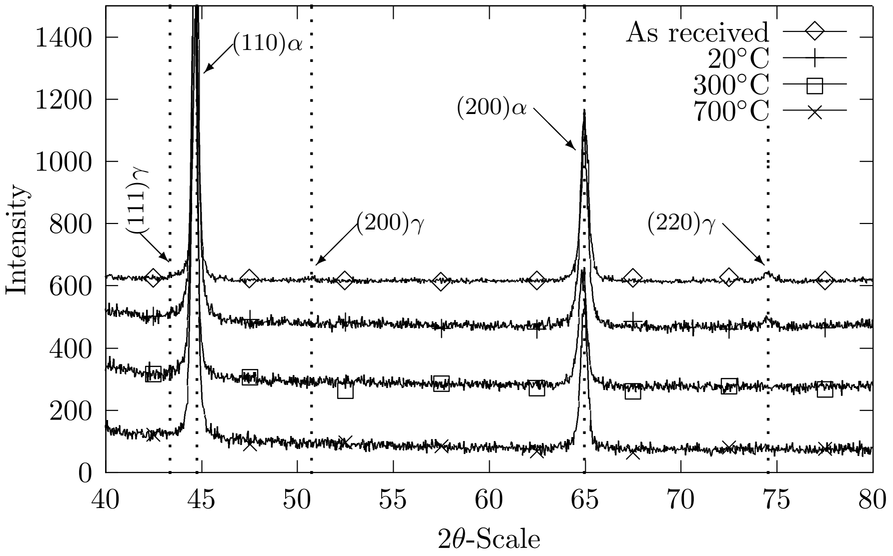

Figure 3.17: Diffractograms of specimens tested at different temperatures.

The micrograph of the specimen tested at quasi-static strain rates and room temperature (Figure 3.16 b) shows a similar microstructure as the initial material. XRD measurements also show a similar diffraction pattern as the initial material. The austenite phase ((220)γ peak) remains in the specimen tested at room temperature, suggesting that dislocation glide is the main deformation mechanism at room temperature.

The micrograph of the specimen deformed at 300°C (Figure 3.16 c) shows a similar microstructure as the initial material. However, XRD measurements do not show any austenitic peak, suggesting the martensitic transformation of the retained austenite. The micrograph of the specimen deformed at 700°C etched with Klemm's agent (Figure 3.16 d) clearly shows that the initial microstructure was transformed. The micrograph shows a well dispersed ultra fine martensite phases in the ferritic matrix suggesting the degradation of the residual austenite and martensite. The same sample etched only with Nital (Figure 3.18) (Nital etchant allows the cementite and ferrite phases to be easily identified) shows an increase of the ferrite-globular cementite phases. XRD results support that a complete transformation of the retained austenite is held in the material (Figure 3.17).

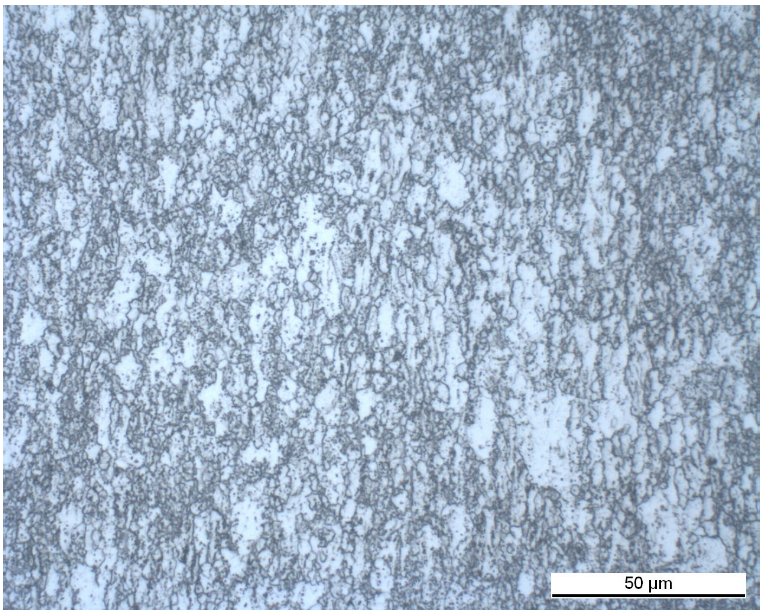

Figure 3.18: Microstructure of the specimen tested at 700°C etched with nital 5%.

3.4.3 Mechanical behavior and microstructure evolution relation

Comparing the microstructures of the as received material (Figure 3.16 a) and the microstructure of the specimen deformed at room temperature (Figure 3.16 b), similar microstructure can be noticed despite a stretching of the grains due to a mechanical loading. The XRD result shows a similar retained austenite fraction in both specimens. It can be concluded that the transformation of retained austenite to martensite due to the mechanical deformation (”TRIP effect”) is not very efficient in this steel at this testing condition and plastic deformation is mainly accommodated in the ferrite matrix [VS06].

The experimental results clearly show that the deformation behavior of the studied CP800 is dependent on the temperature. It is well known that generally the temperature affects steels by decreasing the flow stress and increasing the ductility of the material [Ber08], due to the microstructure changes and the activation of additional slip systems. However, the experimental mechanical tests show the increase of the flow stress and strain hardening at 300°C.

The increase of the flow stress when the temperature is increased has been attributed in some cases to the dynamic strain aging effect, for instance in HSLA-65 steels [NN05] and DP steels [Akb08]. Generally, dynamic strain aging takes place above certain temperature when the solute interstitial atoms such as C or N, activated by the effect of the temperature become mobile enough and can diffuse to the dislocations waiting for the thermal activation. Those diffused atoms fixed the dislocations and increase the strength of the material even increasing the temperature [NN05; Akb08; VDB82]. However, the dynamic strain aging effect is normally accompanied by inhomogeneous deformations, characterized by serrated flow behavior, called Portevin-Le Chatelier effect [NN05; Akb08; VDB82]. In this case, the tensile test results at 300°C do not show any significant serrated flow behavior, which may suggest that other mechanisms cause the increase in the flow stress.

The XRD result of the specimen tested at 300°C does not show $(220)\gamma$ peak related to the austenite phase, suggesting the transformation of the initial retained austenite into martensite. The macroscopic behavior (increase of the flow stress, the elongation at fracture and the strain hardening coefficient) combined with XRD results have previously been related to TRIP effect for materials with compositions different to the material considered in this study [Jac04]. However, it is also generally accepted that the transformation rate is decreased with temperature [VS06]. This suggests that during the heating of the specimen, for this particular composition, retained austenite can be destabilized to such a degree that it might partially transform to untempered martensite [Mei03]. Microstructure analysis supports this reasoning since the untempered martensite's appearance is similar to retained austenite in the micrographs (using Klemm's etchant both the untempered martensite and austenite are not affected by sodium metabisulfate and are left white while tempered martensite is tinted brown [Huh07; Huh02]) and XRD results do not show any austenite peak.

The CP800 shows an increase of ductility at 700°C, increasing the elongation at fracture and decreasing the flow stress. The increase of the ductility of the material is attributed to the decrease of the martensitic phase. The initial retained austenite and martensite degraded into ferrite and cementite phases (Figure 3.18) due to the temperature effect. These microstructural changes contributed to soften the material and increase the ductility [Mor07]. Moreover the thermal activation of additional sliding systems also plays an important role.

3.5 Conclusions

The analyzed steels show a wide range of strengths, MS1200 ($\sigma_{\text{uts}} \approx 1350$MPa) and DC01 ($\sigma_{\text{uts}} \approx 445$MPa). It is shown that the strain rate has little influence on the flow behavior of the different steels at quasi-static strain rates and at room temperature. On the other hand, only DP600 and DC01 materials are influenced by the rolling direction. Both steels show higher σ_{uts} and lower ε_{f} at 45°.

The mechanical characterization at quasi-static strain rates and elevated temperatures of the CP800 steel shows an increase of the tensile flow stress at 300°C with a similar ε_{f} as the specimen tested at room temperature. At 700°C the flow stress is decreased while the elongation at fracture increases by 139%.

The microstructure analysis of the deformed specimens, using optical microscopy and XRD measurements, shows the transformation of the initial microstructure depending on the testing condition. In the specimen tested at 700°C, the degradation of the initial microstructure into ferrite and globular cementite phases is observed, which favors the ductility of the material and decreases the flow stress.

In order to increase the formability of a commercial CP800 steel a minimum temperature of 400°C should be reached in the process. At 700°C the ductility is increased up to 0.7 strain. However, if this material is formed at elevated temperatures, the microstructure is also changed and this effect must be taken into account.

The formability of CP800 material can be increased by means of temperature assistance in processes where the deformation of the workpiece is localized, such as heat assisted bending or heat assisted roll forming [Gei04; MV09]. Thus, process limits can be increased by local heating, keeping the initial properties of the material unchanged in the rest of the workpiece.

Results from this chapter are also of interest for numerical simulations when material is deforming at different strain rate and temperature conditions. In Chapter 4 material data are used based on the results from the current chapter.

Chapter 4

Numerical modeling of roll forming processes

Viam sapientiae monstrabo

“ I will show you the way of wisdom ”

Synopsis

Conventional roll forming and flexible roll forming are complex 3D forming processes, in which the interaction between the rolls and the sheet, must be accurately analyzed. The finite element method is widely used during the design and optimization stages of the product, but additionally, the finite element method helps to understand the nature of the complex failure modes of the roll forming processes. For these reasons, it is essential to develop reliable numerical models.

In this chapter, the hypotheses and equations governing the conventional roll forming and the heat assisted flexible roll forming processes are described. The conventional roll forming process is modeled using a mechanical approach. The heat assisted flexible roll forming process must be modeled using a coupled thermo-mechanical analysis, where the interaction between the mechanical and thermal fields are considered. Additionally, the procedure to fit material data from the mechanical material characterization (Chapter 3) is also explained. Finally, results of the developed numerical models are also shown and the effect of the different parameters are analyzed.

A paper based on the work described in this chapter is published in the *International Journal of Material Forming* [Lar10c]

4.1 Introduction and numerical background of roll forming

The numerical modeling is a key factor in the development and optimization stage of the fabrication processes in order to save time and costs related with the traditionally used trial and error process set-up [Hae05; Wen05].

In the present chapter, the numerical models of conventional and heat assisted flexible roll forming process developed during the dissertation are explained. The chapter begins with the literature review of the most important numerical works performed and analyzing the different simulation parameters in roll forming modeling.

In the second part of the current chapter, a brief explanation of the equations and hypotheses involved in the construction of the numerical model of roll forming process are explained. Results from these models are showed and the effect of the material strength on different roll forming parameters are analyzed.

In the third part of this chapter, equations and hypotheses governing the thermo-mechanical approach of heat assisted flexible roll forming process are explained. Results from the numerical models of heat assisted flexible roll forming process are shown and the effect of the temperature and the heating strategy on the flexible profile geometry are analyzed. Finally, the most important conclusions are summarized.

4.1.1 Background in numerical modeling of roll forming process

Historically, the firsts analytical modeling approaches to roll forming process were developed in order to predict different critical parameters of the process. Semi automatic procedures to determine the number of roll forming passes were proposed by different authors in [Pan92; Hal05; Lin09a].

Bhatacharyya et al. [Bha84b] investigated the influence of the bend angle and of the bend angle increment, on the longitudinal strain. The same author developed [Bha84c; Bha84a] an analytical model to predict the deformation length. On the other hand, Bhattacharyya et al. [Bha87] developed a semi-empirical model for the prediction of the roll load in the cold roll forming process for a U channel, equating the external work to internal dissipation of energy.

Chiang [Chi84] developed an analytical model to predict the longitudinal membrane strain and investigate the effect of the flange length, web width and the bend angle on the web strain and on the longitudinal strain. Zhu [Zhu93] investigated the influence of the flange length, material thickness, bend angle and bend angle increment on the longitudinal strain distribution. The same author studied also the influence of the geometry of the female tool on the bend angle of a U channel and obtained an implicit bend angle curve model.

Panton et al. [Pan92; Pan94] described the fundamental deformation types of roll forming process and developed analytical models to describe the longitudinal stretching, longitudinal bending, shear and transverse bending. The analytical models were developed minimizing the plastic work described by geometrical relations. A strip element of the analytical model developed by Panton is shown in Figure 4.1 [Pan94].

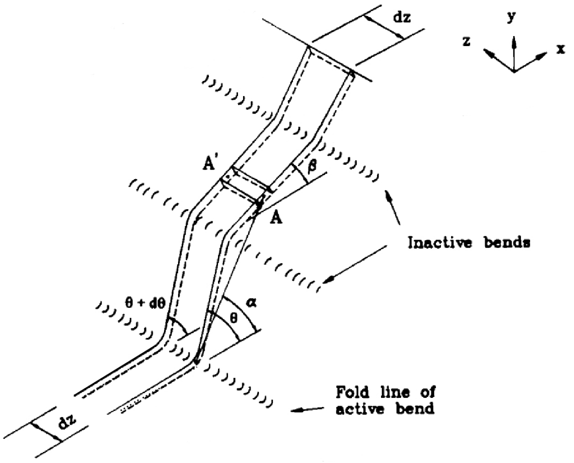

Figure 4.1: Modelization of an element strip isolated from a roll forming pass with a single active bend [Pan94].

More recently, Lindgren [Lin07c] developed analytical models in order to predict the deformation length and the longitudinal peak strain during the roll forming process. For this purpose, a two-level factorial design was done using finite element analysis in order to identify the most significant parameter affecting the deformation length and the longitudinal peak strain. The model was developed based on the results of the factorial design. The same authors [Lin08] developed empiric models for the prediction of the roll load and the roll torque when a U channel profile was roll formed. The models took into account the thickness of the material, the bending angle and the yield strength of the material.

The analytical models can be very useful to predict different parameters of the roll forming process or in order to help in the design process of the roll formed parts.

However analytical models are very limited in complicated geometries, when the forming process must be optimized or when the nature of the complex failure modes must be understood. For these reasons other authors modeled the roll forming process using the finite difference method.

The first numerical models of roll forming process appeared based on the finite difference method in the early 80's. The finite difference method uses an approximative shape function to describe the shape of the profile between two roll forming stands. Kiuchi et al. [Kiu84] used a sinusoidal shape function to describe the shape of the sheet. However, these shape functions are only pure geometric descriptions of the 3D shape of the deformed strip, which do not take into account the stresses. In order to calculate the stresses and strains of the sheet metal the steady-state situation is assumed between the roll forming stands. The strip is first discretized in different elements and then the deformation of the strip is calculated by geometric relationships derived from the shape function. Similar methods of describing the shape of the sheet between two subsequent stations using shape functions were successfully developed by different authors [Ona87; Pan94; Dug95; Dug96; Han01a; Han01b; Han05; Zw02; Taj02]. A discretization of the sheet metal used in the finite difference method is shown in Figure 4.2.

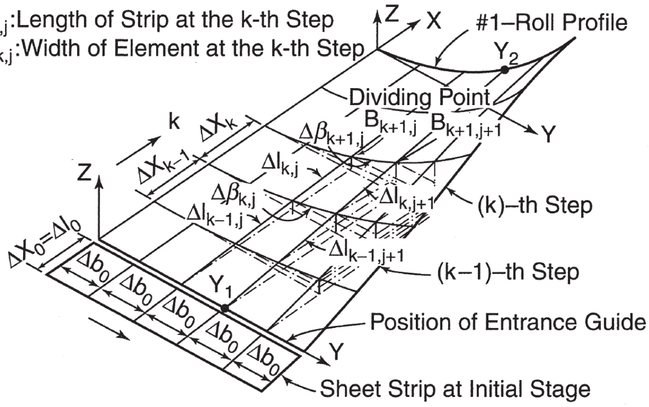
$\Delta l_{k,j}$:Length of Strip at the k-th Step
$\Delta\beta_{k,j}$:Width of Element at the k-th Step
Z
X
#1–Roll Profile
Y_2
Dividing Point
k
ΔX_k
ΔX_{k-1}
$\Delta\beta_{k+1,j}$
$B_{k+1,j}$
$B_{k+1,j+1}$
Y
Z
$\Delta l_{k,j}$
$\Delta\beta_{k,j}$
$\Delta l_{k-1,j}$
$\Delta l_{k,j+1}$
(k)–th Step
$\Delta X_0=\Delta l_0$
$\Delta l_{k-1,j+1}$
(k–1)–th Step
Δb_0
Δb_0
Δb_0
Δb_0
Δb_0
Y_1
Position of Entrance Guide
Y
Sheet Strip at Initial Stage

Figure 4.2: Discretization of the sheet metal in elements [Hal05].

Finally, integrating the geometric relations, strains and stresses in the sheet are obtained. In order to achieve accurate results, a iterative calculation of the strains and stresses must be done. The finite difference method is explained in more detail in [Hal05].

4.1.2 Literature review of finite element models of roll forming process

The roll forming process has been modeled using the finite element method by many authors. However, the objective and the hypotheses taken by the authors to develop the numerical models are different in each case. The aim of this section is to review and analyze the different simulation parameters used by the different authors, in order to select the most suitable parameters to develop a reliable numerical model of roll forming process.

Body discretization

Forming rolls

In all the analysed works the forming rolls were modeled as rigid bodies, since the objective of the numerical models was to describe the forming behavior of the sheet, rather than the calculation of contact stress or roll deformations.

Sheet metal

Shell and solid elements have been used to model the sheet metal in the roll forming process. Shell element is the most extended element type to model the sheet metal in forming processes. In these processes the thickness of the sheet is very small compared with the other two dimensions and the formulation of these types of elements correctly reproduced the behavior of the metal sheet when is formed [Reb92a; Reb92b; She04; Jl05; Teh06; Lin05; Lin07a; Geh07; Sag08; Lun08; Lin08; Zen09; Lun09; Par09b; Dut09]. However, other authors and software developers who modeled the roll forming process used solid elements to model the sheet metal [Hei96; Hon01; Als04; Gul07; Bui08; Jeo08; Par09a; Rou09; Dat10].

Hellorg [Hel07] compared roll forming experimental results with numerical results carried out by reduced integration shell elements (S4R) and reduced integration solid elements (C3D8R) using Abaqus-explicit 6.5. According to Hellborg shell elements better described the deformations and the final geometry than solid elements. However, the forces were better described by solid elements.

Adaptative meshing

Alsamhan et al. [Als04] analyzed the effectiveness of the adaptative meshing on the modeling of roll forming process in order to decrease the computational cost. A remeshing technique was developed to finely remesh those zones where the deformation was maximal. Using the remeshing technique the computational time was reduced considerably.

Material property modeling

Most of the work analysed used the elastic-plastic material model, with isotropic work hardening and an associated work hardening rule. Only few works considered the anisotropy of the material. Other authors, implemented successfully damage criterias in the roll forming process [Lun09].

Boundary conditions

The kinematic of the model

Two different kinematic models were identified during the literature review depending on the considered hypotheses. In order to simplify the numerical models some authors avoided the rolling movement of the rolls. Thus, the sheet was modeled as static and the forming rolls advanced without rolling [Reb92a; Reb92b; Hei96; Hon01; Als04; She04; Jl05; Bui08; Lun08; Par09a; Zen09].

On the other hand, other authors considered the rotational movement of rolls. These authors modeled the roll forming process with rotatory rolls where the sheet metal was pushed through the rolls by the action of the frictional forces [Lin05; Lin07a; Lin08].

Contact conditions, friction

Depending on the objective of the model, some authors neglected the friction between the sheet and the rolls [Reb92a; Reb92b; Hei96; Hon01]. However, other authors considered the friction between the roll and the sheet metal. The Coulomb friction law was used in all work that friction was modeled. A wide range of friction coefficients were used: $\mu = 0.01$ [She06], $\mu = 0.085$ [Lin08], $\mu = 0.1$ [Lin05; Lin07a; Jeo08; Par09a; Lun09] and $\mu = 0.2$ [Teh06; Gul07; Bui08; Rou09; Zen09].

Forming load and torques

In most of the cases, the models were focused in the prediction of the longitudinal strain and the final shape of the profile. Due to the complexity of the friction behavior in roll forming process, only few authors investigated the forming forces and torques using the finite element method. For instance only Lindgren [Lin07b] validated a finite element model for the roll forming of a U channel taking into account the roll loads and torques. The author conducted experimental tests measuring the roll load and torque, the longitudinal and transversal strain and the springback of the profile. The numerical and experimental results were similar except for the springback prediction.

Finite element formulation

Both, the explicit dynamic method [Hei96; Jl05; Teh06; Hel07; Lun08; Jeo08; Lun09] and the static implicit method [Hon01; Als04; Lin05; Teh06; Lin07a; Geh07; Gul07; Lin08; Par09b; Rou09; Dut09] were used to model the roll forming process depending on the used commercial code and the objective of the simulation.

It was not identified any significant advantage using the implicit or explicit method. However, Rebelo et al. [Reb90; Reb92a; Reb92b] compared the effectiveness of the explicit and implicit method to model the roll forming process using Abaqus code. The authors concluded that both approaches were suitable for the modelization of roll forming process.

Finite element commercial codes

Although some authors developed specific finite element codes to model the roll forming process (EPFEP3 developed by [Als04] and Shape RF used by [She06; Jeo08]) most of the works were developed using generalist commercial codes like Abaqus [Reb92a; Reb92b; Teh06; Geh07; Lun08; Zen09; Lun09], MSC.Marc [Hon01; Lin05; Lin07a; Gul07; Lin08; Zen09; Rou09], Ls - Dyna [She04; Jl05; Sag08; Par09a; Par09b; Dut09] or Pam - Stamp [Hei96].

4.2 Conventional roll forming numerical modeling

The main objective of the current section is to develop a reliable numerical model, that can be used not only to predict the failure modes and optimize the roll forming process, but also to predict the forming load and torques. In order to validate the numerical model, four different steels mechanically characterized in Chapter 3 are used, and the effects of the material strength on different roll forming parameters are analyzed. The developed numerical models are compared with experimental results and validated.

In this first approach, in order to simulate the conventional roll forming process, a commercially available finite element software, MSC.Marc - MSC.Mentat was employed. In this section, the hypotheses and equations used in order to develop the numerical model of roll forming process are explained.

4.2.1 Mechanical analysis

A quasi-static mechanical approach was selected to model the roll forming process neglecting inertial terms. In the quasi-static regime, the first law of Newton states that the balance of the force and momentum applied to a solid body must be zero. Therefore, the force-displacement relation of a solid body, can be described by equating the external forces ($\mathbf{F}_{\text{ext}}$), which the body is subjected to, and internal forces (associated with internal strains and stresses):

$$\sum \mathbf{F}_{ext} = \mathbf{K}(\mathbf{F}_{\text{ext}}, \mathbf{u})\mathbf{u} \tag{4.1}$$

where $\mathbf{K}$ is the so called rigidity matrix, defined as the relation between the strains and stresses of the body, and $\mathbf{u}$ is the displacement vector. In the current analysis the nonlinearities from material behavior and from contact procedures were considered in the rigidity matrix $\mathbf{K}$, which was considered to be displacement ($\mathbf{u}$) and external force ($\mathbf{F}_{\text{ext}}$) dependent. The internal forces were determined using experimentally obtained stress-strain relations of the material (results of Chapter 3). The external forces were derived from the boundary conditions applied by the forming rolls. A variational form of Eq. 4.1 is written using the principle of virtual work:

$$\int_{V_0} S_{i,j} \delta E_{i,j} dV = \int_{V_0} b_i^0 \delta \eta_i dV + \int_{A_0} t_i^0 \delta \eta_i dA \tag{4.2}$$

where V_0 is the volume of the solid, $S_{i,j}$ is the second Piola-Kirchhoff stress tensor, $E_{i,j}$ is the Green-Lagrange strain tensor, b_i^0 is the body force tensor and t_i^0 is the traction vector and η_i are the virtual displacements. In the current model the mechanical problem was solved in an implicit mode employing the Updated Lagrangian procedure. The Updated Lagrangian procedure is used in problems with large displacements or deformations and it uses the current configuration as the reference state and is redefined in each iteration. The principle of virtual work can be expressed at increment $n+1$ as:

$$\int_{V_{n+1}} \nabla\eta_{ik}\sigma_{ik}\nabla\Delta u_{i,j}dV = \int_{V_{n+1}} \dot{b}_i\delta\eta_i dV + \int_{A_{n+1}} \dot{t}_i\delta\eta_i dA \tag{4.3}$$

where $\Delta u_{i,j}$ and η_{ik} are the actual incremental and virtual displacements respectively, σ_{ik} is the Cauchy stress tensor, and b_i and t_i are the body force and surface traction respectively in the current configuration. This equation was projected against the shape functions for the finite element discretization and solved using a Full Newton-Raphson Algorithm. This time integration scheme is widely employed and thus it is not explained in the present thesis. Reader is referred to [MSCa] for more details on the mechanical model.

Body discretization

Roll modeling

The rolls were defined as rigid bodies and were composed by different 3D surfaces. The surfaces were described by analytical non-uniform rational B-splines (NURBS) which provide a precise mathematical form capable of representing the common analytical shapes [MSCa].

The geometry of the model was the same as the geometry of experimental trials and is explained in section §5.2 of Chapter 5. The gap between the rolls were 1.5 mm for MS1200, DP600 and DC01 materials and 1.2 mm for CP800 material. The numerical model of roll forming process and a detail of the sheet mesh can be seen in Figure 4.3.

Sheet modeling

The sheet metal was modeled using a full-integration eight node solid element type 7 of MSC.Marc. Element type 7 uses trilinear interpolation functions and the strain tends to be constant throughout the element. This results in a poor representation of bending behavior. The bending behavior was improved using an alternative interpolation function so called assumed strain. Using this element type with this interpolation function, the bending behavior and forming forces can be accurately represented [MSCc; Hel07].

Due to the symmetry of the profile only a half of the sheet metal were modeled. The bending areas of the sheet metal, where the strain concentration was large, were discretized with a smaller elements than the rest of the sheet metal. On the other hand, due to one of the objectives of the current simulation was to model the forming forces and torques, the fine mesh zone was necessary in order to define correctly the interaction between the sheet and the rolls.

However, in order to avoid a large number of elements in the model, two different mesh sizes were used to mesh the initial flat sheet. The central portion of the sheet was meshed with a very fine mesh and the rest of the sheet with a coarse mesh. The fine meshed part had 4 elements in the thickness and the coarse part had 1 element. A detailed fine mesh can be seen in Figure 4.3.

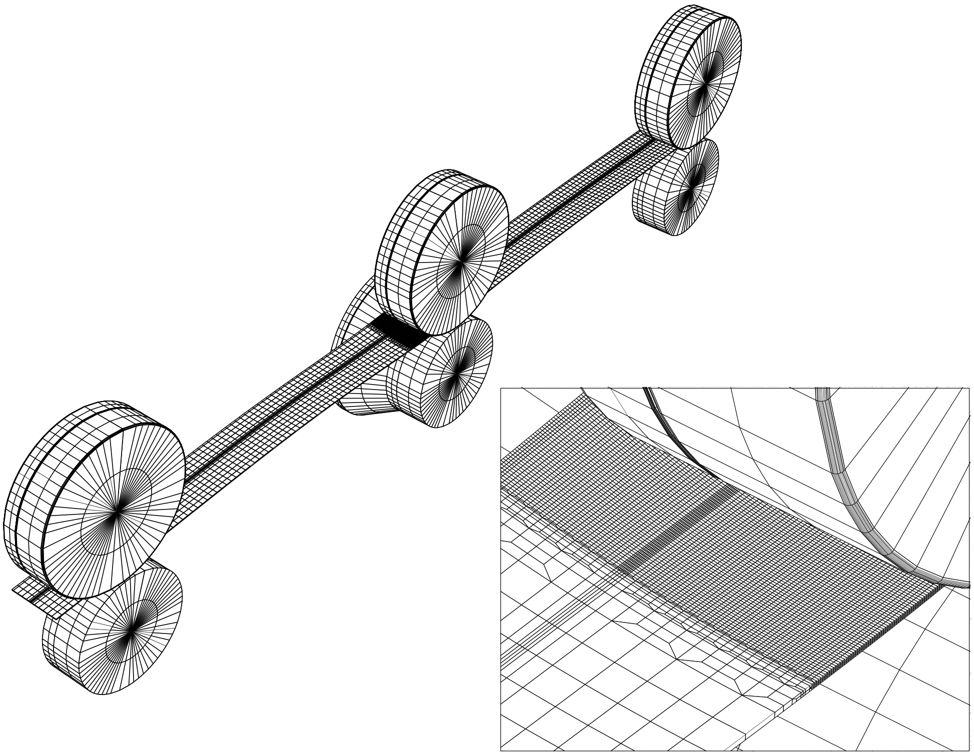

Figure 4.3: Body definition in roll forming numerical models. Rolls were defined as undeformable rigid bodies and the sheet metal was defined by solid elements. Fine mesh was used in bending zones and where the load forces and torques were calculated.

Material property modeling

An elastic-plastic material model was used in the current model where the elastic and plastic behaviors were modeled separately.

Elastic behavior modeling

The elastic behavior of the material was considered isotropic and was defined with the Young's modulus of the material ($E = 210\text{GPa}$), the Poisson's ratio ($\nu = 0.33$) and the shear modulus G. The shear modulus was obtained as:

$$G = \frac{E}{2(1+\nu)} \tag{4.4}$$

The anisotropical behavior of the material was only taken into account in the yield criteria of the material.

Yield function, Hill's criteria

The general expression of the Hill's anisotropic yield function and stress potential are assumed as:

$$\bar{Y_\sigma} = \sqrt{\frac{\left(a_1(Y_{\sigma_\mathrm{y}} - Y_{\sigma_\mathrm{z}})^2 + a_2(Y_{\sigma_\mathrm{z}} - Y_{\sigma_\mathrm{y}})^2 + a_3(Y_{\sigma_\mathrm{x}} - Y_{\sigma_\mathrm{y}})^2 + 3a_4Y_{\tau_\mathrm{zx}}^2 + 3a_5Y_{\tau_\mathrm{yz}}^2 + 3a_6Y_{\tau_\mathrm{xy}}^2\right)}{2}} \tag{4.5}$$

Where $\bar{\sigma}$ is the equivalent tensile yield stress, Y_{σ_x}, Y_{σ_y} and Y_{σ_z} are the yield stress with respect to the axes of anisotropy, Y_{τ_xy}, Y_{τ_yz} and Y_{τ_xz} are the yield stresses in shear with respect to the axes of anisotropy and a_1, a_2, a_3, a_4, a_5 and a_6 are constants that have to be determined experimentally.

Hills [Hil48] yield criterion has been extensively used in sheet metal forming, especially for steel. For this purpose, the material was considered orthotropic with: rolling direction (0°), the direction transverse to the rolling direction in the plane of the plate (90°) and the direction perpendicular to the plate (thickness direction). The axes of anisotropy are shown for the specimen at 0° rolling direction in Figure 4.4.

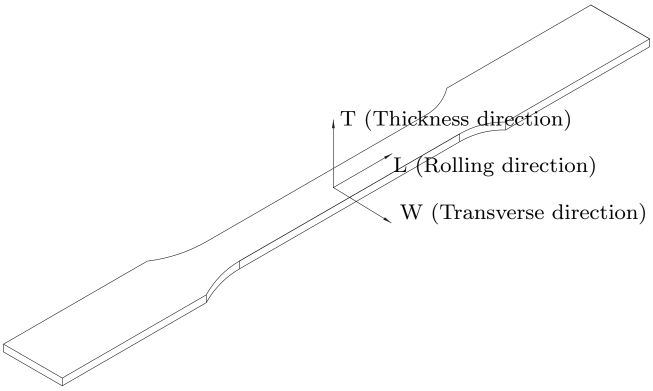

Figure 4.4: Axes of anisotropy for the specimen at 0° rolling direction.

Hill's anisotropy parameters can be calculated from the mechanical characterization of materials. Y_{σ_0}, $Y_{\sigma_{45}}$ and $Y_{\sigma_{90}}$ yield stresses and r_0, r_{45} and r_{90} anisotropy r-values were calculated respectively at 0°, 45°and 90° using results of Chapter 3. The yield stress in the third (thickness) direction is evaluated as:

$$Y_{\sigma_\mathrm{T}} = Y_{\sigma_0}\sqrt{\frac{r_{90}(1+r_0)}{r_0+r_{90}}} = Y_{\sigma_{90}}\sqrt{\frac{r_0(1+r_{90})}{r_0+r_{90}}} \tag{4.6}$$

And the direct stress coefficients are calculated as:

$$a_1 = \left(\frac{Y_{\sigma_\mathrm{av}}}{Y_{\sigma_{90}}}\right)^2 + \left(\frac{Y_{\sigma_\mathrm{av}}}{Y_{\sigma_0}}\right)^2 - \left(\frac{Y_{\sigma_\mathrm{av}}}{Y_{\sigma_\mathrm{T}}}\right)^2 \tag{4.7}$$

$$a_2 = \left(\frac{Y_{\sigma_\mathrm{av}}}{Y_{\sigma_\mathrm{T}}}\right)^2 + \left(\frac{Y_{\sigma_\mathrm{av}}}{Y_{\sigma_0}}\right)^2 - \left(\frac{Y_{\sigma_\mathrm{av}}}{Y_{\sigma_{90}}}\right)^2 \tag{4.8}$$

$$a_3 = \left(\frac{Y_{\sigma_\mathrm{av}}}{Y_{\sigma_0}}\right)^2 + \left(\frac{Y_{\sigma_\mathrm{av}}}{Y_{\sigma_{90}}}\right)^2 - \left(\frac{Y_{\sigma_\mathrm{av}}}{Y_{\sigma_\mathrm{T}}}\right)^2 \tag{4.9}$$

where Y_{σ_av} is the yield stress of the used associated flow stress curve. On the other hand, values for a_4, a_5 and a_6 are evaluated for the orthotropic case as :

$$a_4 = a_5 = 2 \tag{4.10}$$

$$a_6 = \frac{2}{\left(\frac{Y_{\sigma_\mathrm{T}}}{Y_{\sigma_\mathrm{av}}}\right)^2\left(\frac{3}{2r_{45}+1}\right)} \tag{4.11}$$

Hill's yield criteria parameters calculated from the mechanical characterization are summarized in Table 4.1.

Table 4.1: Values used for Hill's yield criteria.

Material	r_0	ς_{r0}	r_{45}	ς_{r45}	r_{90}	ς_{r90}	$Y_{\sigma 45}/Y_{\sigma 0}$	$Y_{\sigma 90}/Y_{\sigma 0}$
MS1200	0.366	0.077	0.446	0.076	0.249	0.130	0.96	0.98
CP800	0.592	0.01	0.747	0.012	0.667	0.005	0.98	1.00
DP600	0.864	0.030	0.735	0.019	0.654	0.027	1.00	0.95
DC01	1.22	0.017	0.76	0.017	1.40	0.017	1.20	1.15

Plastic behavior modeling

The plastic behavior of the material is modeled using an associated flow curve. The associated flow curve or effective plastic strain, is calculated subtracting the elastic portion from the experimental true strain, via:

$$\varepsilon_{\text{eps}} = \varepsilon_{\text{true}} - \frac{\sigma_{\text{true}}}{E} \tag{4.12}$$

where ε_{eps} is the effective plastic strain, $\varepsilon_{\text{true}}$ is the true strain and σ_{true} is the true stress of the material. As an example, the true stress - true strain curves and the subtracted true stress - effective plastic strain curves of the DC01 material are showed in Figure 4.5 a.

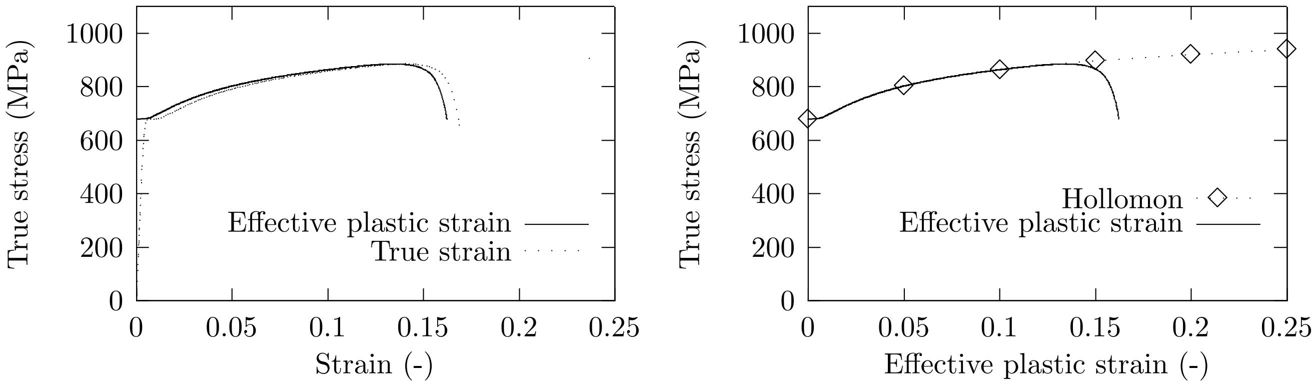

a)

b)

Figure 4.5: (a) Comparison of true stress-strain curve and true stress - effective plastic strain curve and (b) comparison of effective plastic strain curve and the Hollomon's material laws.

In order to model the stress-strain behavior of materials, results from material characterization (Chapter 3) were used, and only some representative curves of the material behavior were selected. At room temperature only the curves at $\dot{\varepsilon} = 10^{-3}$ s^{-1} strain rate and at 0° were considered.

However, using this procedure only the stress-strain behavior of materials can be modeled in the uniform deformation range. The post uniform behavior of the material is defined as the stress - strain relation behavior of the material after the onset of necking on the tensile sample. The post uniform behavior of the material was modeled using the Hollomon's material law.

Post uniform material behavior, Hollomon's material model

Hollomon's material model represent the stress - strain relation of the materials using an exponential relation:

$$\sigma_{\mathrm{Hol}} = K_{\mathrm{Hol}}(\varepsilon_{\mathrm{eps}})^{n_{\mathrm{Hol}}} \tag{4.13}$$

Where σ_{Hol} is the stress of Hollomon's law, $\varepsilon_{\mathrm{eps}}$ is the effective plastic strain, K_{Hol} is the hardening coefficient and n_{Hol} is the hardening exponent. The coefficients K_{Hol} and n_{Hol} were calculated between $\varepsilon_{\mathrm{eps}} = 0.05$ strain and the strain corresponding to the ultimate tensile stress ($\varepsilon_{\mathrm{uts}}$) and minimizing the error between the experimental data and material model Eq. 4.14. The true stress - effective plastic strain curves and Hollomo's material modelization of DC01 material are shown in Figure 4.5 b.

$$\sum_{\varepsilon=0.05}^{\varepsilon=\varepsilon_{\mathrm{uts}}} \sigma_{\mathrm{error}} = \sum_{\varepsilon=0.05}^{\varepsilon=\varepsilon_{\mathrm{uts}}} (\sigma_{\mathrm{eps}} - \sigma_{\mathrm{Hol}}) \tag{4.14}$$

Where σ_{error} is the accumulated error between the experimental stress (σ_{eps}) and the stress from Hollomon's law (σ_{Hol}). Following this procedure, material models for MS1200, CP800, DP600 and DC01 steels were calculated. Table 4.2 summarizes the Hollomon's coefficient for the different materials and Figure 4.6 shows the comparation between the experimental and Hollomon's material laws for each material.

Table 4.2: Values used for Hollomon's material model

	MS1200	CP800	DP600	DC01
K_{Hol} (MPa)	1398.7	1062.7	886.01	569.1
n_{Hol} (-)	0.017	0.089	0.108	0.186

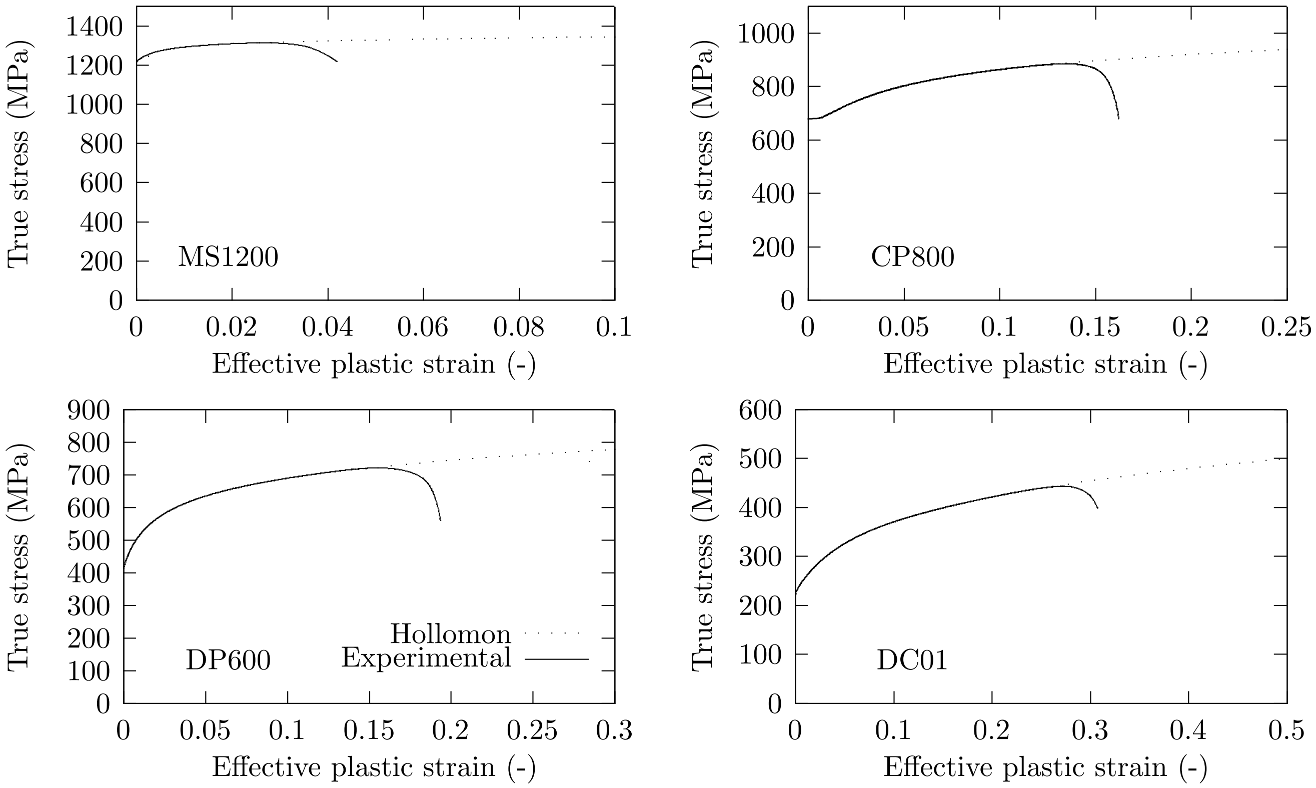

Figure 4.6: Comparison between experimental results and Hollomon's laws.

Boundary conditions

Contact conditions

The mechanical contact employed in the numerical models was based on the so-called direct constraint procedure in combination with the iterative penetration checking [MSCa]. In every time increment Δt the distance between the nodes and the surfaces were calculated and compared with a tolerance in order to detect if contact occurred. If any contact was detected, direct constraints were placed on the nodes in contact using boundary conditions. Both kinematic constraints on transformed degrees of freedom and nodal forces were applied on the nodes in contact. More detailed information about contact procedures is available in [MSCa].

Friction modeling

The friction between the rolls and the sheet was also implemented in the numerical model of roll forming process. Friction modelization was based on the Coulomb formulation, where the stick regime (no relative displacement between the bodies) and the slip conditions (relative displacement between the bodies) were proportional to the normal force. In stick conditions the frictional force is defined as:

$$F_{\mathrm{t}} < \mu \cdot F_{\mathrm{n}} \tag{4.15}$$

where F_{t} is the friction force, F_{n} is the normal force and μ is the friction coefficient. On the other hand, in sliding conditions the frictional force is defined as:

$$F_{\mathrm{t}} = \mu \cdot F_{\mathrm{n}} \tag{4.16}$$

Coulomb frictional model is graphically represented in Figure 4.7 a. For a given normal force, the friction stress has a step function behavior based upon the value of the tangential relative sliding displacement Δu_t. Since this numerical discontinuity in the friction value may cause numerical difficulties different approximations of the step function are used. The friction procedure used in the model is the so called Coulomb bilinear model (Figure 4.7 b [MSCa]).

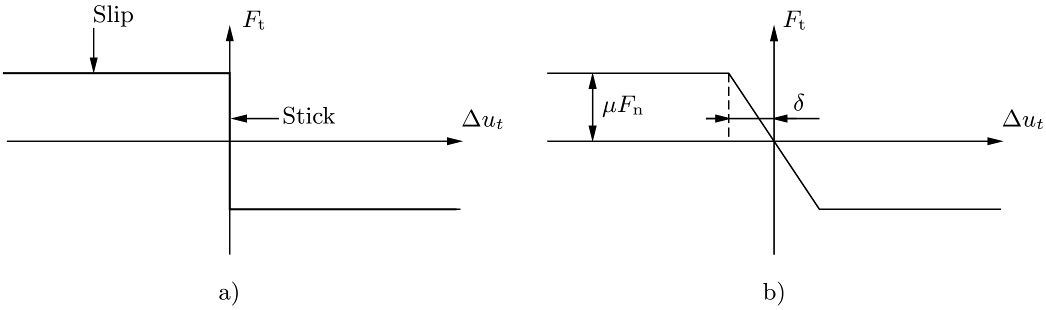

Figure 4.7: (a) Coulomb model of friction and (b) Coulomb bilinear model of friction aproach [MSCa].

The bilinear model assumes that the stick and slip conditions correspond to reversible and permanent relative displacement. For that, a reversible displacement threshold δ is defined below in which sticking is simulated and the friction forces are defined as:

$$F_{\mathrm{t}} = \frac{\mu F_{\mathrm{n}}}{\delta} u \tag{4.17}$$

The value of δ was determined to be 0.0025 times the average edge length of the finite elements defining the deformable contact bodies. In the slip regime the Coulomb friction was defined by the Eq. 4.16.

Different values of μ were used by different authors as it is shown in the literature review section. Values of μ = 0.01 [She06], μ = 0.085 [Lin08], μ = 0.1 [Lin05; Lin07a; Jeo08; Par09a; Lun09] and μ = 0.2 were used depending on the different lubrication conditions. However, a methodology to determine a reliable friction coefficient for modeling the complex frictional behavior between the sheet-roll system is needed. In the current case, a intermediate friction coefficient of μ= 0.15 was selected to perform the simulations.

4.2.2 Results of the conventional roll forming numerical model

In order to validate the numerical model of roll forming process, different parameters of roll forming process are calculated and calculated with experimental results.

Profile geometry

The longitudinal section (section A-A'), longitudinal bow (Δh_{Bow}) and the final angle β are measured from the numerical results (Figure 4.8). The longitudinal bow error Δh_{Bow} is defined as the longitudinally round shape taken by the profile after the forming process. In the current study, transversal cross sections are calculated in the center of the finely meshed zone (Figure 4.8).

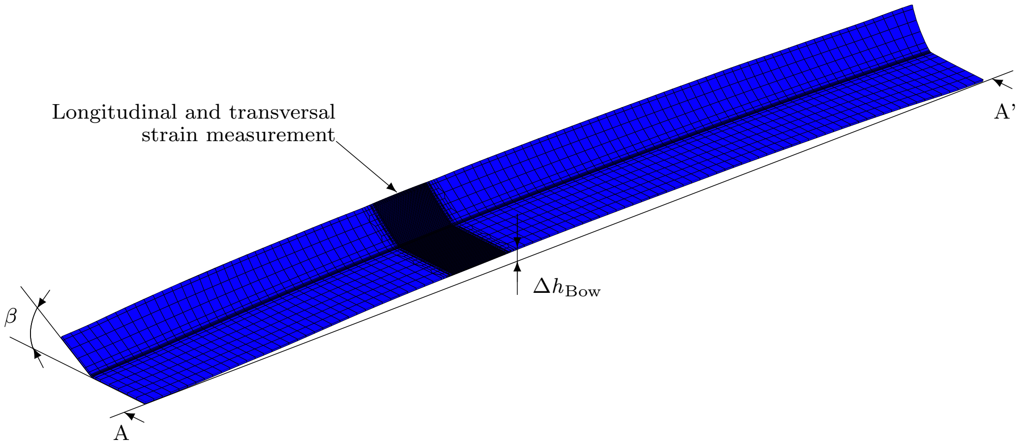
Longitudinal and transversal strain measurement
A'
Δh_{Bow}
β
A

Figure 4.8: Profile calculated using DC01 material properties. The cross section angle (β), the longitudinal bow Δh_{Bow} and longitudinal and transversal strains are extracted from the numerical model.

Longitudinal and transversal strains

Values of the longitudinal and transversal strain were calculated in the edge of the profile, in the center of the fine mesh part (Figure 4.8). The longitudinal and transversal peak and final plastic strain during the forming calculated with DC01 material data are shown in Figure 4.9.

Analyzing the behavior of the longitudinal strain during the forming process, it can be seen that the longitudinal deformation starts between the two forming stations and

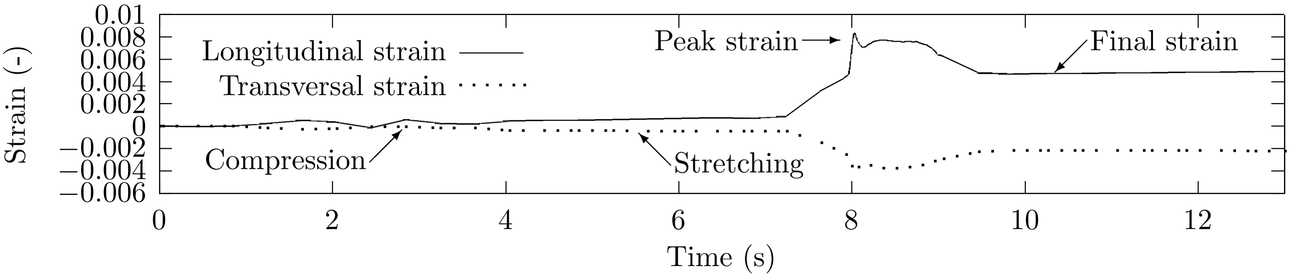

Figure 4.9: Calculated longitudinal and transversal strain during the roll forming.

four different forming stages can be differentiate: i) Longitudinal compression stage, the edge of the flange is not in contact with the roll but the upper surface of the flange is compressed due to the shape taken by the sheet. ii) Longitudinal stretching, the sheet is in contact with the bottom roll and the longitudinal strain starts to increase. iii) Peak strain, before the center of the forming station the longitudinal strain increases rapidly to a maximum value, then decreases rapidly when is approached to the center of the forming station. iv) Final residual longitudinal strains, if the longitudinal strain exceed the elastic limit residual strains and stresses induced geometrical errors in the final profiles. The transversal strains shows a similar behavior as the longitudinal strain.

Forming loads and torques

Forming loads are calculated from the upper roll and the forming torques from the bottom roll of the forming station. In order to approach to the reality and decrease the noise during the calculation of the load and forming torques, the number increment is increased while the rolls are in contact with the fine meshed zone. The forming roll load and torque evolution during the forming process is shown in Figure 4.10.

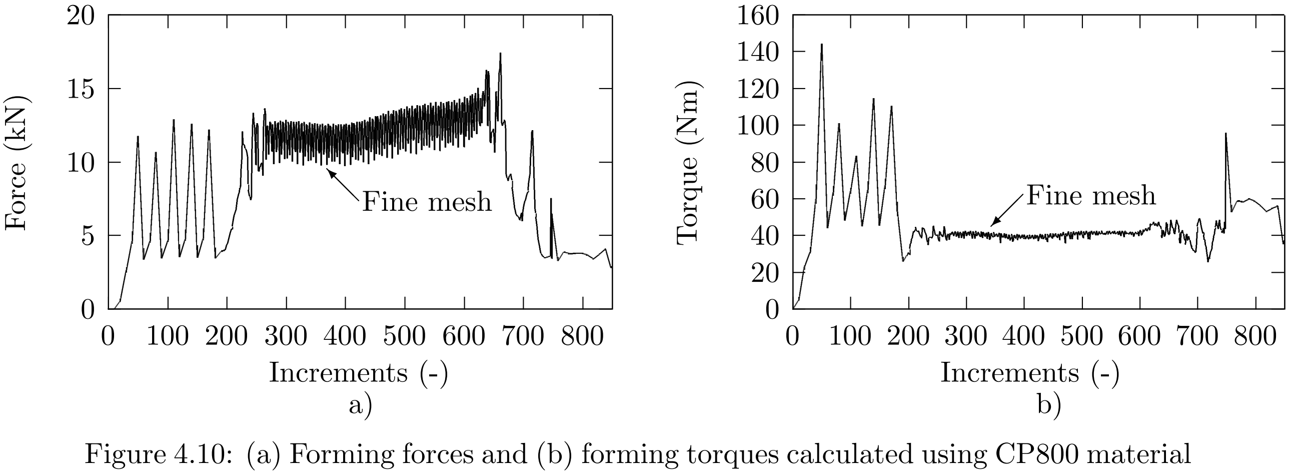

Figure 4.10: (a) Forming forces and (b) forming torques calculated using CP800 material properties.

It is noticed a decrease of the noise in the load and torque calculation in the fine mesh zone. The load and torque computation noise is directly dependent of the sheet-rolls interaction modeling quality. If the number of nodes in contact with the forming rolls is high the computation noise is low and vice versa. In the current case, values of forming loads and torques are calculated averaging the fine meshed zone.

Effect of material strength

Simulations with four different material properties were made in order to account the effect of the material strength on the different parameters of the roll forming process.

Comparing the effect of material strength in the final longitudinal cross section of the different profiles, it is concluded that when the material strength increases the longitudinal bow decreases. The longitudinal bows of the profiles formed with different materials are shown in Figure 4.11 a.

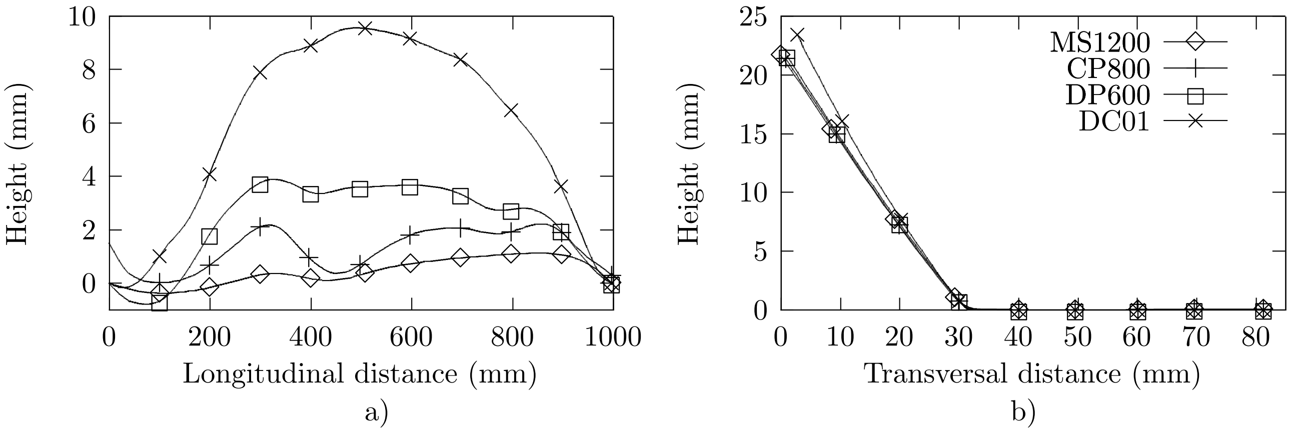

Figure 4.11: Calculated (a) longitudinal section and (b) transversal sections depending on the formed materials.

The longitudinal bow is produced due to the difference in length between the edge of the flange and the bend line of the profile. During the forming process, the edge of the profile is stretched in such a degree that is plastically deformed. After the forming stand, the profile takes a longitudinally round shape in order to reach the equilibrium state [Hal05]. As it was expected, when the strength of the material increases, the springback of the profile increases and the final angle of the profile decreases. However, numerical results showed a higher bending angle than 30°, suggesting a difficulty of the model to reproduce the springback behavior of the process. This effect, will be discussed later on in the validation of the numerical models section §4.2.3.

Figure 4.11 b shows the cross section of the center of the fine mesh zone for different materials. The evolution of the longitudinal bow and measured angle after the forming process for each material are shown in Figure 4.12.

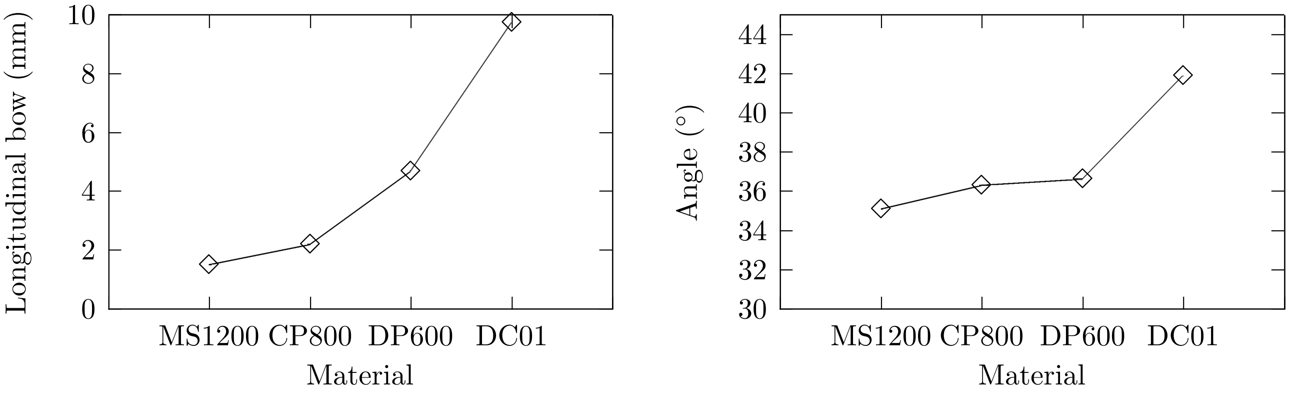

a) b)

Figure 4.12: Calculated (a) longitudinal bow and (b) profile angle values depending on the formed materials.

The computed longitudinal and transversal strains are calculated from the edge of the profile. The computed values of the longitudinal and transversal peak and longitudinal residual plastic strain for each material are shown in Figure 4.13.

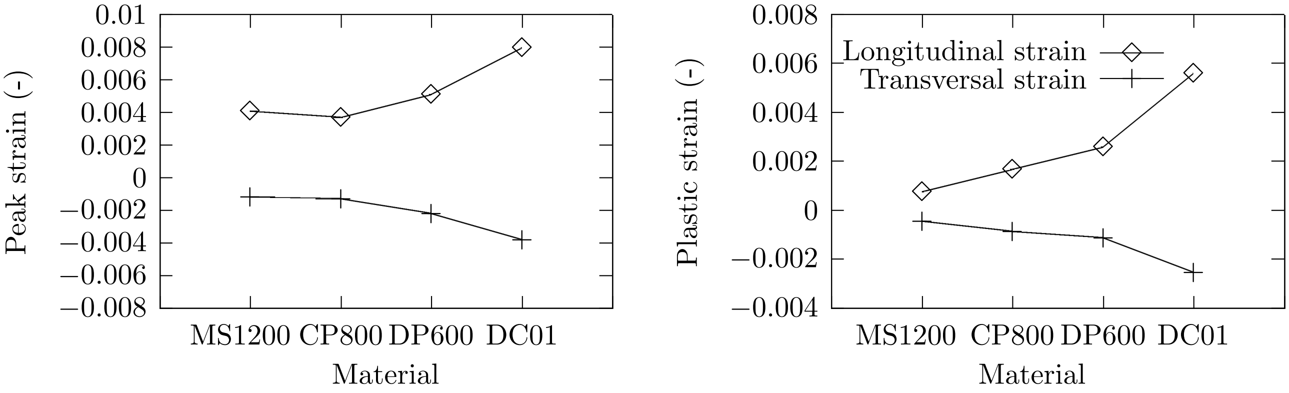

a) b)

Figure 4.13: Calculated (a) longitudinal and transversal peak strain and (b) longitudinal and transversal residual plastic strain values depending on the formed materials.

Comparing the effect of the material strength on the longitudinal and transversal peak and residual plastic strains, can be concluded that: the peak strain slightly increases when the material strength decreases. In the same manner the transversal peak strain increase when the material strength decreases. On the other hand, both, the longitudinal and transversal final residual strains increases when the material strength decreases. Computed forming load and torque values for the different materials are shown in Figure 4.14.

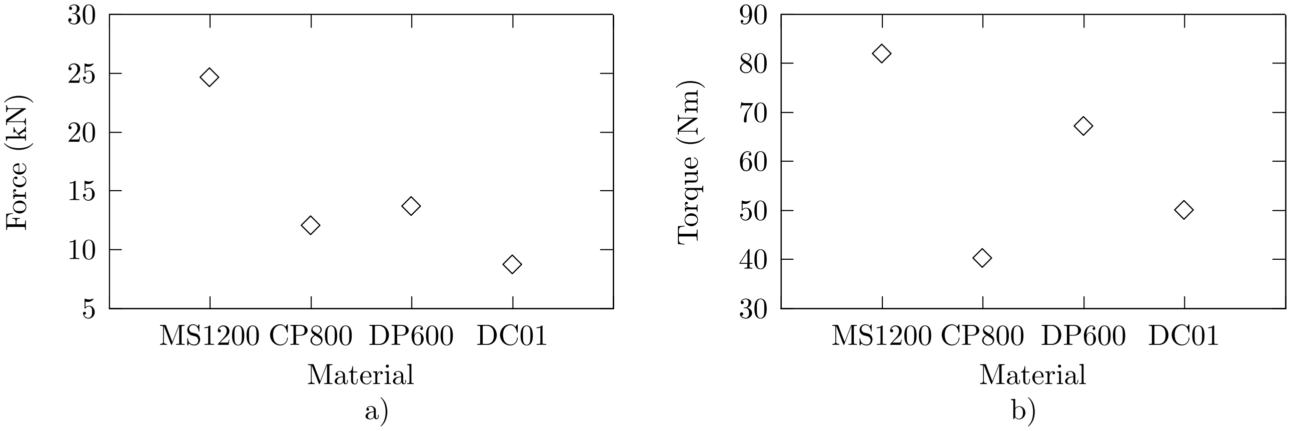

Figure 4.14: Calculated (a) forming load and (b) forming torque values depending on the formed materials.

As it was expected, the forming load and torques increases when the roll formed material strength increases. However, the CP800 material show a lower forming load and torque, due to its smaller thickness.

4.2.3 Validation of the conventional roll forming model

The main objective of the numerical analysis is to gain insight into the different roll forming processes in order to be able to predict the different features occurring in a real process and thus optimize the design of the processes themselves. In order to achieve these objectives, it is essential to analyze the reliability of the developed numerical models comparing numerical and experimental results.

For these purposes, calculated numerical results are compared with experimental results performed with this objective and the strengths and weaknesses of the numerical models are discussed. Experimental values of the profile geometry, longitudinal and transversal strains and the forming load and torques of profiles formed with four different types of steels are used for this purpose. The reader is referred to Chapter 5 section §5.3 in order to know more details of the experimental procedure.

Profile geometry

Values of the numerical and experimental longitudinal bow and the measured angles are shown in Figure 4.15.

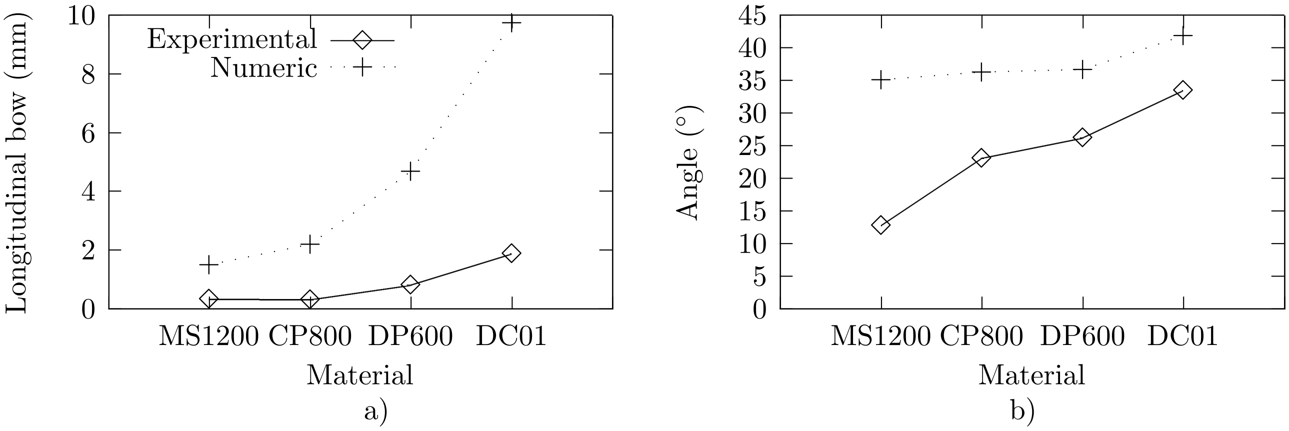

a) b)

Figure 4.15: Comparison of calculated and experimental (a) longitudinal bow and (b) profile angle (β) values depending on the formed materials.

Similar behavior is shown by both numerical and experimental results when different material strength are used. The longitudinal bow increases and the springback effect decreases when the material strength decreases. However, significant differences are obtained comparing numerical and experimental result values.

Comparing numerical and experimental results it can be seen that numerical results overestimated the longitudinal bow error. The longitudinal bow error is defined as the longitudinally round shape taken by the profile after the forming stage and is produced mainly for the longitudinal plastic strains. It is seen later on, that the numerical models overestimated the longitudinal plastic strain in the profile, thus this overestimation of the longitudinal bow is attributed to this difference in the longitudinal plastic strain. However, the error produced in the springback prediction could also affect the longitudinal bow.

Comparing the numerical and experimental cross section, it can be seen that numerical results underestimated the springback effect. All the computed profiles showed a bigger bending angle than 30°, thus it is concluded that the springback effect is poorly represented by the numerical models. This negative springback effect could be attributed to different reasons: i) it is seen in the literature review and in the description of the numerical model that the solid elements poorly represents the springback behavior.

In order to improve the bending behavior an alternative interpolation function so called assumed strain was used. However, the results shows a poor representation of the bending behavior and it would be interesting to test other interpolation functions. ii) The element density in bending zone could be insufficient, in order to accurately describe the springback effect. More investigations are needed in this field in order to improve the springback behavior of the numerical models of roll forming processes.

Longitudinal and transversal strains

Values of numerical and experimental longitudinal and transversal peaks and final plastic strains are shown in Figure 4.16 (a) and (b) respectively.

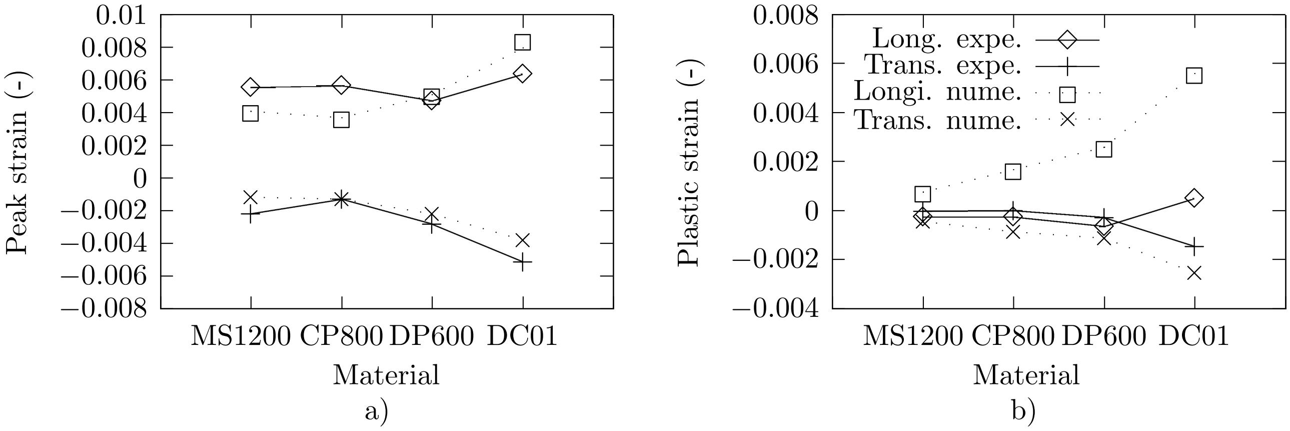

Figure 4.16: Comparison of the numerical and experimental (a) longitudinal and transversal peak strains and (b) longitudinal and transversal plastic residual strain values depending on the formed materials.

Similar behavior is shown by the numerical and experimental results when different materials are used, the longitudinal and transversal peaks and final strains increase when material strength decreases.

Similar values of computed and experimental longitudinal and transversal peak strains are achieved for all the materials. However, the final plastic strain are overestimated by the numerical models. This effect could be attributed to the differences between the real yield limit and the yield limit determined from the tensile tests. It would be interesting to investigate other material characterization methods such as bending tests, in order to approach the numerical model to the real yield limit.

Forming loads and torques

Finally, values of computed and experimental forming load and torques are shown in Figure 4.17 a and b respectively.

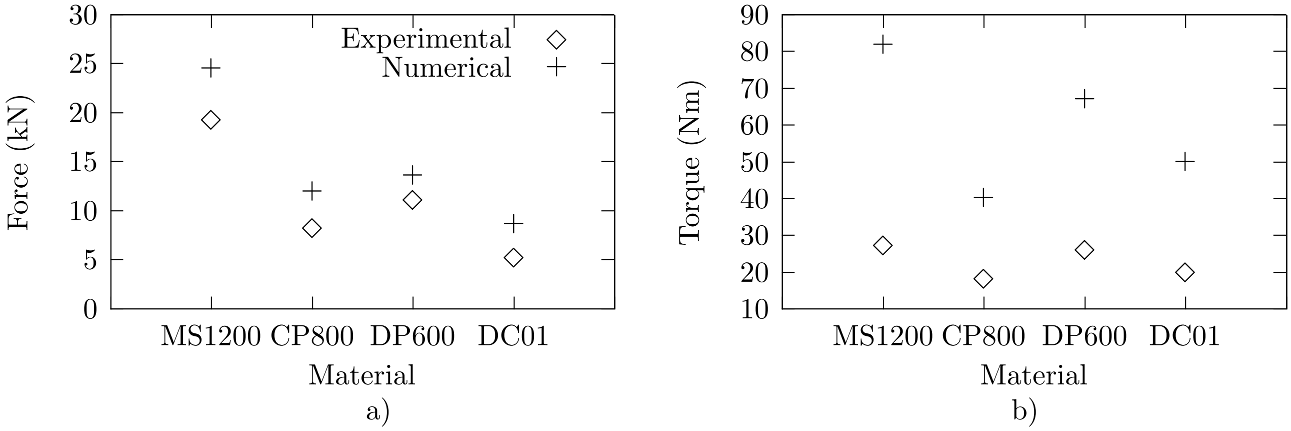

Figure 4.17: Comparison of the numerical and experimental (a) forming loads and (b) torque values depending on the formed materials.

Similar behavior is shown by the numerical and experimental results, the forming load and torque increases when material strength increases. It is also seen that numerical results of forming loads agree well with the experimental ones. However, big discrepancies are found when the numerical and experimental values of forming torque are compared. Computed numerical results overestimated the forming load. Numerous reasons could explain the discrepancies between the experimental and numerical results of forming torque: i) The friction coefficient of μ= 0.15 from bibliography were used due to a lack of an specific methodology to experimentally determinate the friction coefficient for roll forming process. The difference between the real friction coefficient and the numerical one could be the reason of the differences between the numerical and experimental results. ii) In the numerical models the gap between the forming rolls was selected to be the same of the sheet thickness. However, it is known that during the experimentation the shafts of the rolls deflects due to the forming forces, changing the gap between the rolls. This shaft deflection could affect the pressure loads in the forming zone and thus, the forming torque could be affected.

Although, discrepancies are found between the numerical and experimental values of springback and forming torques, the numerical models developed in Chapter 4 shows the same behavior in all the measured parameters and materials. Thus, this numerical model is validated knowing the strengths and weaknesses of the model.

4.3 Heat assisted flexible roll forming numerical modeling

The main objective of the current section is to analyze and optimize the heat assisted flexible roll forming process for the selected profile. For this purpose, a sort of simulations were performed changing the process temperature and the heated zone. The geometry used in the model was the same geometry of the experimentation and is shown in section §5.3 of Chapter 5.

4.3.1 Coupled thermo-mechanical analysis

A coupled thermo-mechanical approach was used to model the heat assisted flexible roll forming process. The effect of introducing a heat source changes the temperature distribution of the workpiece, introduces thermal induced strains and influences the material's mechanical properties. Thus, a coupled thermo-mechanical approach were used. Same hypotheses and procedures were used to model the mechanical part, explained in section §4.2, and this section only is focused on the thermal approach.

In this work, a sequential coupling procedure was used in the coupled thermo-mechanical analysis: In each Δt time increment, the transient heat distribution is calculated, depending on the applied heat sources and boundary conditions, and transferred to the mechanical model. Then, in the mechanical analysis, the deformation of the part is calculated, taking into account the temperature dependent material properties. Finally, the sheet geometry is updated to the thermal analysis in order to solve the next time step. This iterative process is repeated until the thermo-mechanical calculation is solved. The procedure to coupled the thermal and mechanical analysis is shown in Figure 4.18.

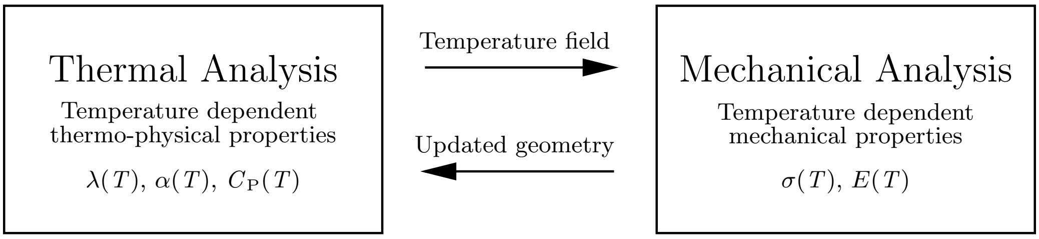
Thermal Analysis
Temperature dependent thermo-physical properties
$\lambda(T)$, $\alpha(T)$, $C_P(T)$
Temperature field
Updated geometry
Mechanical Analysis
Temperature dependent mechanical properties
$\sigma(T)$, $E(T)$

Figure 4.18: Interaction between the mechanical and thermal fields.

Transient thermal analysis

The measure of temperature is based on the establishment of an equilibrium state in the reference body. Meanwhile, thermodynamics is based on the concept of bodies, with negligible representative volume, that during a small interval of time Δt their state is considered to be in equilibrium. The first law of thermodynamics states that for a close system the increase in the internal energy of a system is equal to the amount of energy added to the system, minus the amount lost as a result of the work done by the system on its surroundings, in a rate basis is:

$$\dot{Q} = \dot{W} + \frac{\partial U}{\partial t} \tag{4.18}$$

where $\dot{Q}$ is the heat transfer rate and $\dot{W}$ is the work transfer rate. The derivative $\frac{\partial U}{\partial t}$ is the rate of change of internal thermal energy, U with the time, t.

In any configuration, there are three ways to transfer the heat between two bodies, namely by conduction, convection and radiation. At this point, coming to the heat assisted roll forming process it was necessary to distinguish between the different nature of heating and cooling mechanics:

- The heat generated in the workpiece during the inductive heating and the internal heat transfer through the sheet was considered.
- The heat generated in the workpiece due to plastic deformation and frictional effects was not considered. The quantity of heat generated by these phenomena was negligible compared with the heat generated by the inductive heating.
- The heat transferred by conductive contact with the rolls and blank holders and the convection with the surrounding air was considered during and after the process.
- The heat transfer by thermal radiation was not considered. The quantity of heat lost by radiation is neglected in order to simplify the numerical model and because this cooling down mechanism is negligible compared with conductive and convective heat exchanges.

A unitary volume control of a conductive body with volume V and surface S is defined. In a constant pressure process the internal energy change of the unitary volume control is:

$$\dot{Q} = \frac{\partial U}{\partial t} = \rho C_{\mathrm{p}} \frac{\partial T}{\partial t} \tag{4.19}$$

where C_p is the specific heat capacity at constant pressure. The internal energy change $\dot{Q}$ in the volume control is defined as the heat conducted in the volume through the surface plus the heat generated in the control volume:

$$\dot{Q} = -\int_S (-k_{\text{th}} \nabla T)(\vec{n} ds) + \int_V \dot{q} dv \tag{4.20}$$

where k_{th} is the thermal conductivity coefficient, ∇T is the volumetric temperature gradient and $\dot{q}$ is the heat generated in the unitary volume control due to the inductive heating. Developing the Eq. 4.20 is obtained the general expression of the heat diffusion in three dimensions:

$$\nabla \cdot k_{\text{th}} \nabla T + \dot{q} = \rho C_{\text{p}} \frac{\partial T}{\partial t} \tag{4.21}$$

The temperature distribution within the sheet was calculated solving the Eq. 4.21.

Body discretization

Roll and blank holder modeling

The rolls and blank holders were modeled as rigid bodies where the heat transfer between the sheet and the rolls was considered (see section §4.2.1). The numerical model considered all the blank holder, conventional stand and flexible stands used in the experimental machine.

Sheet modeling

In the mechanical analysis the sheet metal was modeled using a full-integration eight node solid element type 7 of MSC.Marc as is explained in section §4.2.1. In bending zones where the strain concentration was large, were discretized with a smaller elements than the rest of the sheet metal.

In the thermal analysis the sheet metal was modeled using a full-integration eight node solid element type 43 of MSC.Marc. This element uses trilinear interpolation functions, thus, the thermal gradients tend to be constant throughout the element [MSCb].

Material property modeling

As explained in section §4.2.1 an elastic-plastic material law was used in the current model where the elastic and plastic strains were modeled separately.

Temperature dependent elastic behavior

The elastic behavior of the material was considered isotropic and temperature dependent and was modeled with the Poisson's ratio ($\nu = 0.33$) and with temperature dependent Young's modulus (E) (Figure 4.21). Material data for temperature dependent Young's modulus were taken from [Pit05]. These data were calculating following the procedure described in [Ric73] for a given chemical composition of a CP800 steel.

Temperature dependent plastic behavior

The plastic behavior of the material was considered isotropic and temperature dependent. The plastic uniform behavior of the material was calculated subtracting the elastic portion from the experimental true strain - true stress curve, as it is explained in section §4.2.1.

Results from the material characterization (Chapter 3 section §3.4) were selected, and only some representative curves of the material behavior were used. In this case, the effect of the strain rate was considered because its influence specially at highest temperatures (500°C, 600°C and 700°C) is significant.

The post uniform behavior of the material at each temperature was modeled using the Hollomon's material law, as is explained in section §4.2.1. Mechanical properties depending on the temperature and strain rate of CP800 are shown in Figure 4.19 and Figure 4.20.

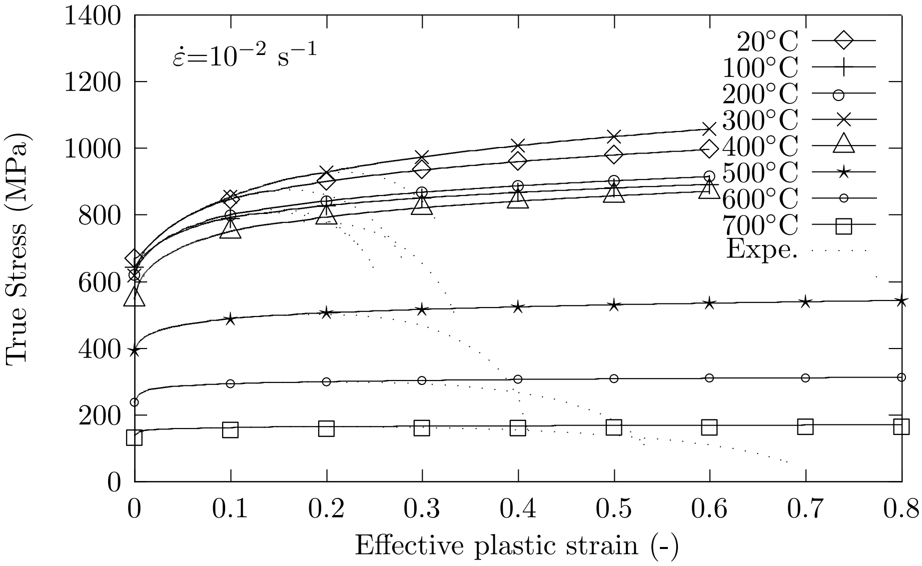

Figure 4.19: Comparison between experimental results and Hollomon's laws at 10^{-2} s^{-1} strain rates. The summary of the results can be seen in Table B.1 of Appendix B.

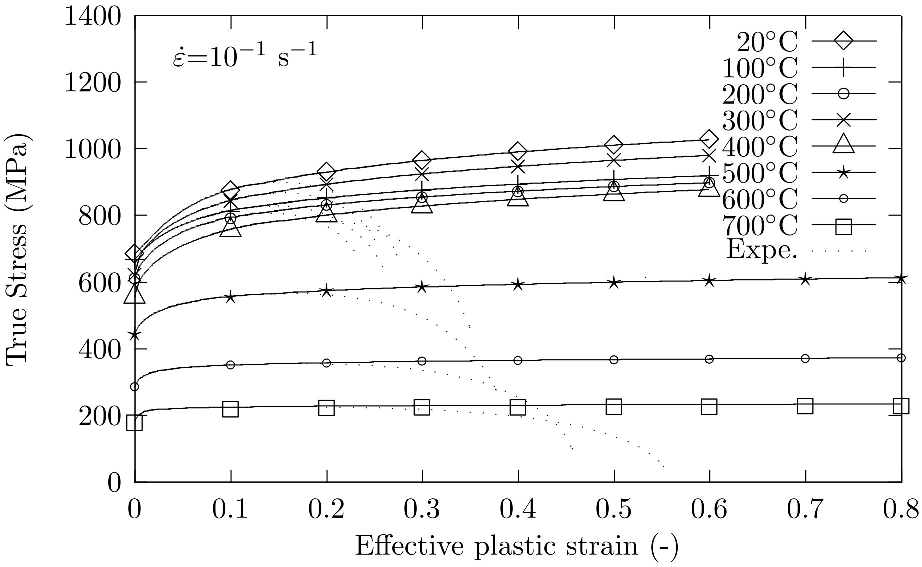

Figure 4.20: Comparison between experimental results and Hollomon's laws at 10^{-1} s^{-1} strain rates. The summary of the results can be seen in Table B.2 of Appendix B.

Thermo-physical properties of the material at high temperature

The most relevant thermo-physical properties are the specific heat capacity (C_p), the thermal conductivity (k_th) and the coefficient of thermal expansion (α). It is out of the scope of the present thesis to perform a deep study on the thermo-physical properties and thus, values for the numerical implementation were taken from literature. Temperature dependent thermo-physical properties used are shown in Figure 4.21.

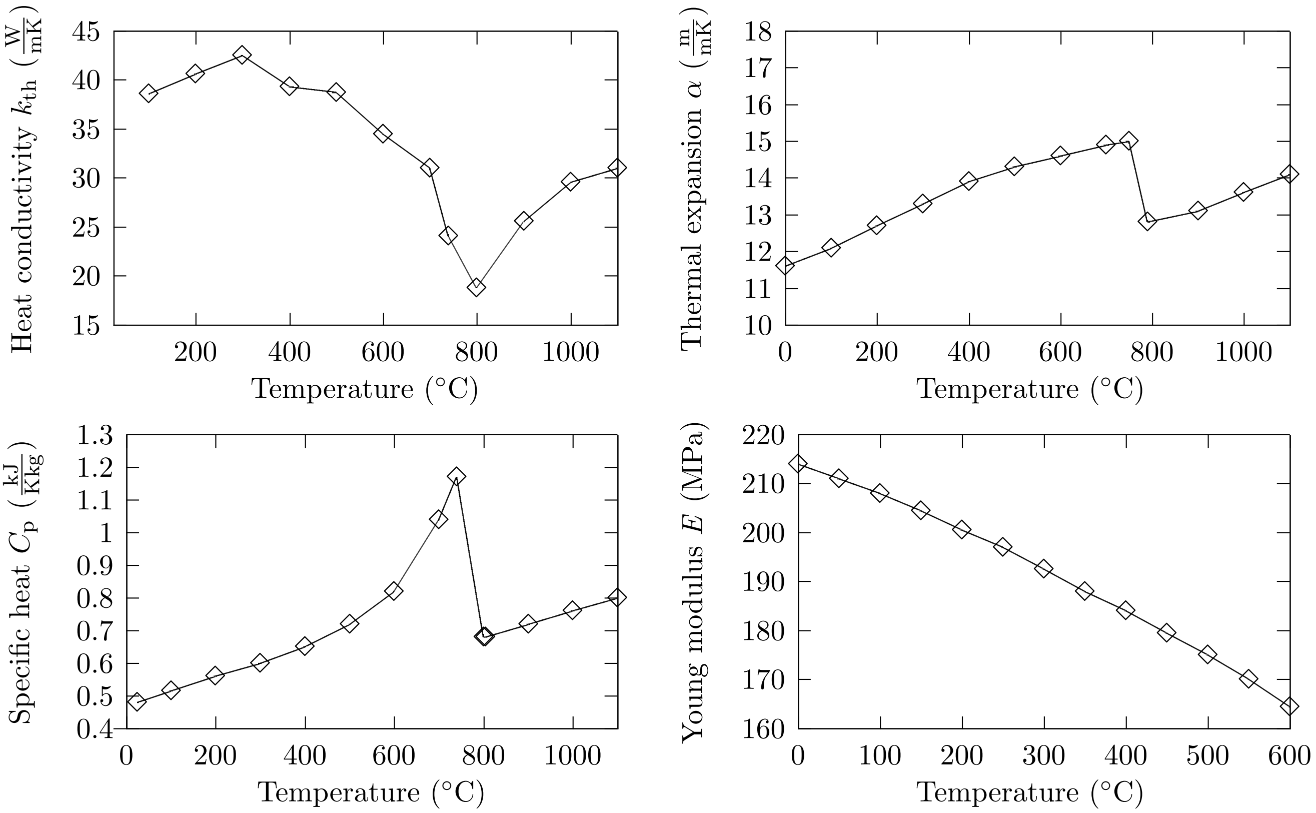

Figure 4.21: Temperature dependent data of the heat conductivity (k_th) and of the specific heat capacity (C_p) are taken from [Mil02], coefficients of the thermal expansion (α) and elastic modulus (E) are taken from [Pit05].

Temperature dependent values of specific heat capacity (C_p) and thermal conductivity (k_th) of ductile steel are taken from [Mil02]. Temperature dependent values of thermal expansion (α) of a CP800 are taken from [Pit05].

Boundary conditions

Contact conditions

The heat transfer by conductive contact between the sheet and the rolls and blank holders was considered in the current model. The conduction between two surfaces will ever form perfect thermal contact when they are pressed together. Since some roughness is always present, a typical plane contact will always include tiny air gaps. Conduction through points of solid-to-solid contact are very effective, but conduction through the gas filled interfaces, which have very low thermal conductivity, can be very poor. Therefore, the heat transfer between two solids in contact is defined as:

$$Q = A \cdot h_{\text{cond}} \cdot \Delta T \tag{4.22}$$

where A is the contacted area, h_{cond} is the interfacial conductance and ΔT is the temperature difference between the two surfaces in contact. The h_{cond} interfacial conductance parameter must be evaluated experimentally. However, in the current dissertation, the steel to steel conductance was selected, h_{cond}=3000 W/m^{2}K, from [Lie87].

Room temperature modeling

A initial temperature of 20°C was applied to the workpiece as room temperature.

Cooling down conditions

The cooling down of the sheet metal was considered only by convection. The quantity of heat lost by radiation effect is negligible compared with convection and conduction effect and in order to simplify the numerical model, radiation terms were not considered. The heat exchange Q with the environment by convection of a body at temperature T can be expressed as:

$$Q = h_{\text{conv}}(T_{\text{S}} - T_{\infty}) \tag{4.23}$$

where Q is the heat flux, h_{conv} is the film coefficient, T_{S} the surface temperature and T_{∞} is the ambient temperature. In the current analysis h_{conv} was considered constant in all the sheet and in all temperature ranges. A film coefficient corresponding to natural convection in gas h_{conv}=4.33 W/m^{2}K was selected [Lie87].

Induction heating modeling

Different heating methods are used in metal forming processes, such as inductive heating, laser heating, heating by resistance etc. The numerical modeling of each heating technology must be done carefully describing the physical heating phenomena. In the current case inductive heating technology was selected to perform the experimental trials of heat assisted flexible roll forming process. However, it was out of the scope of the present thesis to perform an accurate modeling of the inductive heating process. Therefore, the inductive heating source was simplified as a time and position dependent external heat source with a specific area A_{heat} and heat flux F_{heat}. In the beginning of every time increment Δt of the thermal analysis, the geometrical position (x_{c}, y_{c}, z_{c}) of the center of the heating area was calculated by the subroutine Flux depending on the analysis time t. The coordinate positions (x_{c}, y_{c}, z_{c}) were obtained according to the desired heating strategy.

Then, the distances between the center of the heating area and all integration points were calculated. If the distance was smaller than the radius r of the circular heating area A_{heat}, the heat flux F_{heat} was applied directly to the face of the element. In the current numerical model, a circular heating area of 30 mm radius was defined. The value of the heat flux F_{heat} was selected to achieve the desired temperature in the forming zone. The flow chart of the subroutine Flux is shown in Figure 4.22.

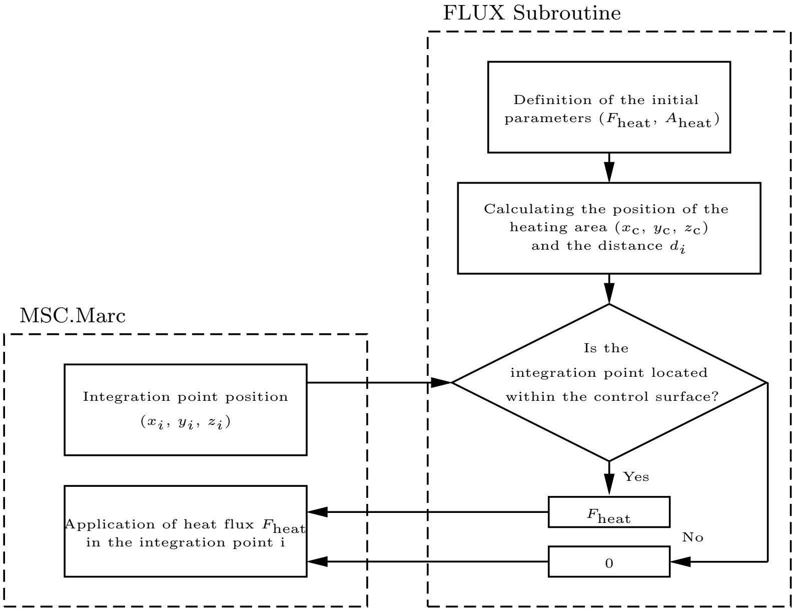
FLUX Subroutine
Definition of the initial parameters (F_{heat}, A_{heat})
Calculating the position of the heating area (x_{c}, y_{c}, z_{c}) and the distance d_i
Is the integration point located within the control surface?
Yes
No
F_{heat}
0
MSC.Marc
Integration point position (x_i, y_i, z_i)
Application of heat flux F_{heat} in the integration point i

Figure 4.22: Flow chart of the FLUX subroutine.

4.3.2 Results of the heat assisted flexible roll forming numerical model

Profile geometry

In order to analyze the effect of heating the different zones of the profile and the effect of the process temperature, different cross sections of the final profiles are compared: The longitudinal section (Section A-A') and the cross sections of the wide and slim part of the profiles are compared, see Figure 4.23.

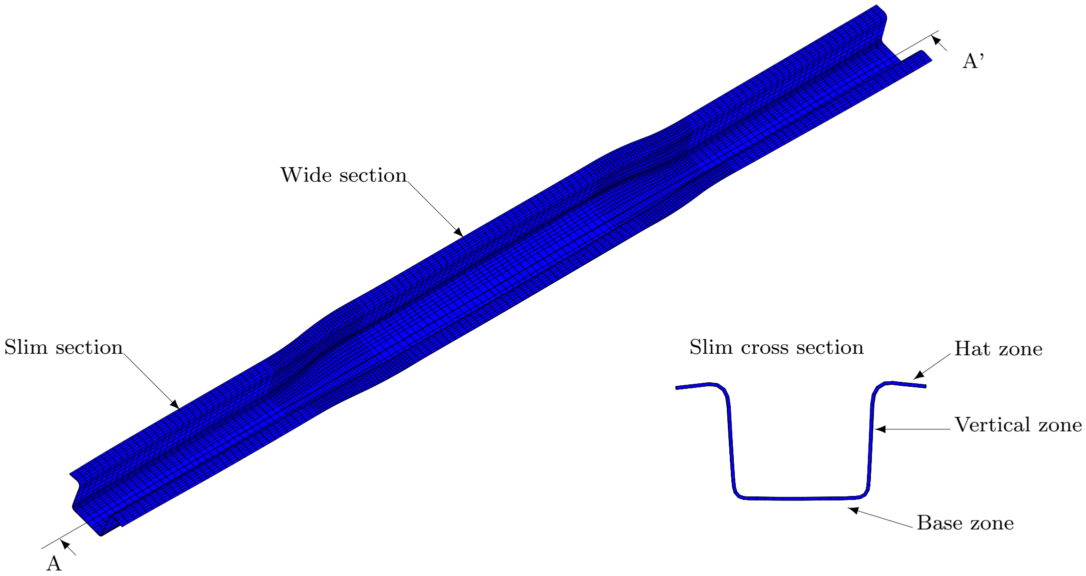

Figure 4.23: The longitudinal and transversal cross sections and different heated zones of the profile.

Longitudinal web warping definition

The web warping is defined as the height deviation of the profile web from the entry of the transition zone to the exit. As is explained in Chapter 2 the web warping is caused by the resulting insufficient longitudinal plastic strain in the flanges of the transition zone. If the plastic deformation of the flange is insufficient, the sheet reacts to the stresses generated during the forming and changes its shape until a state of equilibrium is reached. This effect deforms the transition zone, raising the compressed zone and lowering the stretched zone [Abe08]. For example, a characteristic longitudinal section of a flexible roll formed profile (section A-A') is shown in Figure 4.24.

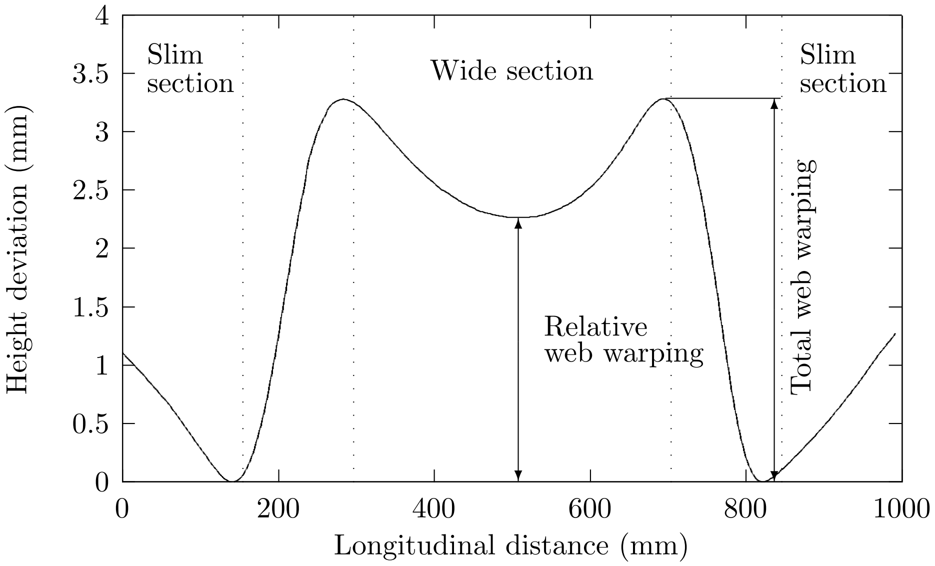

Figure 4.24: The height deviation of a real flexible roll formed profile at room temperature along the longitudinal direction.

However, it is also interesting to analyze the so called relative web warping. The relative web warping of the profile is defined as the height deviation between the lower point of the profile and lower point of the wide section. This difference in height is important since this profile must be welded with the car frame and from a technological point of view this value must be minimal.

Strain distribution within the workpiece and heating strategy

In order to optimize the heating strategy and the heating temperature, it is interesting to analyze the strain distribution along the profile produced at room temperature. Identifying the strain distribution of the profile, those zones that must be longitudinally deformed can be heat assisted increasing locally the formability of the material and achieving the desired longitudinal strains. If the achieved longitudinal deformations in transition zones are large enough the flange warping and web warping can be avoided. The computed strain distribution on the flexible profile formed at room temperature can be seen in Figure 4.25.

The simulation results of the profile formed at room temperature show a longitudinally compressed and stretched areas in the flexible part of the profile. Not only in the hat part of the profile is compressed and stretched, but also the vertical zone of the profile. Thus it is concluded that, the vertical and hat zones of the profile are the most interesting zones to be heat assisted.

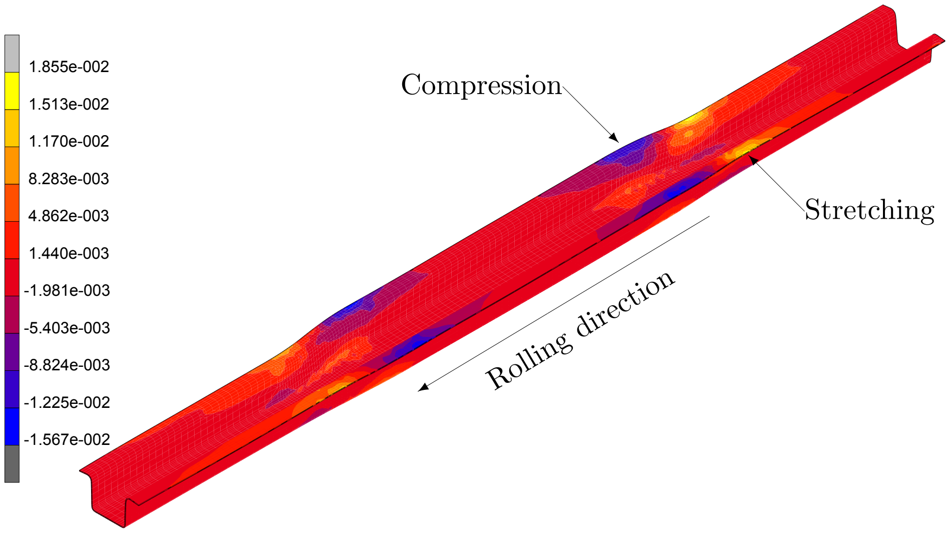

Figure 4.25: Calculated longitudinal strain distribution on the profile after forming at room temperature.

In order to analyze the effect of the temperature on the final geometry of the profile, simulations at 5 different process temperatures were performed. In Chapter 3 it is shown that the minimal temperature to increase the formability of the material is 400°C and at 600 °C is reached the highest formability level. Thus, numerical simulations were performed at nominal temperatures of 20°C, 300°C, 400°C, 500°C and 600°C.

In order to analyze the effect of the heating strategy, three different heating zones were defined (Figure 4.23) and simulations heating these zones were performed. Due to the highest formability were obtained in the mechanical characterization at 600°C, simulations to analyze the effect of the heating zone were performed at this temperature.

Heat distribution

As explained in a precedent section §4.3.1, the power of the heating flux is adjusted to achieve the desired temperature in the forming zone. However, the heat distribution within the profile must be analyzed. As an example, the heat distribution on the profile during the heat assisted flexible roll forming simulation at 400°C are shown in Figure 4.26.

The profile is heated 100 mm before the forming stand, due to the space limitation in the real experimental roll forming machine and in order to avoid collisions between the inductive coils and forming rolls. The computed temperature evolution between the

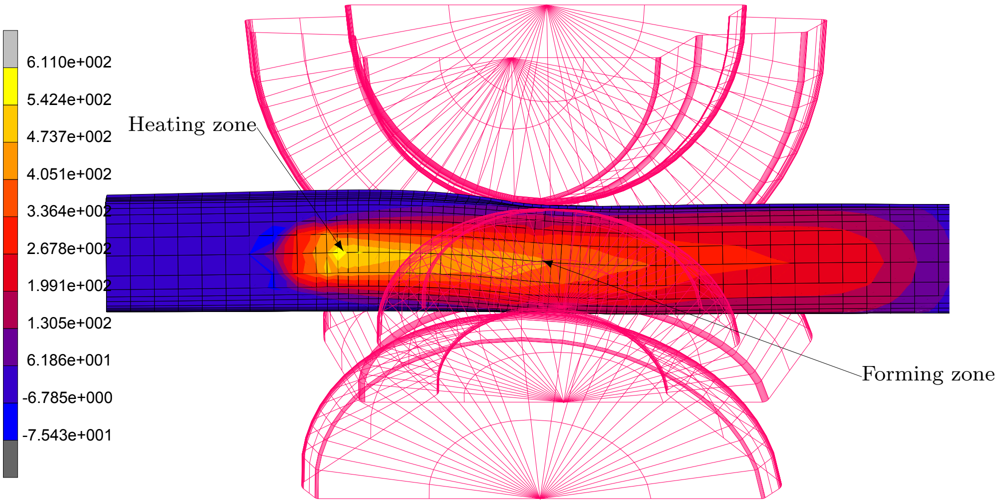
6.110e+002
5.424e+002
4.737e+002
4.051e+002
3.364e+002
2.678e+002
1.991e+002
1.305e+002
6.186e+001
-6.785e+000
-7.543e+001
Heating zone
Forming zone

Figure 4.26: Calculated temperature distribution during the forming of flexible profile at 400°C.

heating and the forming zones are shown in Figure 4.27.

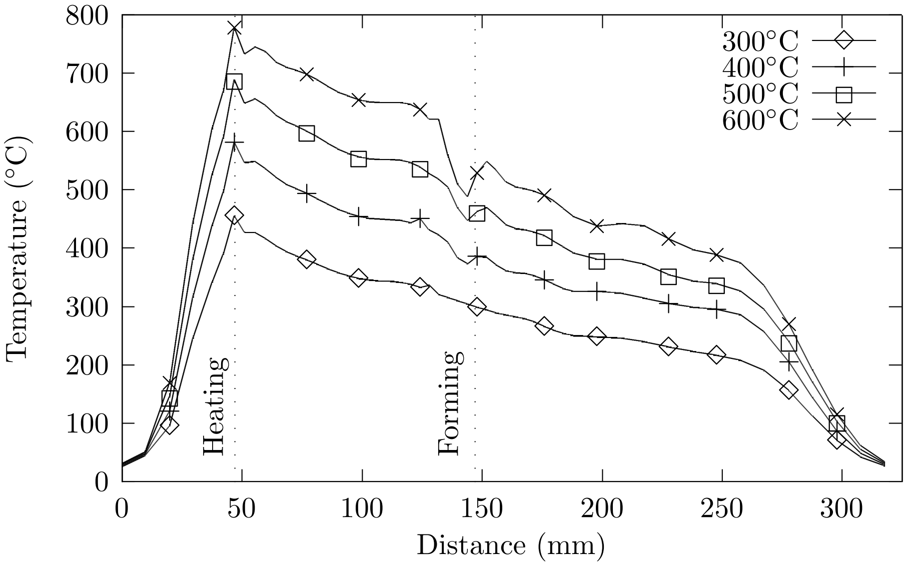

Figure 4.27: Calculated temperature evolution from heating to forming zone.

The maximum temperature is obtained in the heating zone and the temperature decreases due to the convection and conduction effects, obtaining the nominal temperature in the forming zone. Furthermore, a temperature drop is noticed in the forming zone, due to the conductive heat transfer in the contact area between the sheet and the forming rolls.

Effect of the temperature in the longitudinal web warping

The longitudinal sections of the computed flexible profiles roll formed at different temperatures are shown in Figure 4.28.

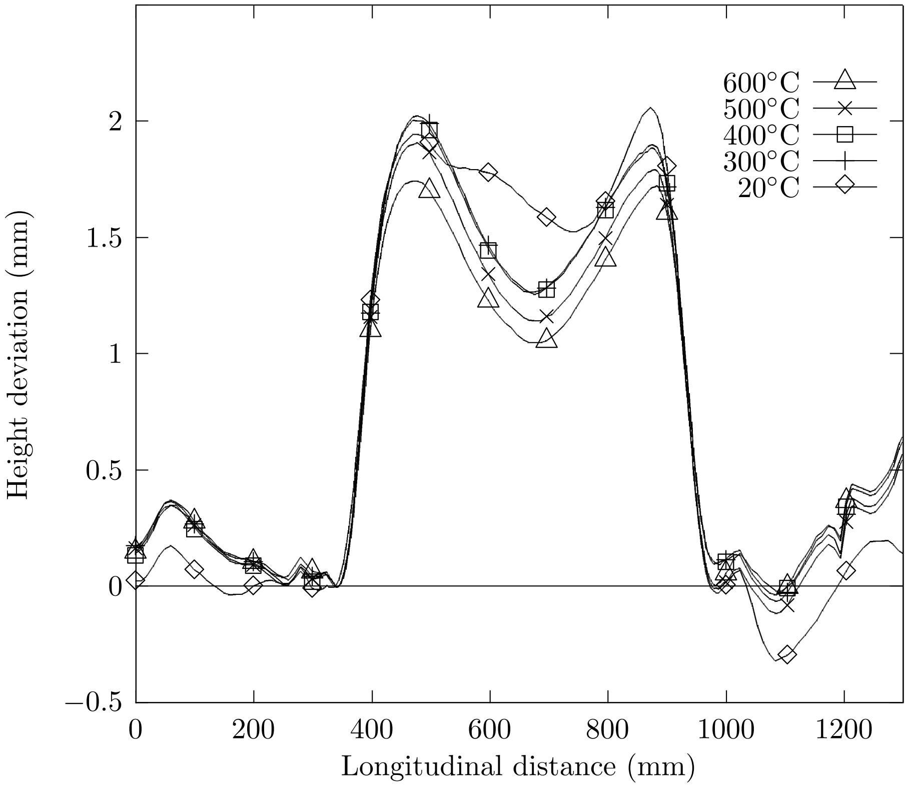

Figure 4.28: The height deviation of the numerical flexible roll formed profiles within the longitudinal direction for different temperatures.

The total web warping is temperature dependent and the minimal value is calculated in the profile at 600°C. Computational results shows a decrease of 17% at 300°C, 17.6% at 400°C, 25.1% at 500°C and 31.3% at 600°C for the relative web warping. On the other hand, the total web warping decreases by 1.7% at 300°C, by 2.6% at 400°C, by 7.4% at 500°C and by 15.3% at 600°C. The computed values of the total and relative web warping depending on the temperature are graphed in Figure 4.29.

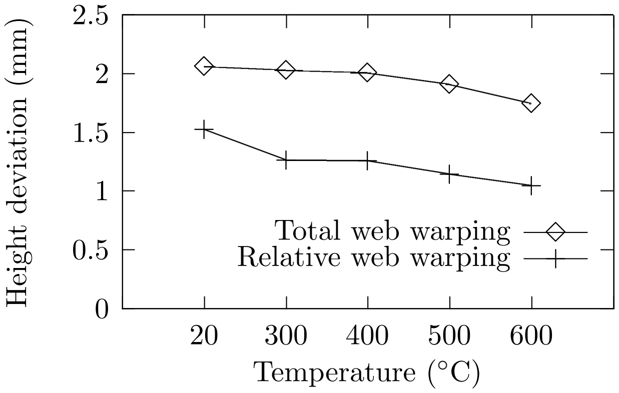

Figure 4.29: Calculated values of the total web warping and relative web warping depending on the process temperature.

The numerical results show a significant decrease of the relative and total web warping when the flexible profiles are heat assisted. On the other hand, it is seen that as higher as the temperature is, lower are the total and relative web warping.

Effect of the temperature on the profile cross section

The cross sections of the computed heat assisted flexible profiles are subtracted from the slim and wide section (Figure 4.23) and angles β_1, β_2, β_3 and β_4 are calculated. As example, the computed cross sections of the slim and wide part of profiles formed at room temperature and at 600°C are graphed in Figure 4.30 a and b respectively.

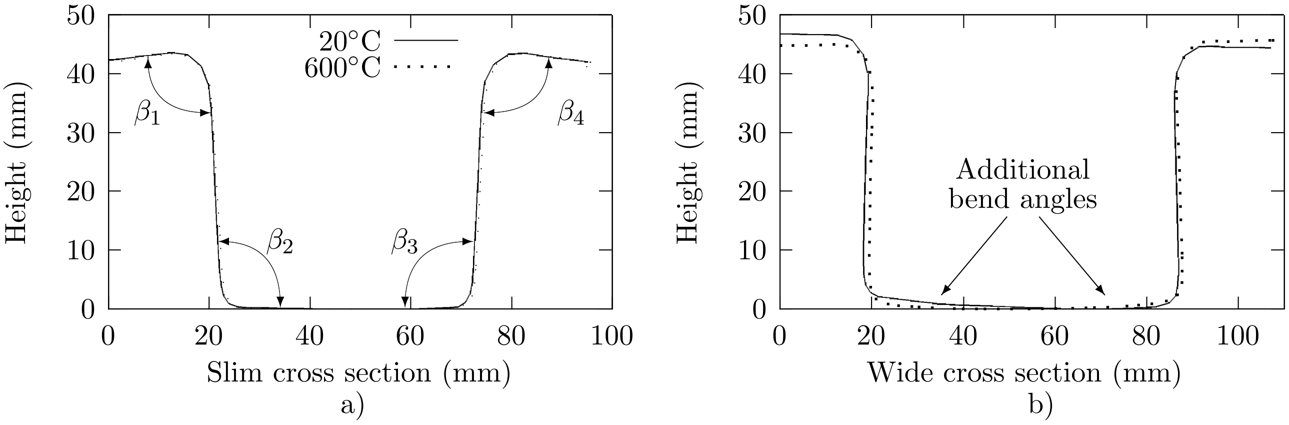

a) b)

Figure 4.30: Calculated (a) slim and (b) wide cross sections at room and 600°C temperature.

The evolution of the angles β_1, β_2, β_3 and β_4 of the slim and wide section depending on the temperature are shown in Figure 4.31 a and b respectively.

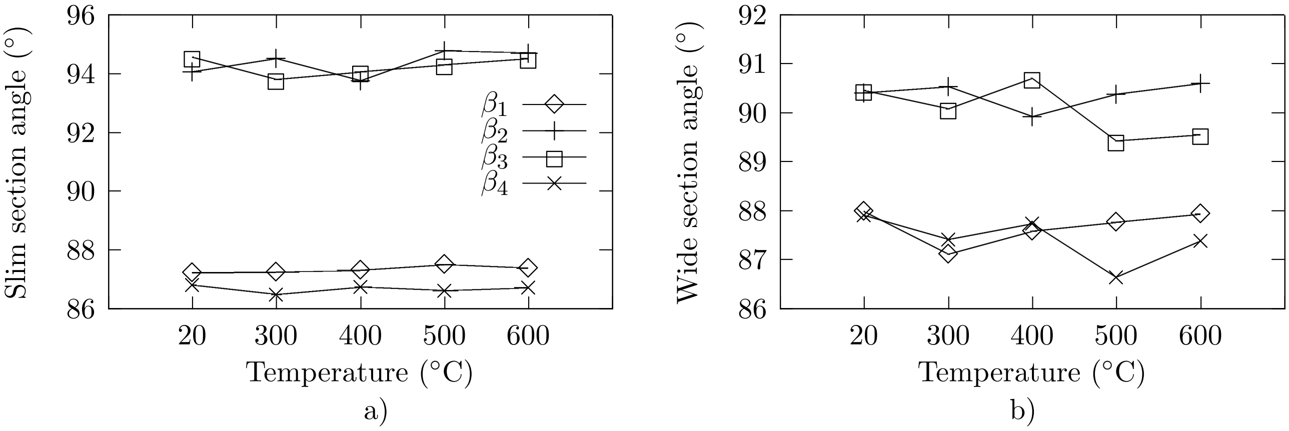

Figure 4.31: Calculated angles β_1, β_2, β_3 and β_4 of the (a) slim and (b) wide section depending temperature.

Similar values of β_1 and β_4 are computed in both slim and wide cross section for all the temperature range. However, values of β_2 and β_3 differ more between the slim and wide section. On the other hand, additional bend angles are identified in the base of the profile, produced by the static blanc holders.

Effect of the heated zone in the longitudinal web warping

Calculated longitudinal sections of flexible roll forming profiles, heat assisted in different zones of the profile are shown in Figure 4.32.

The minimal value of the total and vertical web warping is achieved when the vertical part of the flexible profile is heat assisted at 600 °C. Computational results show a decrease of 20.6% in the relative web warping heating the base, 25.7% heating the hat part and 31.3% heat assisting the vertical part. On the other hand, the total web warping increased by 0.2% heating the base of the profile and 7.5% heating hat zone. A decrease of 15.3% is seen in the total web warping when the vertical part of the profile is heat asisted. The computed values of the total and relative web warping depending on temperature are graphed in Figure 4.29.

Analyzing the different heating zones it is concluded that the best improvements in both, the total and relative web warping, are achieved when the vertical part of the transition zone are heated at 600°C.

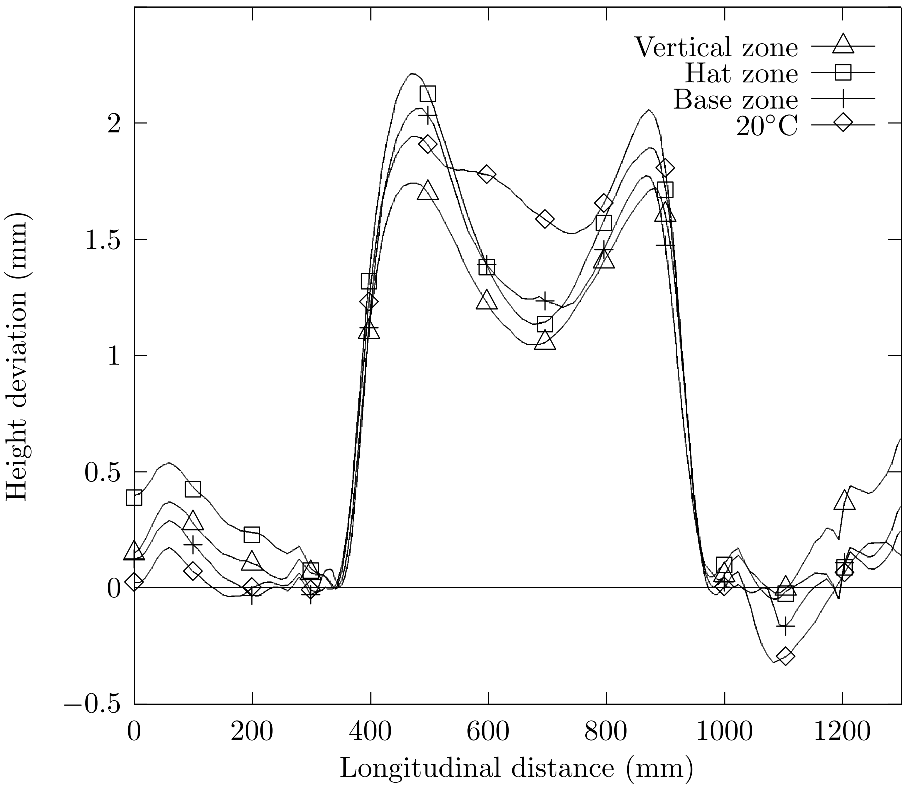

Figure 4.32: Calculated height deviations of the flexible roll formed profiles within the longitudinal direction for different heated zones.

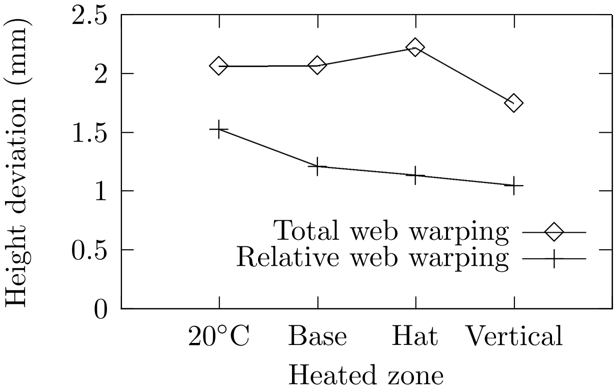

Figure 4.33: Values of calculated total web warping and relative web warping depending on the heating condition.

Effect of the heated zone on the profile cross section

The cross sections of the computed heat assisted flexible profiles were subtracted from the slim and wide section (Figure 4.23) and angles β_1, β_2, β_3 and β_4 were calculated. The measured angles β_1, β_2, β_3 and β_4 of the slim and wide section depending depending on the different heating zones are shown in Figure 4.34 a and b respectively.

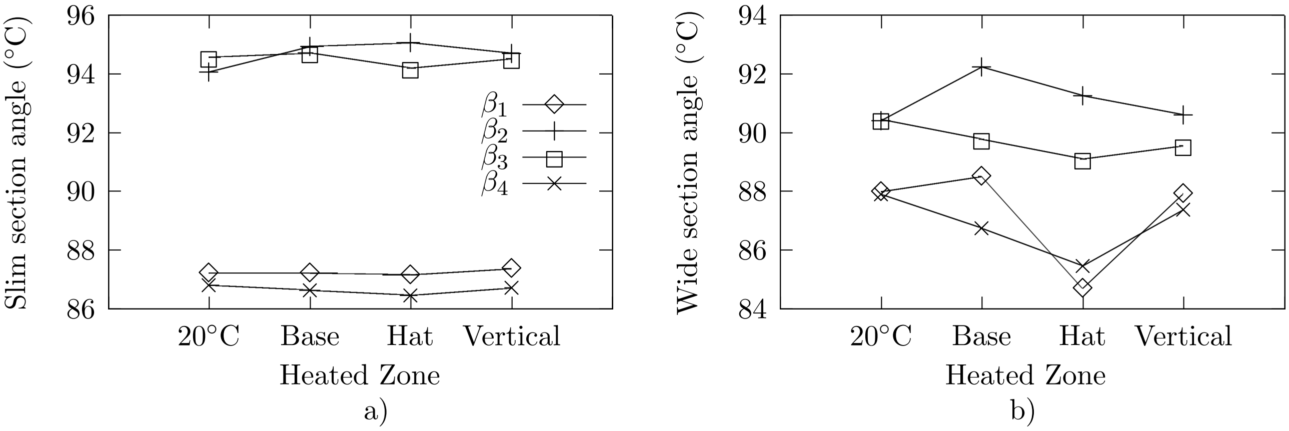

Figure 4.34: Values of total web warping and relative web warping depending on the heating condition.

Similar values of β_1, β_2, β_3 and β_4 are achieved in the slim section of the profile when different zones of the profile are heated. On the other hand, a sligth improvement of angles β_2 and β_3 are achieved when the vertical zone is heat assisted.

4.3.3 Validation of the heat assisted flexible roll forming model

Experimental and numerical results are compared in order to analyze the reliability of the developed numerical model of heat assisted flexible roll forming process. Experimental values of the total and relative web warping and values of the angles in the wide and the slim section are used for this purpose. The reader is referred to Chapter 5 section §5.2 in order to know more details of the experimental procedure.

However, it is out of the scope of the present thesis to perform an accurate modeling of the inductive heating process, thus numerical results from the heating process are not compared with experimental ones. Values of the computed and experimental total and relative web warping are shown in Figure 4.35 (a) and (b) respectively.

Similar behavior is shown by both, the numerical and experimental results for all the temperature range. The relative and total web warping decreased when the temperature of the process increased. The only discrepancy between the numerical and experimental results is seen at 600°C. It is explained in Chapter 5, that the profiles formed at 600°C showed a local buckling of the profile web. The representation of the buckling behavior is always a numerical nonlinearity and additional hypotheses must be taken

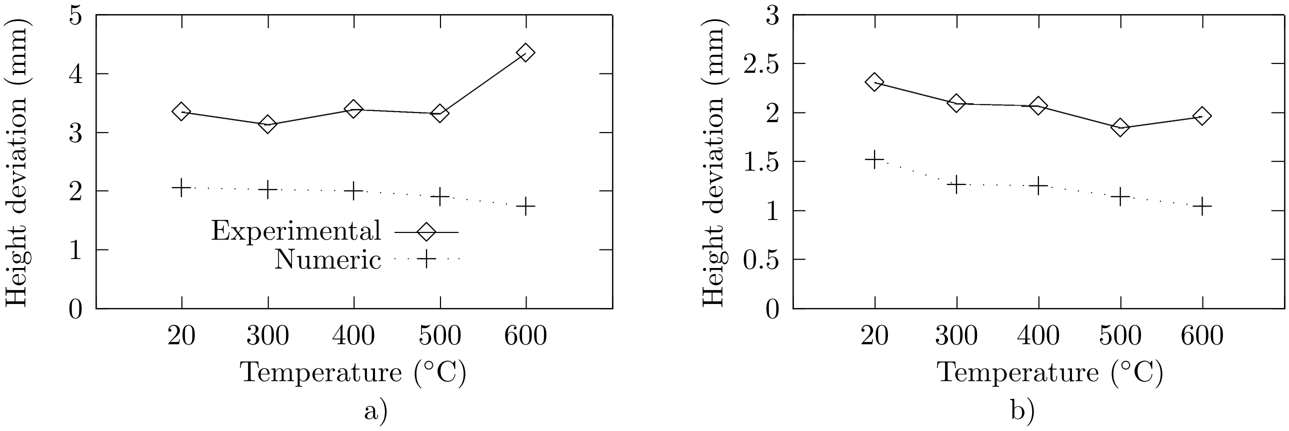

Figure 4.35: Comparison of numerical and experimental (a) total warping and (b) relative web warping depending on the temperature.

into account in the numerical model. In the current developed models these hypotheses were neglected and thus the buckling of the profile is not computed.

Comparing the numerical and experimental angles of the slim and wide sections of the flexible profiles, it is concluded that both numerical and experimental results shows a similar behavior when the process temperature increases. However, discrepancies in numerical and experimental values are attributed to the aforementioned problems of modeling the spring back behavior. Values of the computed and experimental β_1, β_2, β_3 and β_4 of the slim and wide cross sections are shown in Figure 4.3.3.

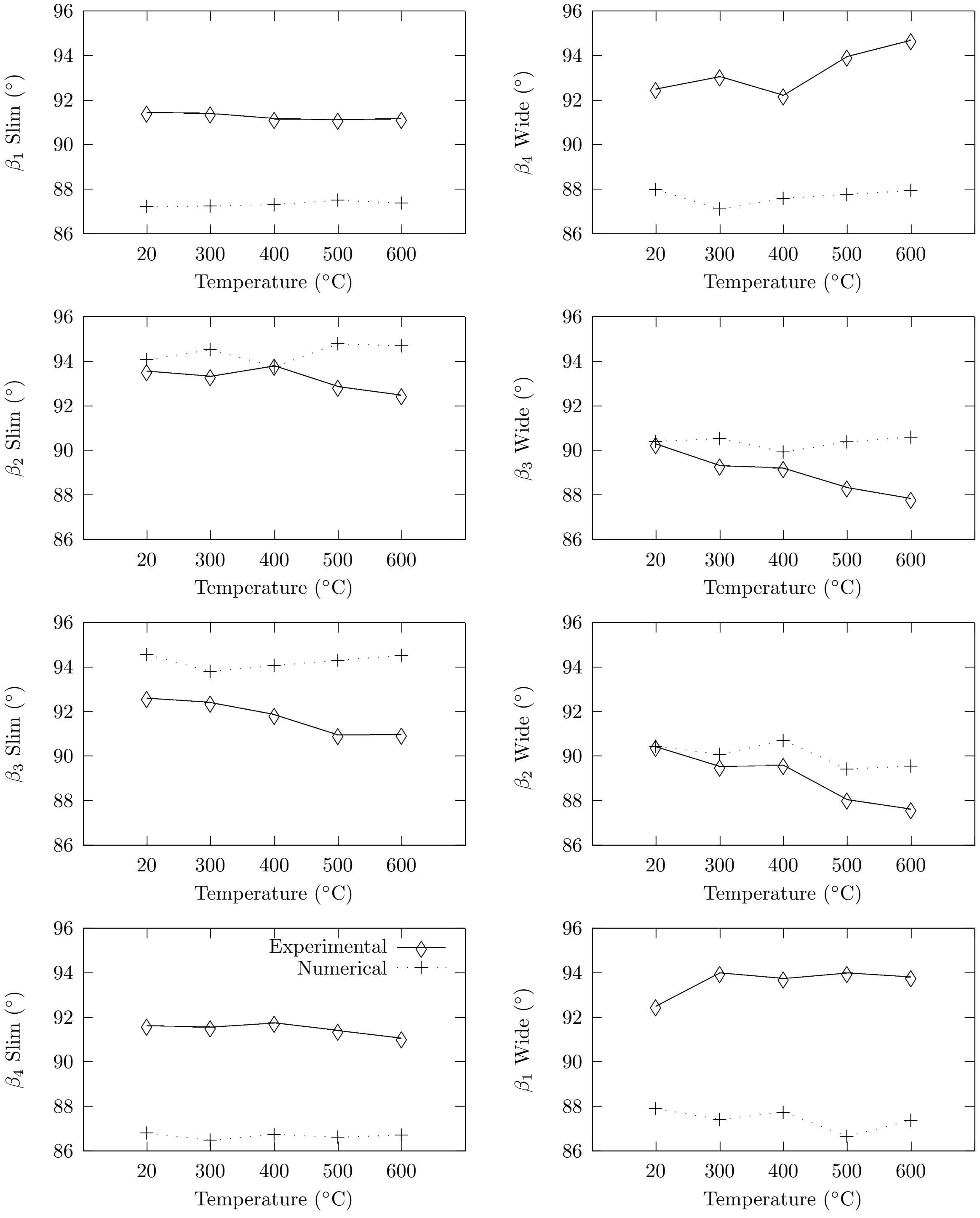

Figure 4.36: Comparison between experimental and numerical values of β_1, β_2, β_3 and β_4 of the slim and wide sections depending on the process temperature.

4.4 Conclusions

Conventional roll forming process is modeled in a first step, in order to analyze the reliability of the developed numerical models. For this purpose, experimental and numerical values of the longitudinal bow, transversal angle, the peak strain and final residual strain in the longitudinal and transversal directions, the forming loads and torques are compared for different material strengths. The numerical and experimental results shows a similar behavior for different material strengths in all the analyzed parameters. However important differences are achieved when numerical and experimental values of bent angles and forming torques are compared.

Heat assisted flexible roll forming process is modeled in order to identify the most appropriated heating strategy and heating temperature during the experimental work. The numerical results show a decrease of 31.3% and 15.3% respectively on the relative and total web warping when the flexible profile is heat assisted in the vertical zone at 600°C. Numerical results shows that the heat assistance is a suitable procedure to decrease the characteristic web warping of flexible roll formed profiles.

Chapter 5

Experimental tests

Perita manus mens exculta

" A skilled hand cultivated mind "

Synopsis

Very little research has been performed in the field of heat assisted roll forming of sheet metals. Therefore, in this chapter heat assisted flexible roll forming experiments carried out for CP800 material are exposed. In the first part, experiments carried out at room temperature in a conventional roll forming machine are described. These experiments, were carried out in order to validate the numerical roll forming models developed in Chapter 4. Additionally, the influence of the material strength is analyzed on different important parameters of roll forming process.

In the second part of the current chapter, experiments of the heat assisted flexible roll forming process are explained. Experiments, performed in a semi industrial machine showed a significant reduction of the web warping when the profiles were heat assisted. Finally, the benefits of the heating are outlined and the microstructure and the final properties of the formed profiles are analyzed.

A paper based on the work described in this chapter was presented in *Advances in Materials and Processing Technologies conference, AMPT2010,* [Lar10a]

5.1 Introduction

Due to the fact that the flexible roll forming and heat assisted roll forming processes are relatively new processes, Chapter 2 is dedicated solely to explaining and reviewing the investigations performed in the field of roll forming, flexible roll forming and heat assisted roll forming technologies. Thus, the reader is referred to Chapter 2 in order to understand in detail the basic problems of the cited technologies.

The first part of the present chapter deals with the experimental work carried out in order to validate the numerical model of the conventional roll forming process developed in Chapter 4. For this purpose, MS1200, CP800, DP600 and DC01 sheet materials mechanically characterized in Chapter 3 are roll formed in the specially designed roll forming machine at the laboratories of the Mondragon University. During the experiments, the longitudinal and transversal strains, the forming loads and torques and the final geometry of the profile are measured.

The second part of the present chapter deals with the heat assisted flexible roll forming of CP800 material experiments. The experiments carried out in a semi-industrial flexible roll forming prototype showed a slight reduction of the longitudinal web warping when the flexible profiles are heat assisted. Finally, different experiments to analyze the effect of the heat assistance in the local and global properties of the profile are also shown. Tensile tests and microstructural analysis with samples extracted from the heat affected area are performed in order to analyze the effect of the temperature in the local properties of the profile. On the other hand, bending and torsion tests ae performed in order to quantify the effect of the heat assistance in the global structural behavior of the profiles.

5.2 Conventional roll forming experiments

5.2.1 Objectives of the experimentation

In order to validate the numerical models of conventional roll forming process, simple roll forming experiments were carried out. Roll loads, roll torques, the longitudinal and transversal strains and the geometry of the profile were measured experimentally. The experimentation was performed using MS1200, CP800, DP600 and DC01 sheet steels in order to validate the numerical models in a wide range of material strength.

5.2.2 Experimental procedure

Conventional roll forming prototype

Basic experiments of conventional roll forming were carried out in the laboratories of the Mondragon University. For this purpose, a roll forming prototype was designed and fabricated. The roll forming prototype was composed of two forming lines, which were composed at the same time of three roll forming stations. This machine configuration was selected to save fabrication costs and space, and allows the forming of two different profile geometries at the same time. Additionally, both forming lines can be combined, forming the workpiece first in one forming line and subsequently in the second forming line.

The machine configuration allows the modification of different important parameters of roll forming process: the distance between the stations, the distance between the rolls, the speed of the line and the geometry of the roll formed profile combining different rolls. The roll forming prototype was also provided by forming load and torque measurement systems. The design and the experimental roll forming prototype are shown in Figure 5.1 a and b respectively.

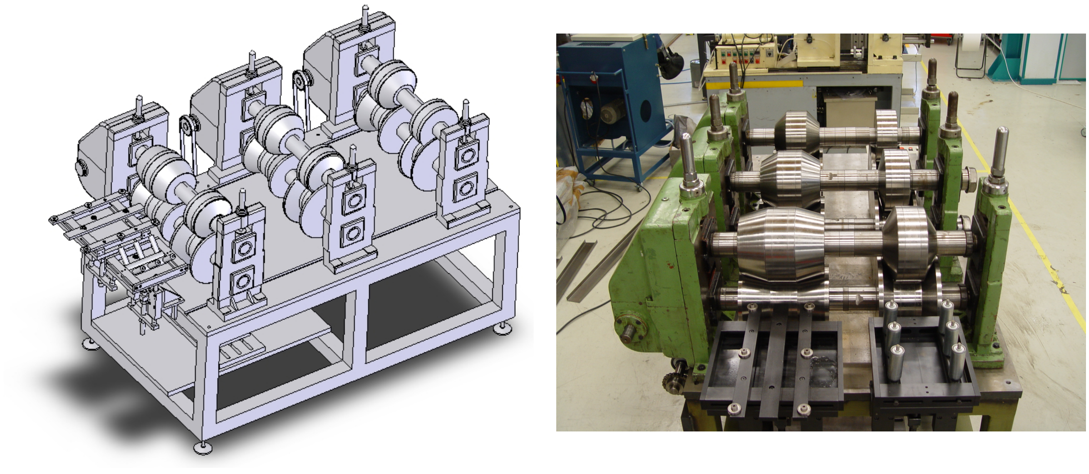

a) b)

Figure 5.1: (a) Conventional roll forming prototype design and (b) conventional roll forming prototype.

Profile geometry and forming sequence

The selected profile for the study was a U channel profile. The undeformed strip was bent in one step to 30°. The final profile is composed by 37.5 mm flange length, 93 mm width and an 2 mm inner radius. The profile was made by e = 1.5 mm thick sheets of MS1200, DP600 and DC01 materials and e = 1.2 mm thick sheets of CP800 steel. The geometry of the selected profile and the forming rolls are shown in Figure 5.2 a and b respectively.

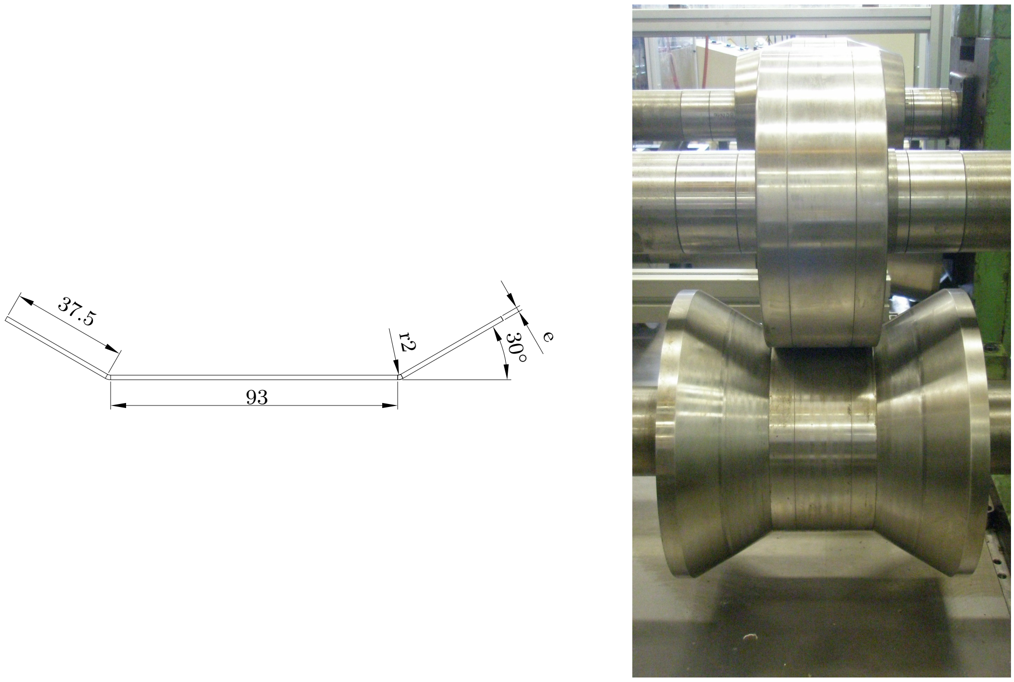

a) b)

Figure 5.2: (a) Selected U profile for the study and (b) rolls used to roll form the profile.

In the current study, only one line of the conventional roll forming prototype was used. The first and the last stands were used as flat rolls and in the second stand the sheet was bent to 30°. The radius of the upper and bottom rolls were 192.2 mm and 99.3 mm respectively. The upper roll of the second stand was not motor driven and rotates freely while the bottom roll applied the torque to form the sheet.

This simple configuration was selected in order to avoid any influence of the first and third stands and between the upper and lower roll, during the torque and load measurement. The distance between the roll forming stations was 750 mm and 2 m long precut sheets were used.

The load and torque are directly dependent on the gap between the forming rolls and on the sheet thickness. Thus, the same gap as the sheet thickness was selected for the study. A distance of 1.5 mm was used with MS1200, DP600 and DC01 materials, and 1.2 mm with CP800 material.

Force and torque measurement

Two Kistler 91071A load cells mounted between the shafts and the machine frame were used to measure the forming load. The roll torque was measured using a Burster 8645-E torque sensor. The torque sensor was mounted within the kinematics of the machine. The position of the load and torque sensors mounted in the roll forming machine can be seen in Figure 5.3 a and b.

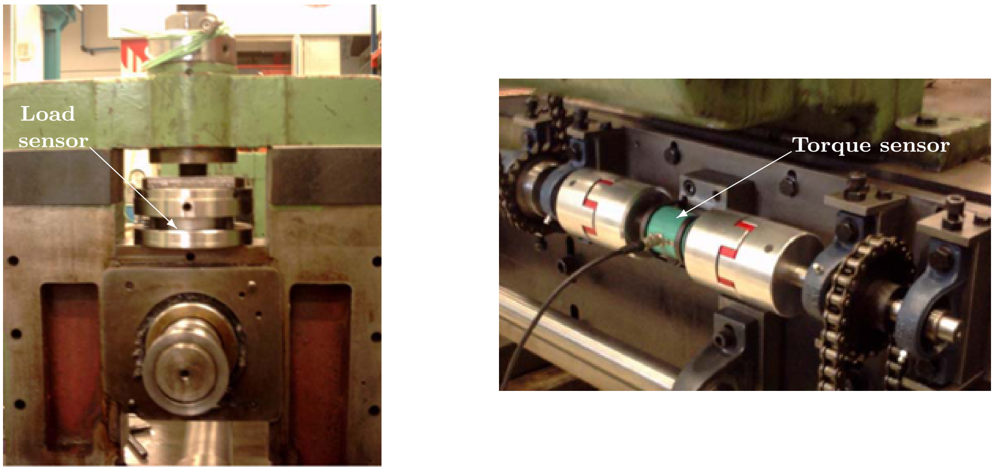

a) b)

Figure 5.3: (a) Kristler 91071A load cells and (b) Burster 8645-E torque sensor used to measure the forming load and torques during experimentation.

The lineal speed of the profile was fixed to 5 m/min and was measured using an encoder. The data acquisition was carried out using equipment from National Instrument and LabVIEW software.

Longitudinal and transversal strain measurements

The longitudinal and transverse strains on the upper surface of the flange edge were measured using CEA-06-125UT-350 type strain gages from Vishay Micro-Measurement. These gages were glued longitudinally in the center of the sheet and at 1.5 mm from the edge. The strain gages were composed of two measurement grids, one grid was used to measure the longitudinal strain (0°) and the second was used to measure the transversal strain (90°). The strain measurement, was carried out using a quarter Wheatstone bridge for each strain gage. The strain gages installation consisted of first cleaning the surface with acetone and grinding the surface at 0°, 45° and -45° using 120 grit SiC paper and then using 400 grit SiC paper. The strain gages were glued using a M-Bond 200 adhesive from Vishay [Vis09].

5.2.3 Experimental results of conventional roll forming test

Profile geometry

Roll formed profiles were measured using a 3D coordinate measuring machine Mitutoyo BHN710. Cross sections at 500 mm, 1000 mm and 1500 mm from the edge of the profile were measured, and the angles β were calculated. The measured cross sections are shown schematically in Figure 5.4.

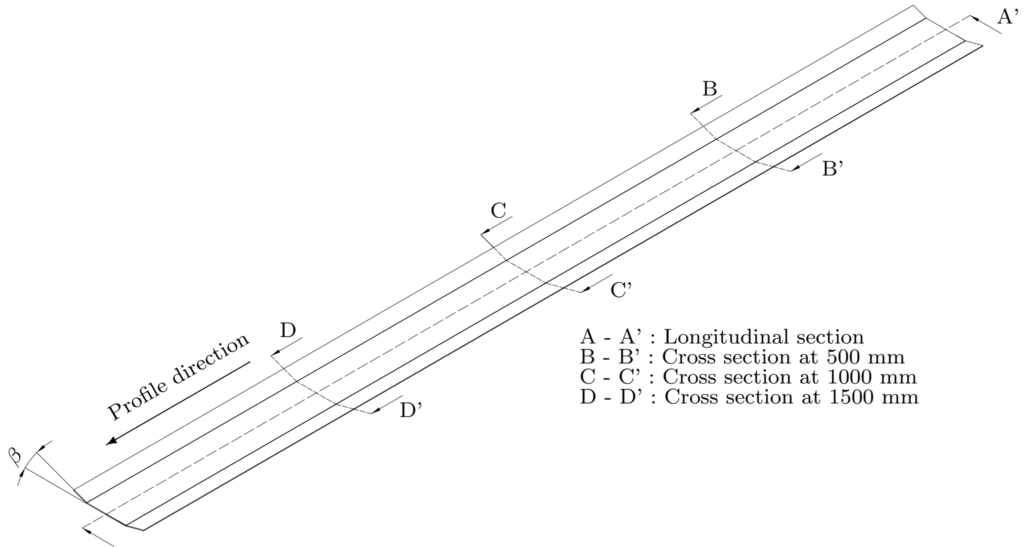
A'
B
B'
C
C'
D
D'
Profile direction
β
A
A - A' : Longitudinal section
B - B' : Cross section at 500 mm
C - C' : Cross section at 1000 mm
D - D' : Cross section at 1500 mm

Figure 5.4: Measured longitudinal and transversal cross sections at 500 mm, 1000 mm and 1500 mm from the edge of the profile.

Due to the space limitation only 1 m long cross sections can be measured using the 3D measurement machine. For this reason, the longitudinal bow was measured only in the middle of the profile, along the cross sections, between 500 mm and 1500 mm (cross sections A-A' is shown in Figure 5.4).

Effect of the material strength in the longitudinal and transversal cross sections

The longitudinal bow error is defined as the longitudinally round shape taken by the profile after the forming stage, (see Figure 2.6). Profiles produced with different materials are shown in Figure 5.5.

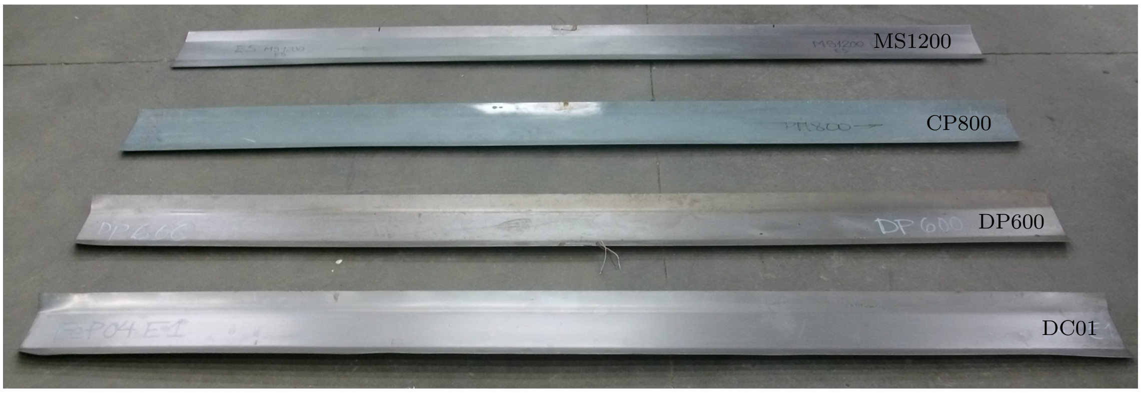

Figure 5.5: Profiles fabricated with different materials show different longitudinal bow deffect.

Analyzing the effect of the material strength in the final longitudinal bow, it can be concluded that: when the roll formed material strength increases the longitudinal bow decreases. The longitudinal bows of the profiles formed with different materials are shown in Figure 5.6.

The longitudinal bow is produced due to the difference in length between the edge of the flange and the bending line of the profile. During the forming process, the edge of the profile is stretched to such a degree that it is plastically deformed. After the last forming stand, the profile takes a longitudinally round shape in order to reach the equilibrium state [Hal05].

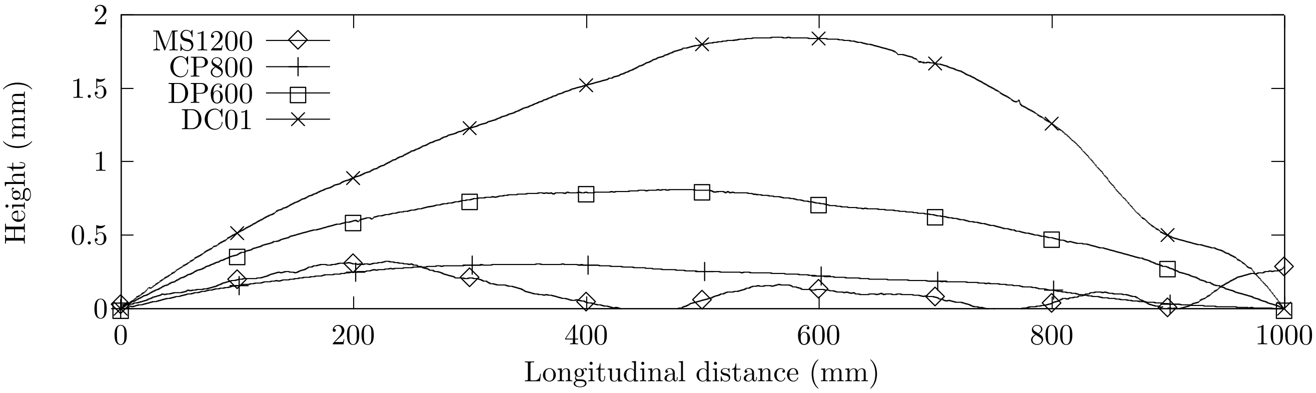

Figure 5.6: Longitudinal bow of profiles fabricated with different materials.

It is seen later on that DC01 and DP600 materials exceeded the longitudinal plastic limit in the flange of the profile leading to residual longitudinal strains and thus to a high values of longitudinal bow error. Longitudinal bow error is larger for these materials than MS1200 and CP800 materials, which do not present any longitudinal plastic deformations. Figure 5.7 shows measured and experimental cross sections at 1000 mm from the edge of the profiles formed with different materials.

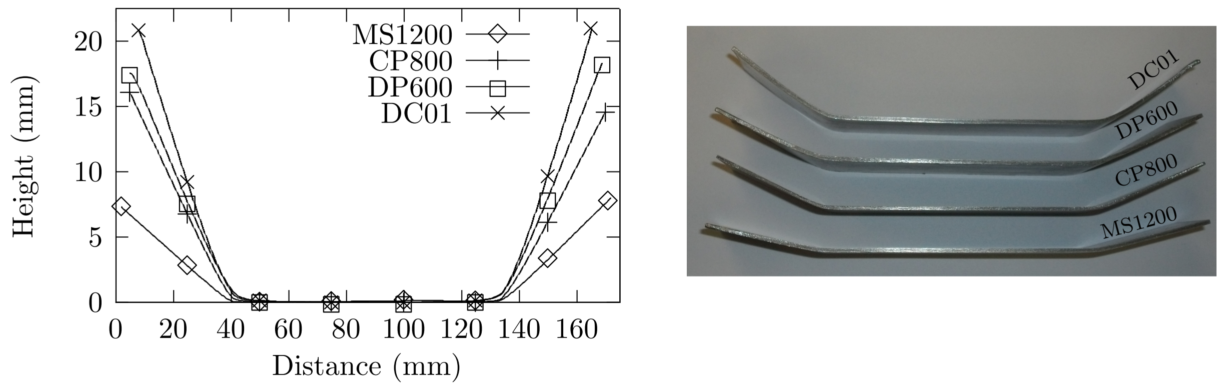

a) b)

Figure 5.7: (a) Measured and (b) experimental transversal cross sections.

The evolution of the longitudinal bow and measured angle depending on the material strength are shown in Figure 5.8. As it was expected, when the strength of the material increases, the springback of the profile increases and the final angle of the profile decreases.

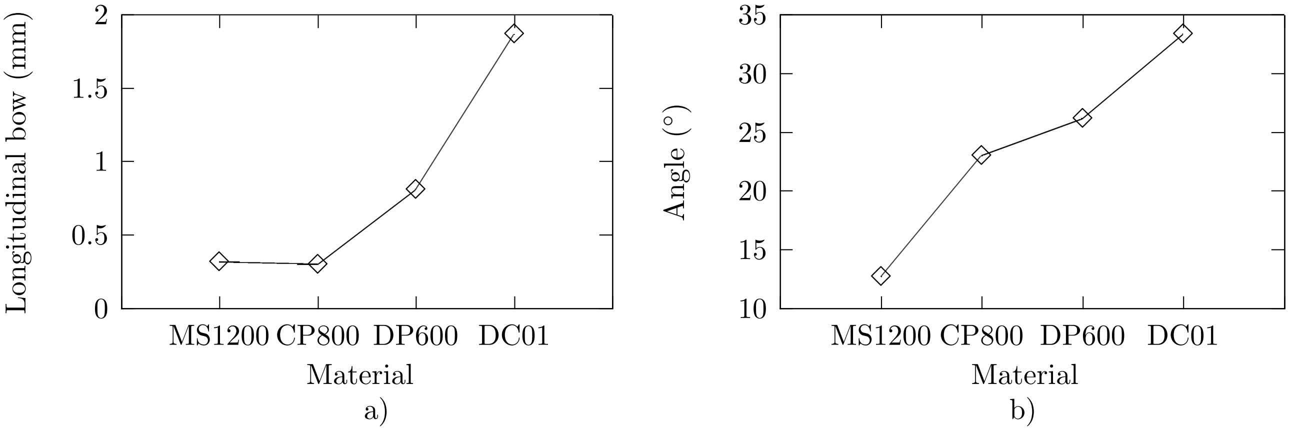

Figure 5.8: (a) Longitudinal bow and (b) measured angle depending on the material strength. The average and standard deviation values of the measured longitudinal bow and angles are summarized in Table C.1 of appendix C.

The profile formed with DC01 material presents a higher bending angle than 30°. The flange presents a transversal bow error and the flange is arc-shaped, (see Figure 5.7). In soft materials like DC01, if the forming step is too severe, as is the case, not only longitudinal, but also transversal bow occurs. Transversal bow occurs before the forming station due to the shape taken by the profile [Hal05]. Measurements show a bend angle of 30° near the radius and 34° near the edge of the flange. High strength steels do not show this effect.

Effect of the material strength on the longitudinal and transverse strains

The longitudinal and transversal strains were measured in the edge of the profile using strain gages. The different measurements of the longitudinal and transversal strain can be seen in Figure 5.9.

Analyzing the longitudinal strains during the experiments, four different deformation stages are identified as described in section §4.2.2: Longitudinal compression stage, longitudinal stretching, peak strain and final residual longitudinal strains. The transversal strains show a similar behavior as the longitudinal strains. Comparing the effect of the material strength on the longitudinal and transversal peak strain and on the residual strains, it can be concluded that: The longitudinal and transversal peak strain slightly increases when the material strength decreases, while the longitudinal and transversal final residual strains increases when the material strength decreases. These results are in concordance with results obtained by Lindgren [Lin07a] and Zhu [Zhu93].

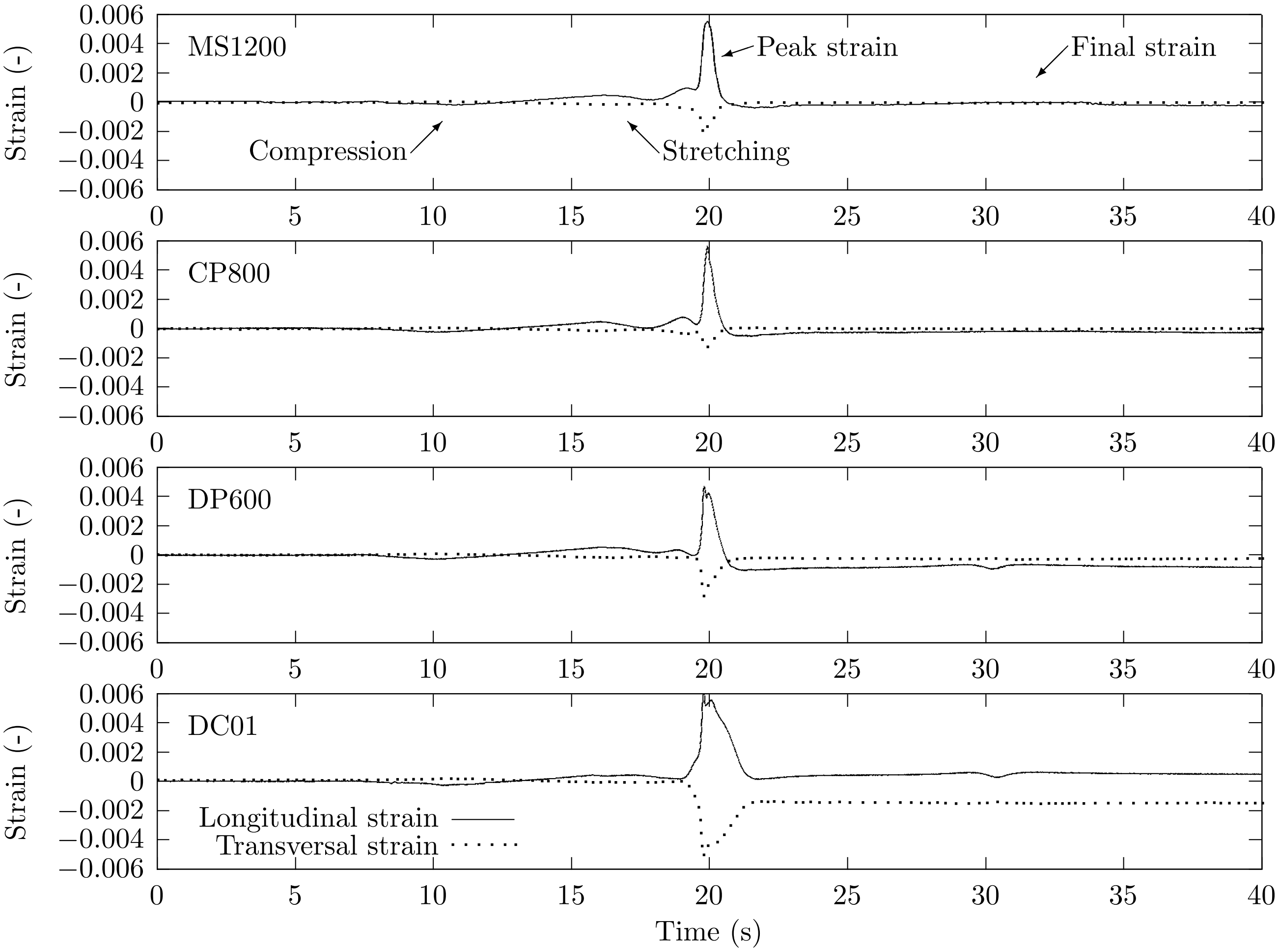

Figure 5.9: Longitudinal and transversal strains of the edge of the profile for different materials.

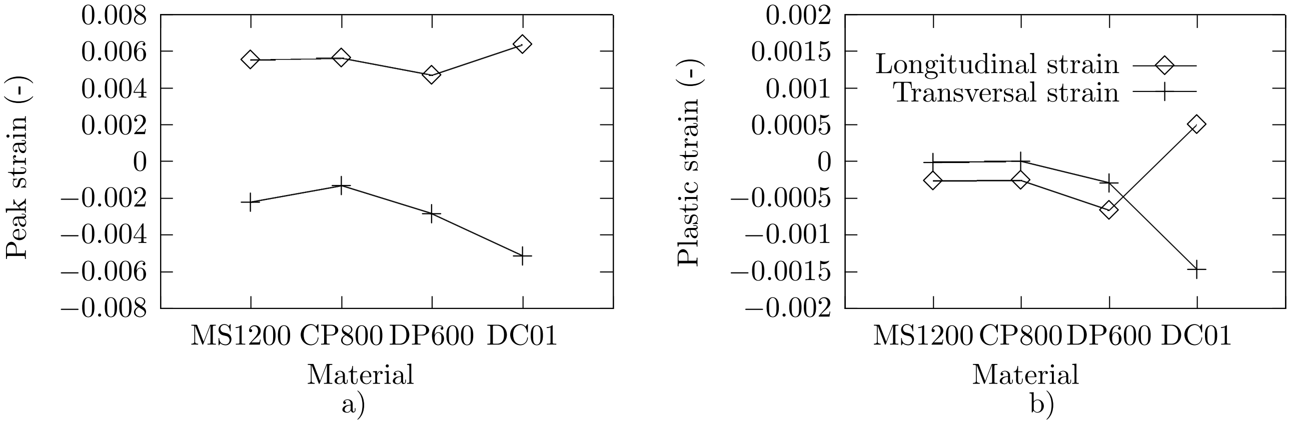

Figure 5.10: Longitudinal and transversal (a) peak strains and (b) residual plastic strain values depending on the material. The average values are summarized in Table C.2.

Effect of the material strength on the forming forces and torques

The forming load and torques were measured during the forming of the profile. As example, the load and the torque corresponding to CP800 material roll forming experiment is shown in Figure 5.11.

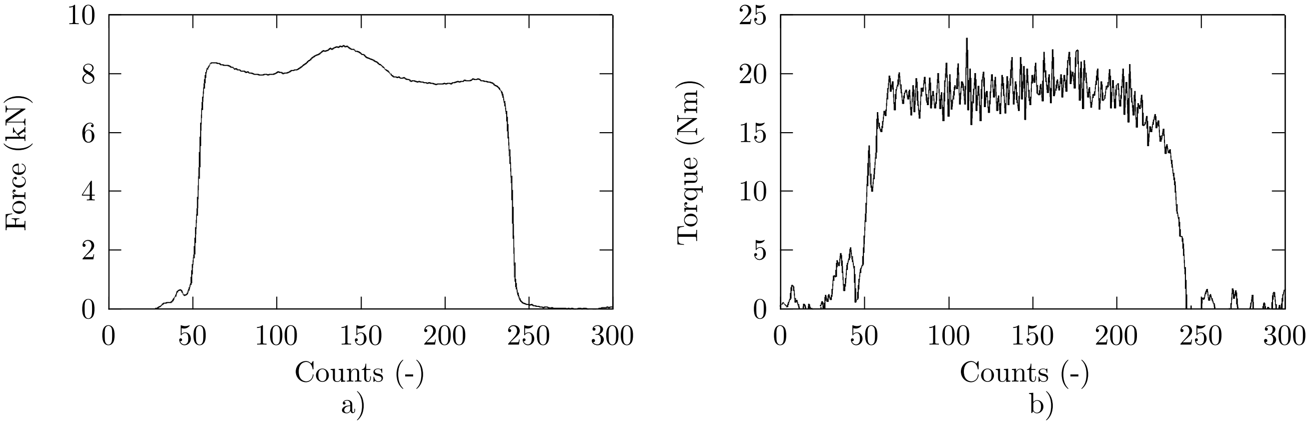

Figure 5.11: Measured (a) forming forces and (b) forming torques during the forming of CP800 material profile.

In all the experiments, similar values of forming loads and torques were obtained for each material. The oscillation of the load and torque values during the forming is attributed to the eccentricity of the forming rolls. When the gap between the rolls decrease, the forming loads and torques increase. The effect of the material strength on the forming load and torques is shown in Figure 5.12.

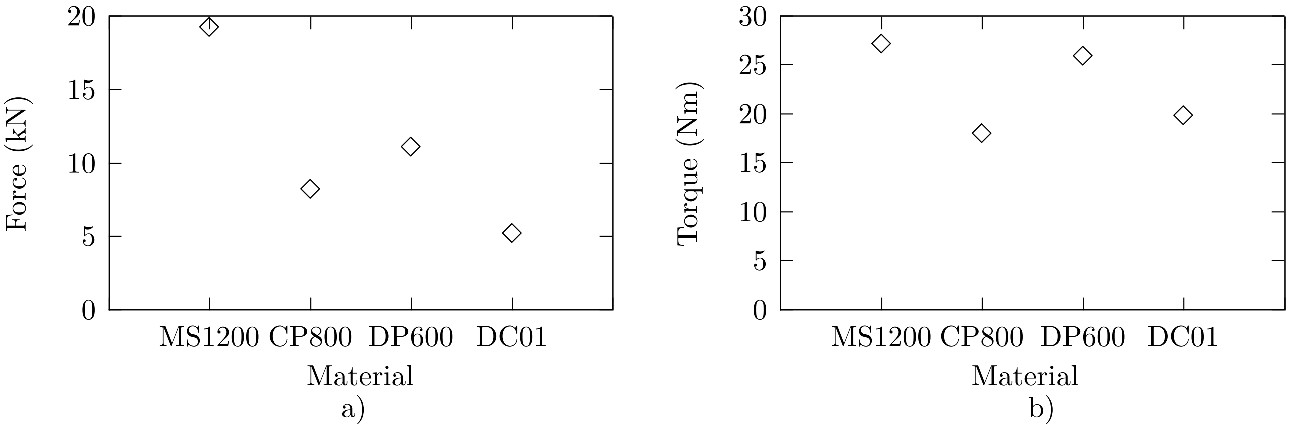

Figure 5.12: (a) Forming loads and (b) torques depending on the formed materials. The average and standard deviation values of the measured forming loads and torques are summarized in Table C.3 of appendix C.

As it was expected, the forming load and torques increase directly when the roll formed material strength increases. However, the CP800 material shows a lower forming load and torque, due to its smaller thickness. Similar load and torque values were obtained by Lindgren in [Lin07b], when a U channel was roll formed.

5.3 Heat assisted flexible roll forming experiments

5.3.1 Objectives of the experimentation

As it is explained in Chapter 1, the main objective of the present thesis is to study and developed a method to increase the geometrical accuracy of flexible roll formed parts by means of local heating. Heat assisted flexible roll forming experiments were performed in order to study the limits of the new method in terms of geometrical accuracy.

5.3.2 Experimental procedure

Proform flexible roll forming prototype

Heat assisted flexible roll forming experiments were carried out in the laboratories of Labein-Tecnalia. An experimental roll forming line designed and built up during the Proform European project was used for this purpose. In order to know more about the objectives and the developments of the Proform project, the reader is referred to [Eur10].

The flexible roll forming line was composed by a decoiler and straightener, a flexible laser cutting system and by the flexible roll forming line. The combination with the laser trimming unit was necessary to realize profiles with constant flange length since the initial strip metal was variable in width. Each stand was motorized by a 3 kW geared motor and the maximum speed of the line was 10 m/min. The flexible roll forming line was composed of 9 conventional stands, 8 flexible stands and blank holders positioned successively. The setup of the laser trimming unit and the a flexible roll forming stand, static blank holder and conventional stand are shown in Figure 5.14 a and b respectively.

The forming sequence features a simultaneous forming of the profile leg and profile flange in forming angles of 15°/30°/50°/70°/80°/90°. Because of the slim width of the profile, the last two bending angles of 80° and 90° were formed side by side. The forming sequence of the Proform profile and the disposition of the forming rolls and support rolls are shown in Figure 5.14 a and b successively.

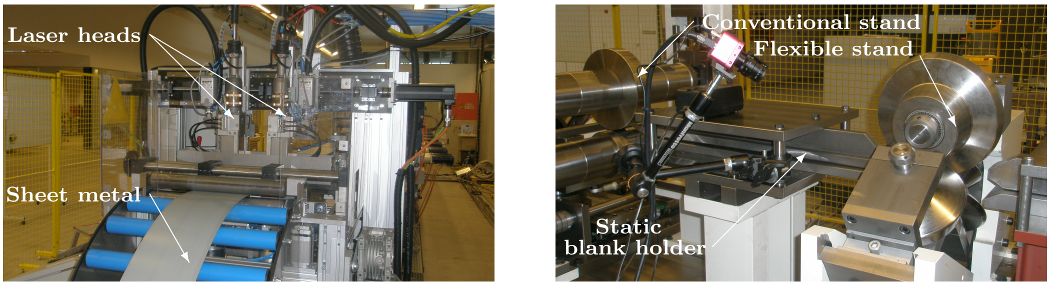
Laser heads
Sheet metal
Conventional stand
Flexible stand
Static
blank holder

a) b)

Figure 5.13: (a) Laser trimming unit and (b) flexible roll forming stand with static blank holder and conventional stand.

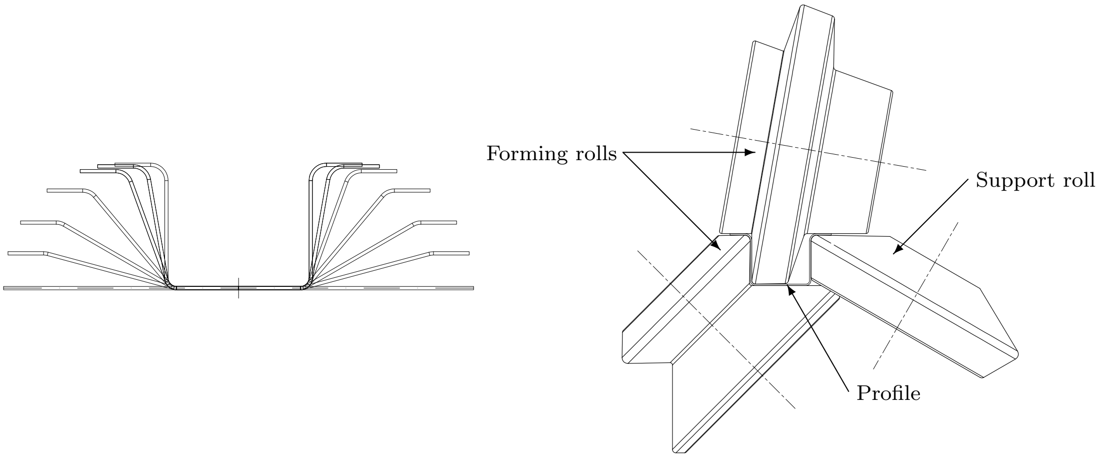
Forming rolls
Support roll
Profile

a) b)

Figure 5.14: (a) Forming sequence of the Proform profile and (b) one side flexible forming stand.

Static blank holders at the entry and the exit of the flexible forming stands were added to support the forming in the transition zones. Only by the effect of the heat assistance was not sufficient to correct the geometrical deviations of the flexible roll formed profiles and additional blank holders were used. In [Abe08] it was shown, that blank holders were necessary to increase the geometrical accuracy of the flexible roll formed U profiles.

Profile geometry and forming sequence

The principle target geometry produced in the Proform line was a width changing hat profile. Within the Proform project a part family was designed to show the flexibility advantages of the flexible roll forming. The parts were manufacturable by modifying the contour in the machine control, but without changing the tools in the line. The target geometry selected for heat assisted flexible roll forming process experiments is shown in Figure 5.15.

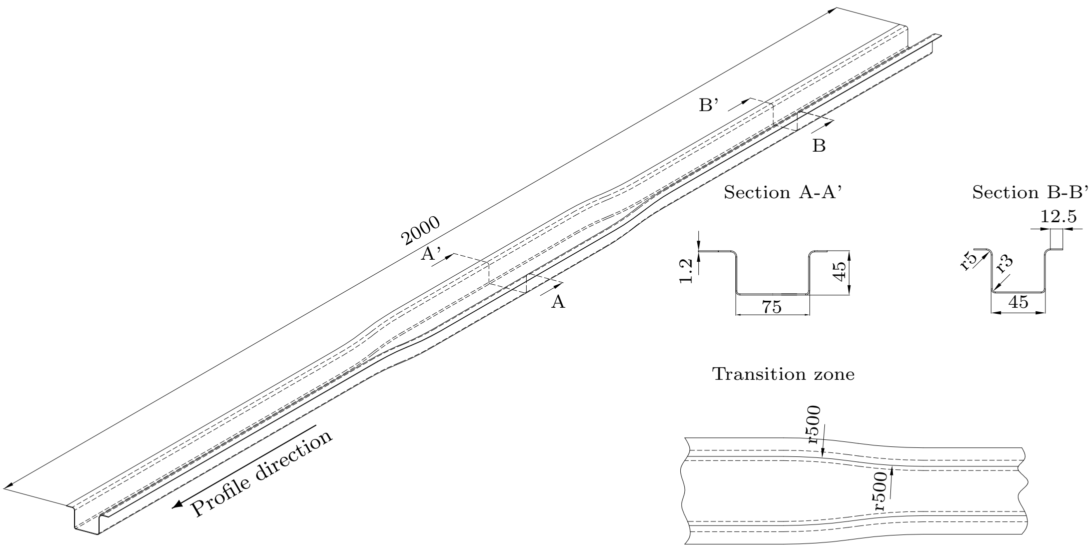

Figure 5.15: Geometry of selected profile for heat assisted flexible roll forming experimentation.

The selected geometry had a contour radius of r = 500 mm. This means a change in the width of 20 mm over a length of 141 mm. During the Profom project, the trends and needs of the automotive industry in the field of BW construction were analyzed by the consortium and the basic profile was selected in order fulfill these requirements. The selected profile is representative of different profiles used in the BW construction, such as offset reinforcement profiles.

Heating method and set-up

The heat assistance to the flexible roll forming was performed using inductive technology. Other heating methods such as resistance heating or laser heating were rejected because: i) By using inductive heating technology bigger areas were able to be heated than by using a laser technology, ii) due to the fact that the heating had to be performed during the fabrication of the profile, heating by means of resistance heaters was not technologically possible, iii) additionally, inductive technology needed smaller investments than laser technology.

The heat assistance was performed using two identical inductive coils and inductive ovens. In order to guaranty the following of the profile contour by the inductive coils, a special mechanical arm was designed and installed in the Proform line. It is out of the scope of the present thesis to perform a deep study on the inductive heating technology and thus the development and optimization of the inductive coils and ovens was subcontracted. The inductive heating system was applied 100 mm before the last forming station. The inductive heating set-up installed in the Proform flexible roll forming line is shown in Figure 5.16.

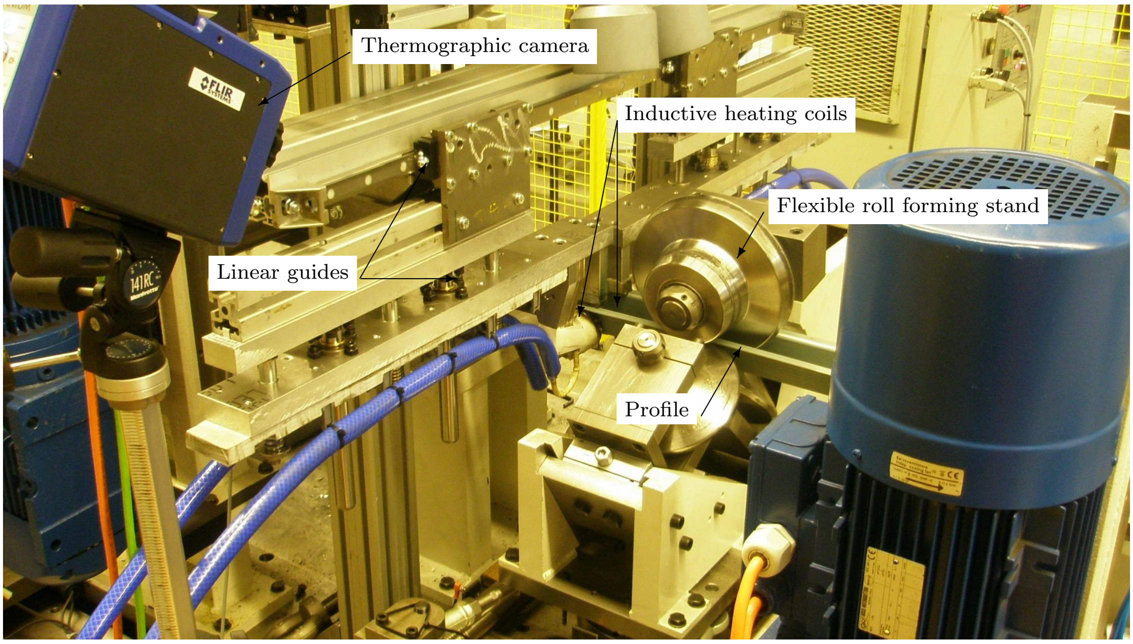

Figure 5.16: Inductive heating device installed in the Proform machine.

The influence of different heating strategies on the web warping are studied numerically in Chapter 4 section §4.3.2. Numerical results showed the biggest improvements when the vertical part of the transition zones were heated. In order to experimentally study the influence of the heat assistance in the final web warping, flexible profiles of CP800 material at five different temperatures (room temperature, 300°C, 400°C, 500°C and 600°C) were manufactured using this inductive heating system.

Temperature measurement by means of calorimetry

Due to the special characteristics of the process, the measurement of the process temperature was dealt by radiation thermometry. Other contact temperature measurement systems such as thermocouples or thermometers were rejected because: i) the thermocouples or thermometers need to be in contact with the surface to measure the temperature, and the measured temperature is dependent on the quality of the contact between the surface and the thermocouple. Since, in roll forming process the sheet is continuously moving, it is difficult to guarantee proper contact conditions. ii) The response time of thermocouples or thermometers is too high to measure the real temperature change during the heating and cooling in heat assisted roll forming processes. iii) Only a punctual temperature measurement can be made using thermocouples and in heat assisted roll forming processes it is interesting to analyze the temperature distribution within the profile.

During the experimentation, the temperature was controlled using a TITANIUM 550LI BB F/3 high speed thermographic camera from Flir System. The camera head was comprised of a 320 by 256 Indium-Antimonide detector array, sensitive to the mid-wavelength infrared (MWIR) (1.0 - 5.0 μm) spectral. The detector assembly was filtered, thus only the radiance signal in the 3.9 μm wavelength was captured. The camera was able to record approximately 400 frames per second in 320 x 256 format.

It is out of the scope of the present thesis to perform a deep study on thermal thermography. Therefore, in the current section only some basics of thermal thermography are explained. Publications about thermal thermography can be found elsewhere (e.g. [DeW88]).

Principles of calorimetry and radiation measurements

The complete electromagnetic spectrum is delineated in Figure 5.17. It is the intermediate portion of the spectrum, which extends from approximately 0.1 to 1000 μm and includes a portion of the ultraviolet, all the visible and infrared, that is termed thermal radiation.

All body at a given temperature emits thermal radiation. Since the emitted radiation is depending on the temperature, the body temperature can be determined by measuring the amount of radiation emitted by the body [DeW88]. However, the radia-

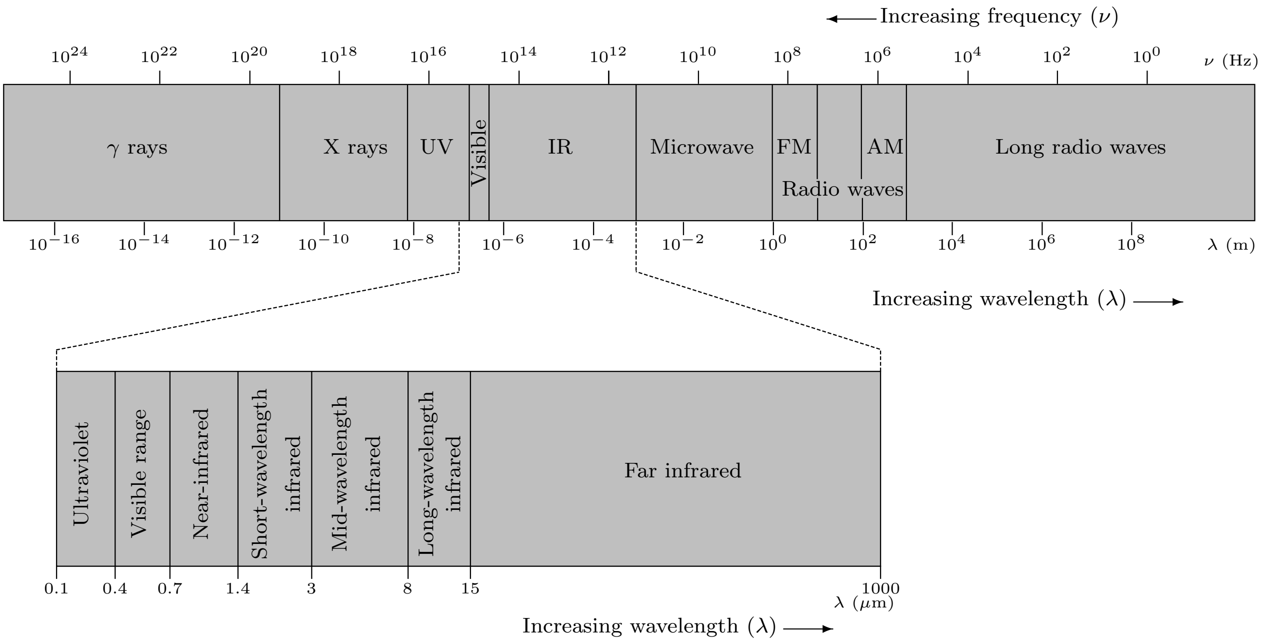
Increasing frequency (ν)
10^{24} 10^{22} 10^{20} 10^{18} 10^{16} 10^{14} 10^{12} 10^{10} 10^{8} 10^{6} 10^{4} 10^{2} 10^{0} ν (Hz)
γ rays
X rays
UV
Visible
IR
Microwave
FM
AM
Radio waves
Long radio waves
10^{-16} 10^{-14} 10^{-12} 10^{-10} 10^{-8} 10^{-6} 10^{-4} 10^{-2} 10^{0} 10^{2} 10^{4} 10^{6} 10^{8} λ (m)
Increasing wavelength (λ)
Ultraviolet
Visible range
Near-infrared
Short-wavelength infrared
Mid-wavelength infrared
Long-wavelength infrared
Far infrared
0.1 0.4 0.7 1.4 3 8 15 1000
λ (μm)
Increasing wavelength (λ)

Figure 5.17: Thermal radiation spectrum comprises part of ultra violet, visible and infrared radiation portion.

tion emitted by a body not only depends on the temperature of the body.

It is considered an object at higher temperature than its surrounding, which around the body exists vacuum and is subjected to a radiation flux from elsewhere. The vacuum condition is important in order to avoid convective and conductive therms. The incoming radiation is absorbed, transmitted or reflected by the body depending respectively on the absorptivity (α_λ), reflectivity (ρ_λ) and transmissivity (τ_λ) of the body. The first law of thermodynamics states that the energy is conserved, thus the incoming radiation quantity must be the same of the sum of reflected, transmitted and absorbed radiation:

$$1 = (\alpha_\lambda + \rho_\lambda + \tau_\lambda) \tag{5.1}$$

However, in order to maintain constant the temperature of the body, the body not only must absorb radiation, it must also loose some energy. Otherwise, the temperature of the body would always increase. Bodies at certain temperature absorb and loose energy emitting radiation. The capability to emit radiation is called emissivity ε_λ. Thus, in thermal equilibrium state, the absorbed and emitted radiation by a body must be the same.

$$\alpha_\lambda = \varepsilon_\lambda \tag{5.2}$$

Absorptivity and emissivity as well as reflectivity and transmissivity varies with the wavelength λ, temperature T and with the angle θ between the body and the incoming radiation.

At this point, it is interesting to explain the concept of the black body, gray body and real bodies. The black body is an ideal emitter or absorber, this means that all radiation (independently of the wavelength or temperature) that it receives is absorbed and emitted. In nature, real black bodies do not exist and the concept of grey bodies is used. Grey bodies have constant emissivity, absorptivity and transmissivity. The term real bodies refers to anything that is not a blackbody nor a greybody.

Spectral nature of radiation

A unity of radiative flux emitted by a black body in certain wavelength λ and at certain temperature T for an infinitesimal solid angle is defined by the Planck's law:

$$R_{\lambda,\mathrm{b}}(\lambda,T) = \frac{2\mathrm{hc}^2}{\lambda^5\left[e^{(\mathrm{hc}/\lambda \mathrm{C}_{\mathrm{Bolt}} T)} - 1\right]} \tag{5.3}$$

where h is the Plank's constant, c is the speed of the light in vacuum and $\mathrm{C}_{\mathrm{Bolt}}$ is the Boltzmann's constant. The Planck law for different temperatures is plotted in Figure 5.18 a.

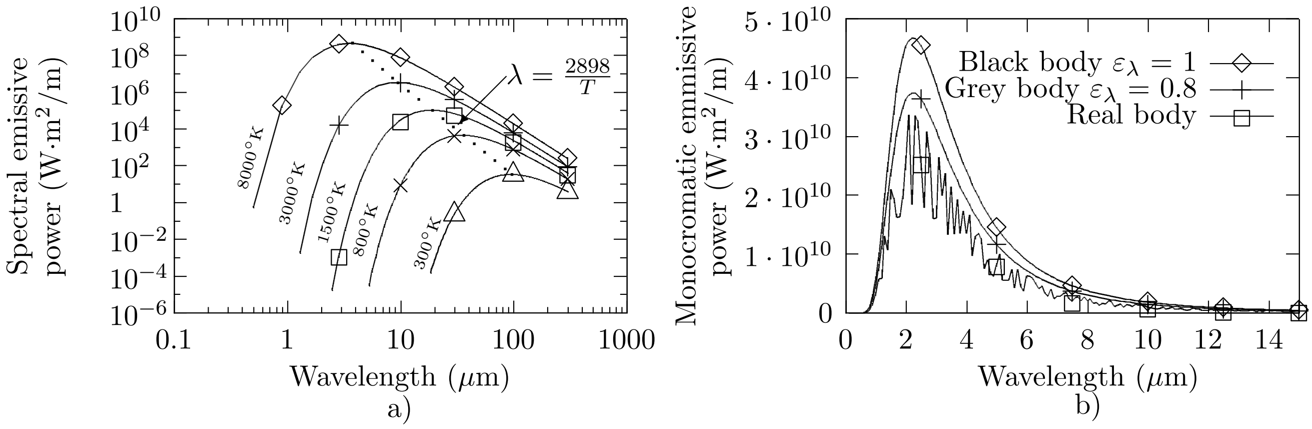

Figure 5.18: (a) Spectral radiance of a black body at different temperatures and (b) comparison between the emissive power of different body types at 1000°C.

It can be noted that, the emitted radiation varies continuously with wavelength, at any wavelength the magnitude of the emitted radiation increases with increasing temperature and the spectral region in which the radiation is concentrated depends on temperature. Additionally, the spectral distribution of the black body is characterized by a maximum. Knowing the spectral radiance of the blackbody as given by the Planck distribution law, (Eq. 5.3), the total existence can be identified integrating the Eq. 5.4 as:

$$M_{\mathrm{b}} = \int_0^\infty M_{\lambda,b} \cdot d\lambda = \int_0^\infty \frac{2\mathrm{hc}^2}{\lambda^5 \left[e^{(\mathrm{hc}/\lambda \mathrm{C}_{\mathrm{Bolt}} T)} - 1 \right]} \tag{5.4}$$

with the results that

$$M_b = \mathrm{C}_{\mathrm{Bolt}} \cdot T^4 \tag{5.5}$$

These results, termed the Stefan-Boltzmann law, enables calculation of the radiant flux density emitted in all directions and over all wavelengths simply by knowing the temperature of a blackbody.

On the other hand, it is interesting to know the range at which the radiance intensity is maximum. The maximum of spectral distribution is described by the Wien's displacement law that is temperature dependent. The locus of the points described by the Wien's displacement law (Eq. 5.6) is plotted as the dashed line in Figure 5.18 a.

$$\lambda_{max} = \frac{2897.7}{T} \tag{5.6}$$

It can be noted that the maximum of the spectral radiance is displaced to shorter wavelengths with increasing temperature. This expression is important since the Wien's law expressed the maximum emitted radiance depending on the temperature, and only measuring a short wavelength region around the peak, the greatest part of the radiance can be measured.

However, real radiation measurements systems acquire the radiance in a narrow spectral range and the detectors are calibrated to measure the temperature depending on the received radiation. In the current case, the TITANIUM 550LI BB F/3 high speed thermographic camera from Flir System provided by filter only captured 3.9 μm wavelength radiance. The temperature range that it was able to measure was adjusted with the so called integration time.

The integration time is defined as the time that the detector is exposed to the radiation source. If the source of radiation is faint the captor needs higher integration time to capture a measurable quantity of radiation. On the other hand, if the received radiation is too high the integration time must be smaller. In the current thesis the integration time was selected to measure temperatures between 300°C and 1700°C.

Emissivity concept

However, in grey or real bodies the emissivity of the surface must be taken into account. As it is explained in section §5.3.2, the emissivity of a real body is always lower than the emissivity of a black body. The relation between the spectral radiance of a real body at certain temperature and the spectral radiance of a black body at the same temperature is defined as the spectral emissivity. Thus, the emissivity is the relation between the emitted energetic flux by a real body and a black body at certain wavelength.

$$\varepsilon_\lambda(T,\lambda,\theta) = \frac{R_\lambda(T,\lambda,\theta)}{R_{\lambda,b}(T,\lambda,\theta)} \tag{5.7}$$

The emissivity is a superficial property of materials, and it depends on the temperature, measured wavelength, surface roughness, physical state of the material, the surface oxidation and the angle between radiation source and receptor. Additionally, the accuracy of the temperature measurement depends on the emissivity value. The smaller the emissivity of the body is, the higher the uncertainty of the temperature measurement is [Ald09].

Emissivity measurement experimental procedure

It can be concluded that, during the temperature measurement of real surface, the emissivity plays a significant role. Thus, the measurement of the emissivity is also important. Currently, no theory exists to determine the emissivity of real bodies, thus, emissivity must be experimentally determined. There are different ways to determine and control the emissivity of real surfaces:

- Heat a sample material to a known temperature, using a precise sensor, and measure temperature using an IR instrument. Then adjust the emissivity value to force the indicator to display the correct temperature.
- For relatively low temperatures (<300°C), the temperature of a piece of masking tape, with an emissivity of 0.95 for example, can be measured using an IR instrument. Then the emissivity value is adjusted to force the indicator to display the correct temperature of the material
- For medium-high temperatures, if the material or a portion of it, can be coated with a dull black paint it will have an emissivity value of aproximatly 1.0. Measure the temperature of the paint, and then adjust the emissivity to force the indicator to display the correct temperature.

- For high temperature measurements, a hole (depth of which is at least 10 times the diameter) can be drilled into the object. This hole acts as a blackbody with emissivity of approximately 1.0. Measure the temperature in the hole, and then adjust the emissivity to force the indicator to display the correct temperature of the material

During the experimentation, in order to control the emissivity, the surface of the profiles were coated with a commercial dull black paint before the heating process. A commercial silicon based paint for high temperature applications from Motip Dupli GmbH was used. According to the specifications the paint was able to resist temperatures up to 690°C.

The emissivity of the black paint was determined experimentally using a Fourier transformer spectrometer type FT-IR, at the Department of Condensed Matter Physics at the University of the Basque Country. The experimental setup permits the measurement of the emissivity depending on the wavelength, emission angle and the sample temperature. The experimental setup is provided with an hermetic chamber which permits the measurement of the emissivity in different atmospheric conditions [CG07]. The emissivity was determined comparing the acquired signal spectrum of a black body $S_{\lambda,b}(T)$ and the real body $S_\lambda(T)$ for different temperatures and wavelengths.

$$\varepsilon_\lambda(T,\lambda) = \frac{S_\lambda(T)}{S_{\lambda,b}(T)} \tag{5.8}$$

Emissivity measurements were made at different temperatures starting from 100°C up to 500°C and between the 1.5 and 25 μm wavelengths. A maximal initial temperature of 600°C was selected, however at 500°C the painted samples were damaged, thus the emissivity measurement was stopped. Emissivity measurements were made only taking into account the temperature and wavelength effect. Other affecting parameters rather than measurement angle between emitter and receptor, or the oxidation of the surface were not considered.

5.3.3 Experimental results of heat assisted flexible roll forming test

Emissivity experimental results

High values of emissivity are obtained for the selected black paint in all the wavelength range. At short wavelengths ($\lambda < 7\mu$m) similar values of emissivity are obtained for all temperatures. However, at larger wavelength the dispersion between the emissivity values increase. This dispersion is higher at low temperatures and at high temperatures similar values of emissivity are obtained. The emissivity values depending on the temperature and the wavelength are shown in Figure 5.19 a.

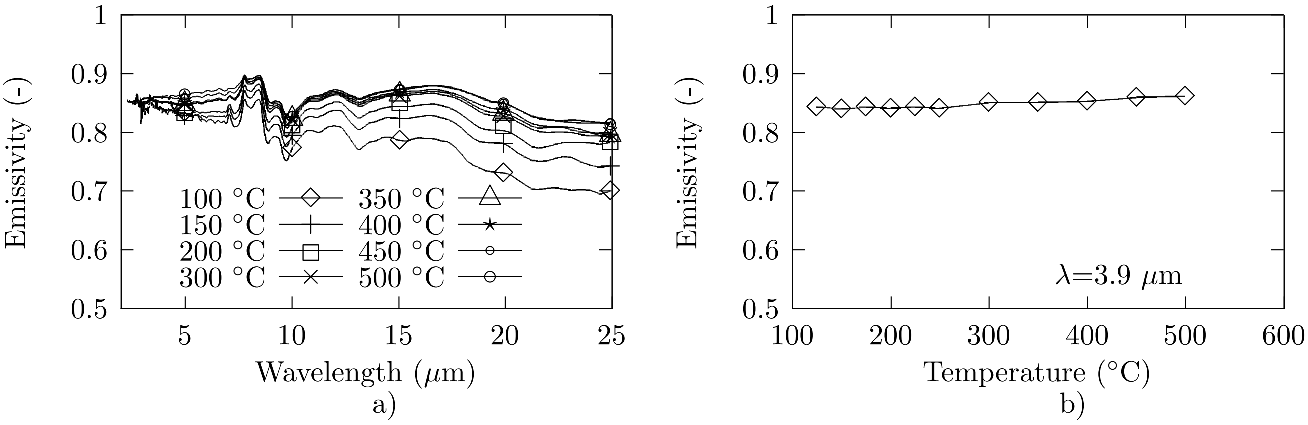

Figure 5.19: (a) Emissivity values of used black paint depending on the wavelength and temperature and (b) emissivity values at different temperatures at 3.9 μm wavelength.

Emissivity values depending on the temperature for 3.9 μm wavelength are shown in Figure 5.19 b. Similar values of emissivity are obtained for all the temperature range. However, a slight increase of the emissivity value can be noticed when the temperature increases. In the current dissertation, the average value of the emissivity $\varepsilon_\lambda = 0.848$ with the standard deviation of $\varsigma_{\varepsilon_\lambda} = 0.008$ was selected.

Heating experiment results

During the experimentation, the camera is positioned in such a way that it is able to measure the temperature in both heated surfaces. The thermal image of the heated area is shown in Figure 5.20.

Due to the fact that during the experimentation it is difficult to control the temperature distribution along the profile, the temperature distribution is not homogeneous in the profile. The inductive coil heating area was bigger than the surface to be heated, and consequently the inductive coils concentrated the highest temperatures in the bottom

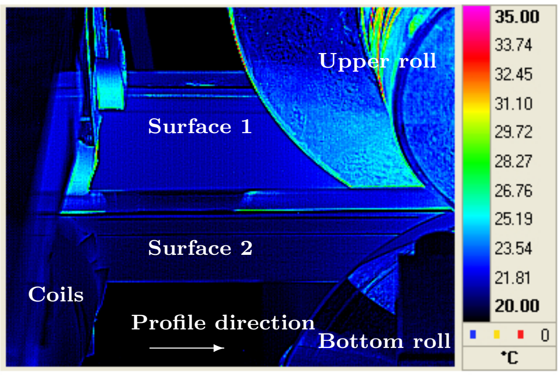
Upper roll
Surface 1
Surface 2
Coils
Profile direction
Bottom roll
35.00
33.74
32.45
31.10
29.72
28.27
26.76
25.19
23.54
21.81
20.00
0
°C

Figure 5.20: Thermal image of the controlled surfaces in the profile.

side of the vertical flange. However, it is show in Chapter 4, that the strain concentration was higher in the upper part of the profile. It would be more interesting to achieve the highest temperatures in those zones where the strains were larger. For example the temperature distribution along the vertical flange during the heat assisted flexible roll forming trial is shown in Figure 5.21 a. The temperature change along the profiles 1 and 2 are plotted in Figure 5.21 b.

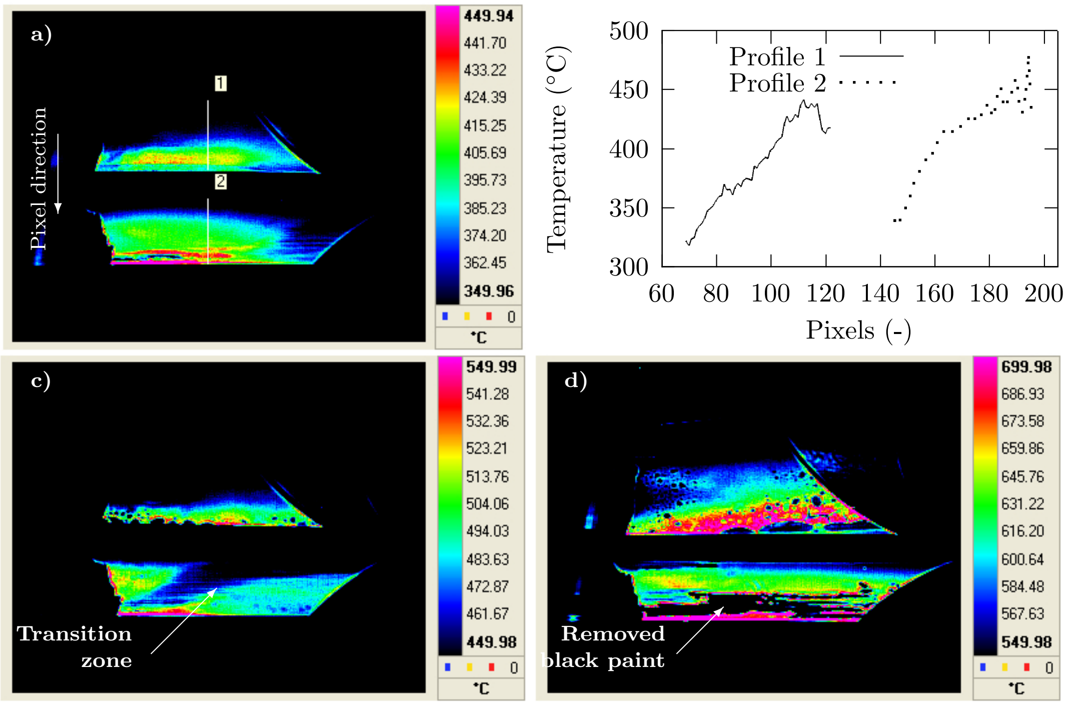

Figure 5.21: (a) and (b) not homogeneous temperature distribution in the profile, (c) zones in transition remains without heating and (d) at highest temperatures the black paint is removed in certain zones.

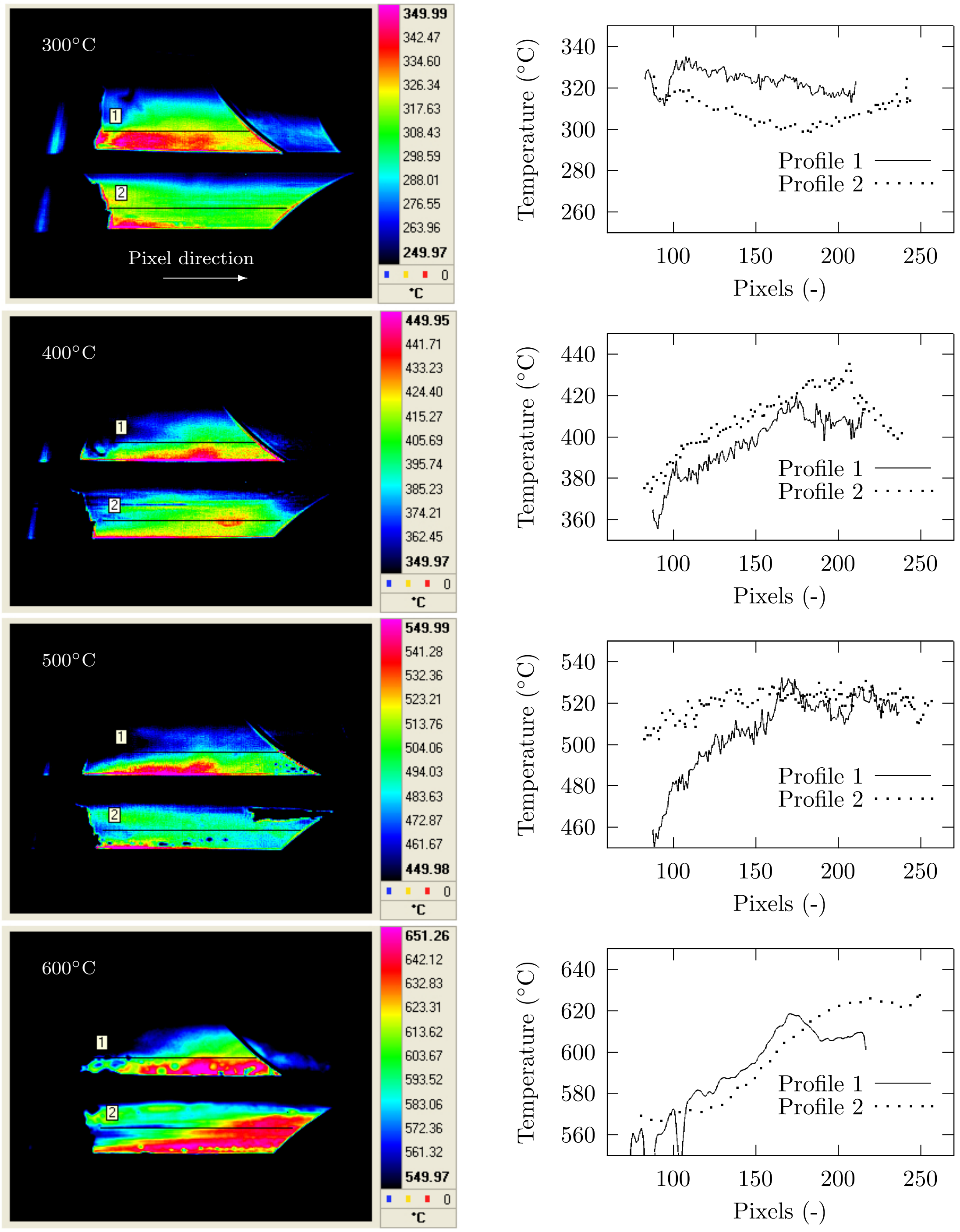

Figure 5.22: Temperature distribution during the heating process at different temperatures and the temperature evolution along the profile.

When using the inductive heating technology, it is very important the relative position between the inductive coils and the surface. In the current case, an special tool is designed to ensure the contact between the heating coil and the surface. An insulator material with 1 mm thickness is used to cover the inductive coils in order to avoid shortcuts. However, due to the geometry of the profile, in transition zones the distance between the coils and the surface is not always the same because the curved areas are not covered by the flat coil geometry. Thus, the heat distribution is not homogeneous in those zones.

At highest temperatures (> 500°C) the black paint is damaged in such a degree that in some parts is removed. In these cases, the emissivity of the profile change making it difficult to measure the temperature in these zones.

However, after a trial and error process, the inductive ovens are set-up to achieve a more homogeneous and stable temperature distribution. The temperature distribution in the profile during the heating process and the temperature profiles along cuts 1 and 2, from the heating coil to the flexible forming roll, are shown respectively in the left and right side of Figure 5.22.

Profile geometry

Heat assisted flexible roll formed profiles are measured using a 3D coordinate measuring machine Mitutoyo BHN710. The longitudinal section (Cross section A-A') and the cross sections at 500 mm (B-B'), 1000 mm (C-C') and 1500 mm (D-D') are measured in order to analyze the effect of the heat assistance in the final profile geometry as it is shown in Figure 5.23.

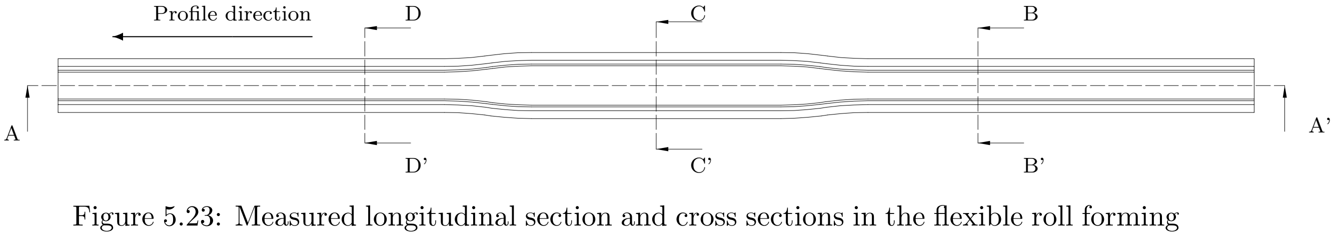

Figure 5.23: Measured longitudinal section and cross sections in the flexible roll forming profile.

Flexible profiles formed at room temperature and at 600°C are shown in Figure 5.24.

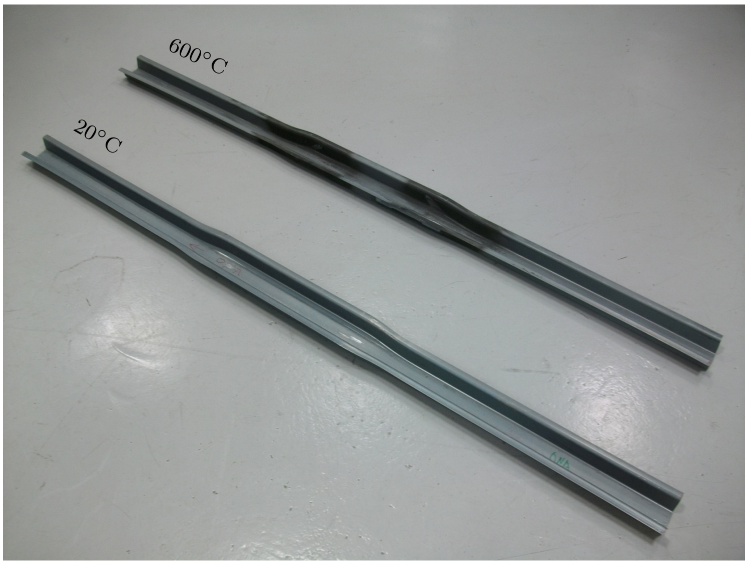

Figure 5.24: Flexible profiles formed at room temperature and at 600°C.

Effect of the temperature in the longitudinal web warping

The longitudinal section of the flexible profiles at different temperatures are shown in Figure 5.25. The average values and the standard deviations of the total and relative longitudinal web warping are summarized in Table C.4 of appendix C. The reader is referred to section §4.3.2 in order to know the definition of the longitudinal total and relative web warping.

The total web warping is temperature dependent and the minimal value is achieved experimentally in profiles fabricated at 300°C. The total web warping decreased by 9% at 300°C and 7% at 400°C, while, at 600°C, the total web warping increases by 32% with respect to the profile formed at room temperature. The average values of the total and relative web warping depending on the temperature are graphed in Figure 5.26 a.

The relative web warping is also temperature dependent and the minimal value is achieved in the profiles fabricated at 500°C. Heat assisting the profile the web warping decreased by 9.3% at 300°C, 10.5% at 400°C and by 20.1% at 500°C. On the other hand, at 600°C the web warping value decreases only by 15% in respect to the profile formed at room temperature.

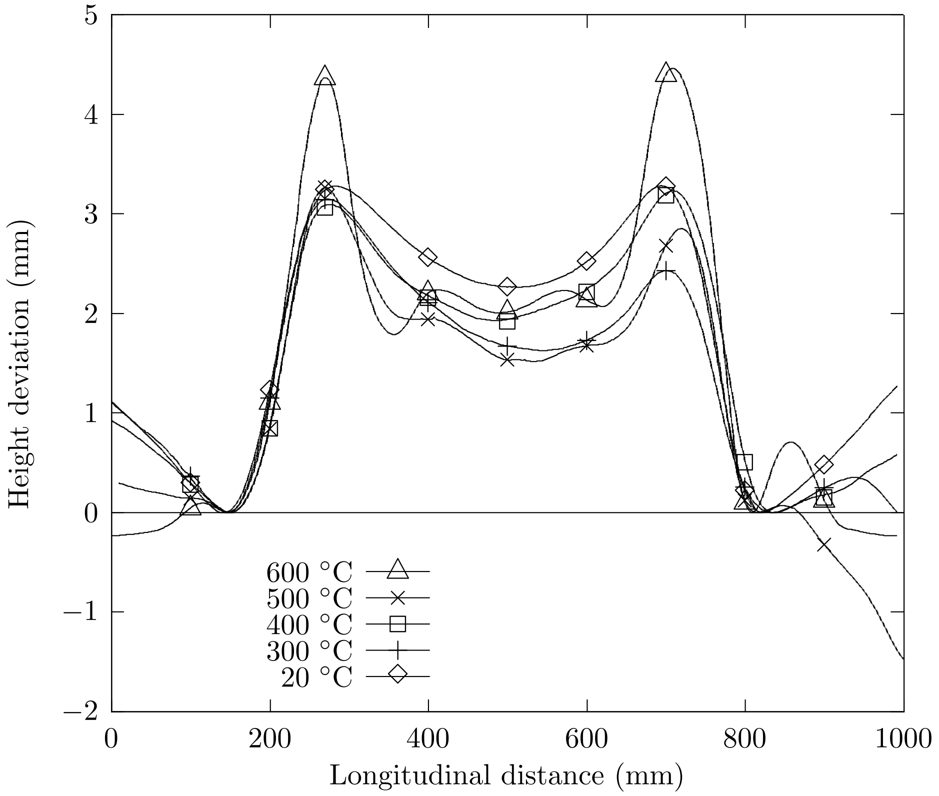

Figure 5.25: Longitudinal sections of flexible profiles at different temperatures.

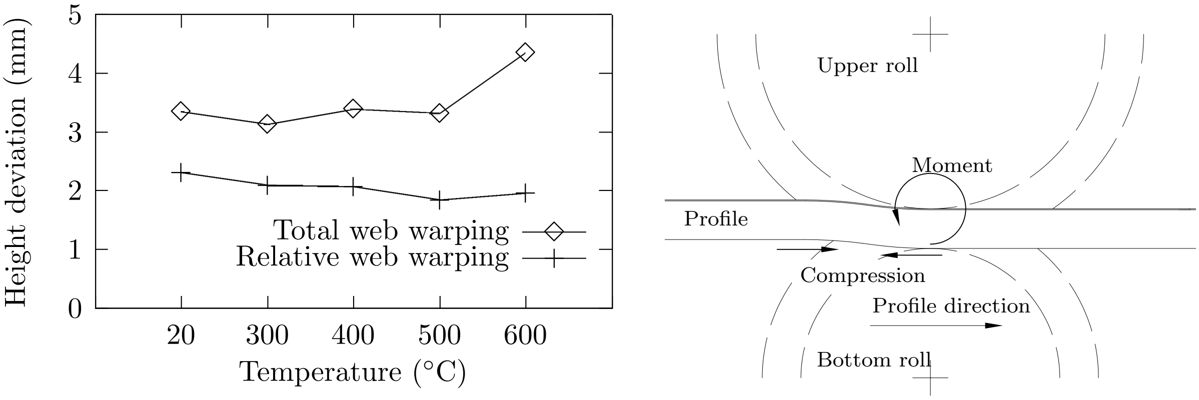

a) b)

Figure 5.26: (a) Total web warping and relative web warping depending on the process temperature and (b) web buckling. The average and standard deviation values are summarized in Table C.4 of Appendix C.

The increase of the total web warping at 600°C is attributed to the local buckling of the web part of the profile due to an excessive softening of the material. After the heating process when the profile is formed by the last forming station, the forming rolls exert a bending moment due to the difference in height between the slim and wide part of the profile. This bending moment induces longitudinal compression forces in the web part of the profile. The material in the bottom part of the profile is more ductile due to the temperature difference, the material reacts by producing localized buckling (Figure 5.26 b).

Effect of the temperature on the profile cross section

The cross sections of the heat assisted flexible profiles were measured at 500 mm, 1000 mm and 1500 mm (section B-B', C-C' and D-D' respectively) and angles β_1, β_2, β_3 and β_4 were calculated. The cross section of the slim and wide part of the profiles formed at room temperature and at 600°C are graphed in Figure 5.27.

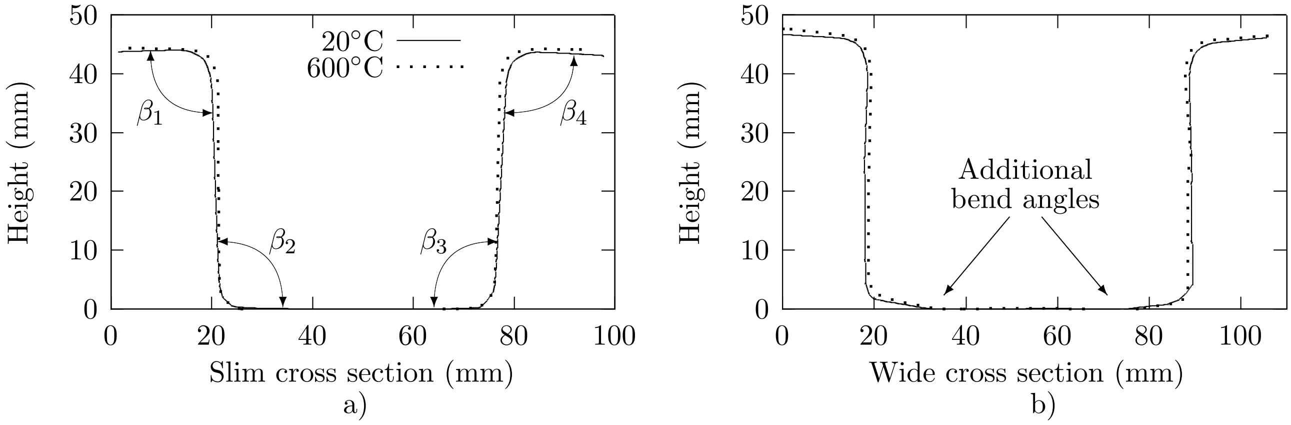

a) b)

Figure 5.27: (a) Slim and (b) wide cross sections, of profiles flexible roll formed at room and 600°C temperature.

The slim section, cross sections at 500 mm and at 1500 mm, showed a higher bend angle than 90° in all the measured angles. This effect is attributed to the springback effect of the material.

However, in all the profiles the cross section measured at 1000 mm (wide part) showed a smaller bend angle than 90° for β_2 and β_3. Additionally, all the cross sections measured at 1000 mm showed two additional bending zones, created for the effect of the static blank holders. The bend angles of the profiles formed at different temperatures were measured and the average values of angles β_1, β_2, β_3 and β_4 are shown in Figure 5.28.

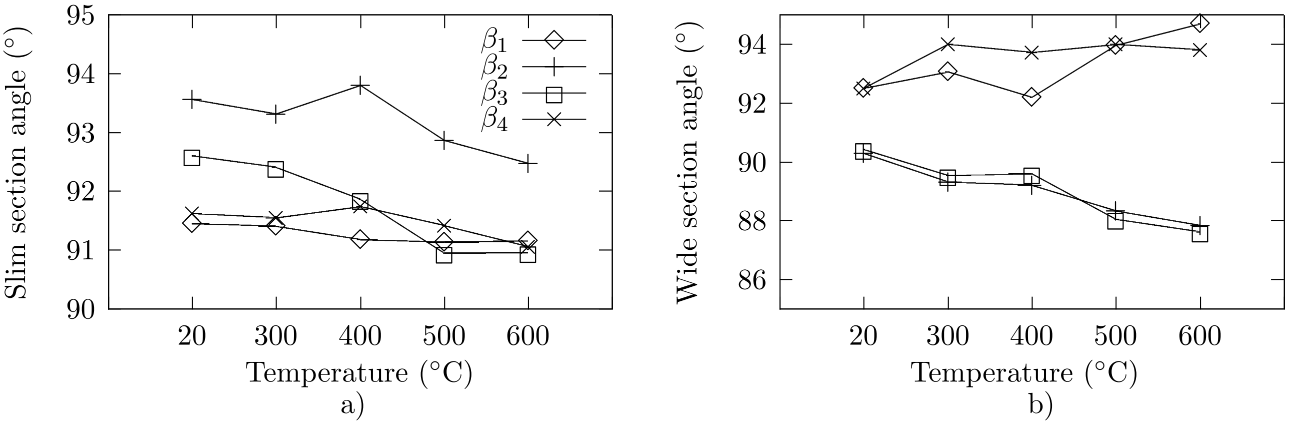

Figure 5.28: Evolution of the different angles depending on the process temperature at the slim (a) and wide part (b). The average and standard deviation values are of the angles of the slim and wide sections are summarized respectively in Table C.5 and Table C.6 of Appendix C.

It can be seen that generally the springback effect decreases when the forming temperature is increased in the slim cross section. However, the effect of increasing the process temperature decrease the β_2 and β_3 angles of the wide section.

5.3.4 Final properties of heat assisted flexible profiles

In order to account for the effect of the temperature in the local and global properties of the profile, different experimental tests were performed. The microstructure and the mechanical properties of the heat affected zones were analyzed by means of optical micrographs and tensile tests. Microstructure analysis and tensile test samples were extracted from the heat assisted area of the flexible profiles (see Figure 5.29).

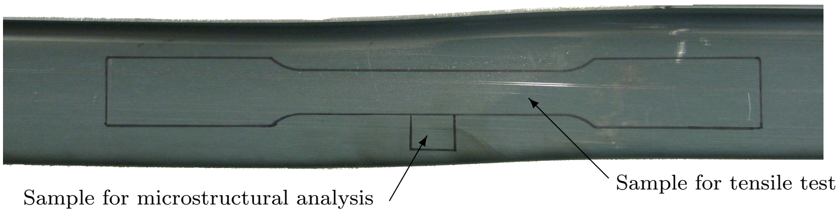

Figure 5.29: Tensile tests specimen and microstructural analysis samples.

On the other hand, the global structural behavior of the heat assisted profiles was analyzed by means of bending and torsion tests. The results shown in this section are used only to measure and quantify the effect of the heating in the profile structure. It is out of the scope of the present thesis to perform a deep study about the effects of the inductive heating on the microstructure and the local mechanical properties.

Microstructural analysis of heat assisted areas

Optical micrographs were obtained from the heat assisted part of the flexible zone in order to evaluate the effect of the temperature on the microstructure of CP800 material, (Figure 5.29). The extracted samples were etched using Klemm's agent. Information regarding the sample preparation is explained in section §3.4.1.

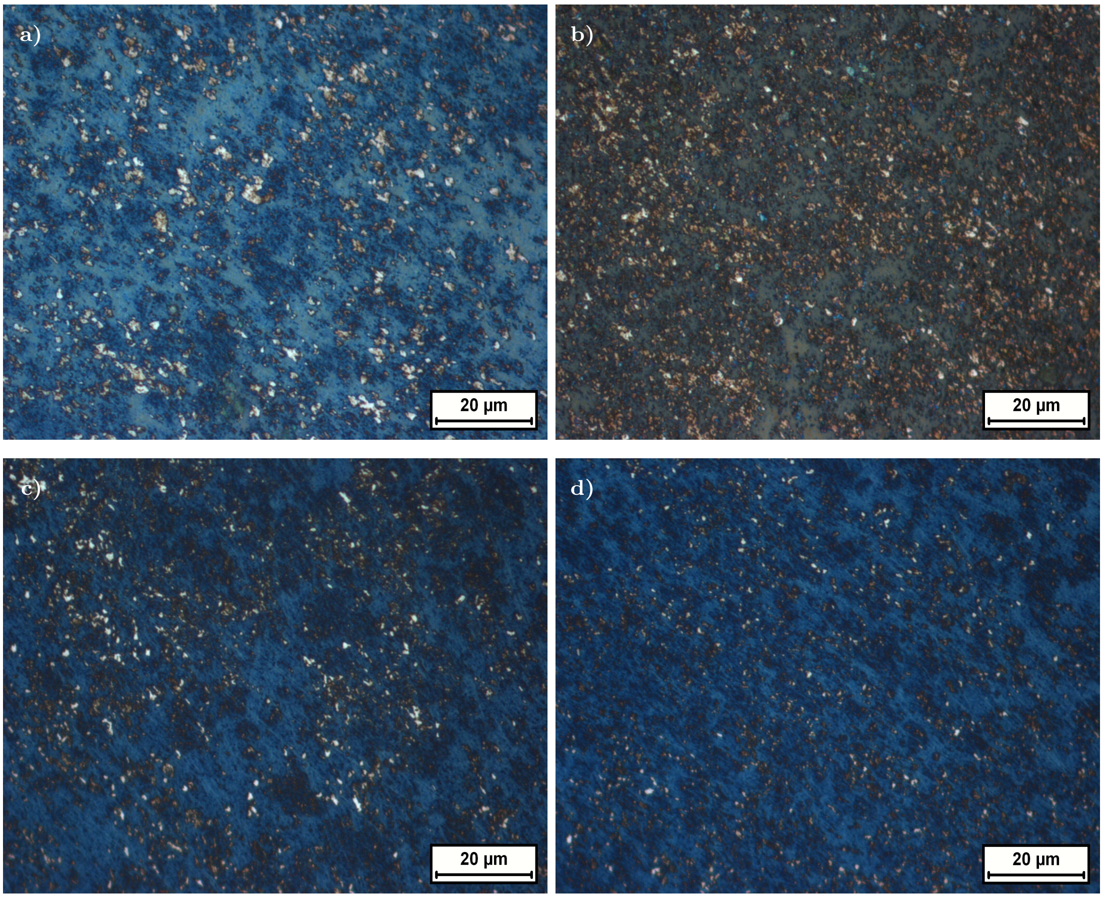

Figure 5.30: Microstructures of the heat assisted zones of profiles formed at (a) 300°C, (b) 400°C, (c) 500°C and (d) 600°C. The extracted samples were etched using Klemm's agent. Information regarding the sample preparation is explained in section §3.4.1.

The micrographs of the profile formed at 300°C show a similar microstructure as the received material, (see Figure 3.3). However, the micrographs of the profiles formed at 400°C, 500°C and at 600°C shows the transformation of the microstructure due to the temperature effect. Analyzing the effect of the temperature in the microstructure, it is found an increase of the ferrite-cementite phases at highest temperatures, suggesting the degradation of the residual austenite and martensite.

Tensile test of the heat affected area

Tensile test of heat assisted areas were performed in order to analyze the effect of the temperature in the local properties of the profile, (see Figure 5.29). Quasi-static tensile tests at room temperature were carried out in the laboratories of Mondragon University. Information regarding the sample preparation and tensile testing is explained in Chapter 3 section §3.3.1. Results of the different tensile tests with samples extracted from flexible roll formed profiles at different temperatures are shown in Figure 5.31.

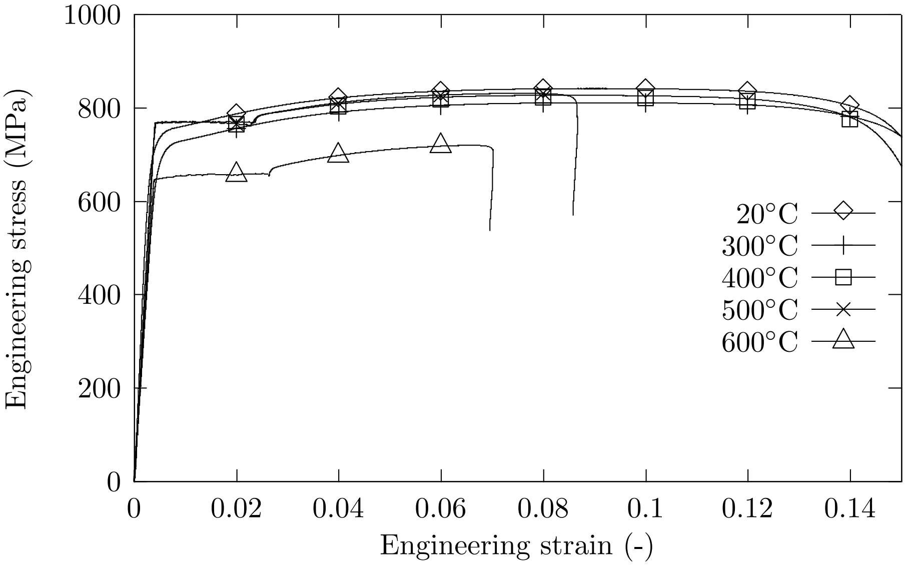

Figure 5.31: Engineering strain - stress curves of samples extracted from heat assisted flexible profiles at different temperatures.

The results of the different tensile tests show that initial properties of the material change locally due to the effect of the heat assistance. There are no significant differences in the tensile behavior between the specimen extracted from the profile formed at room temperature and the specimens extracted from the profiles formed at 300°C and 400°C. However, the decrease of the flow stress and the reduction of the elongation at higher temperatures than 500°C is seen. Additionally, results with samples extracted from profiles at 500°C and 600°C, show perfect plastic behavior at the initial states of the tensile testing. It would be interesting to know the reasons of this behavior and the effects on the material microstructure. However, as it is mentioned previously, it is not the main scope of the present dissertation to analyze deeply these effects.

Bending tests

Bending tests of heat assisted flexible profiles were performed in the laboratories of Centro Ricerche Fiat (CRF) in order to analyze the effect of the temperature in the global behavior of the profile. Three different profiles formed at room temperature, at 300°C and at 600°C were tested.

In an initial stage, the profiles were closed by 1.2 mm thick CP800 material flat sheet. Offset reinforcement profiles are closed in the real applications of the BW constructions, in order to be able to compare the global structural behavior of profiles formed with conventional technologies, such as stamping, and profiles formed with flexible roll forming. A CP800 material flat sheet was welded by means of resistance spot welding technology with spots every 50 mm. A closed profile can be seen in Figure 5.32 a. Three point bending tests were performed in a Zwick 1474 bending test machine using a 20 mm radius tool. The bending tests were performed at 10 mm/min vertical velocity and with 1600 mm distance between the supports. The Zwick 1474 bending machine is shown in Figure 5.32 b. Bending tests result performed with heat assisted flexible profiles are shown in Figure 5.33.

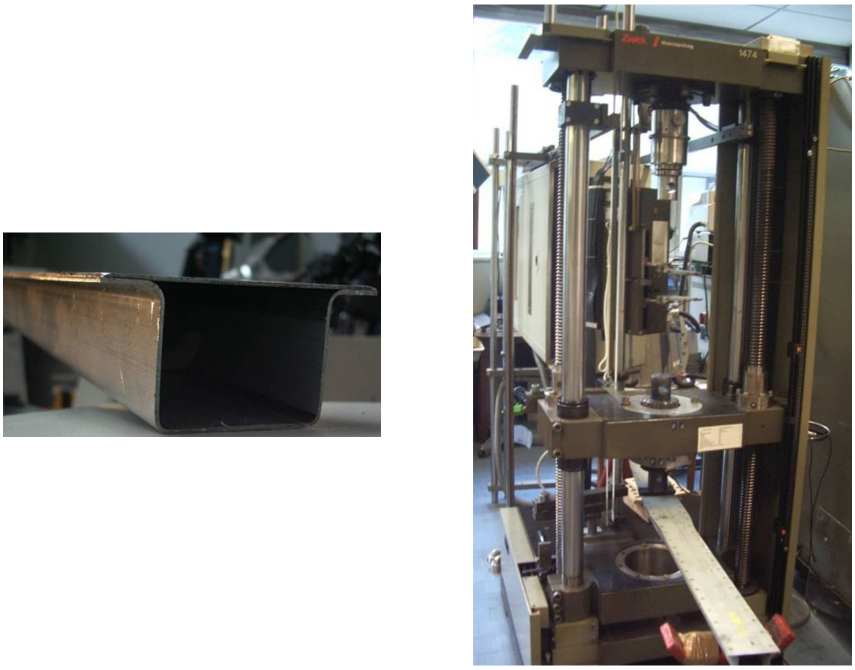

a) b)

Figure 5.32: (a) Closed profile and (b) Zwick 1474 bending test machine.

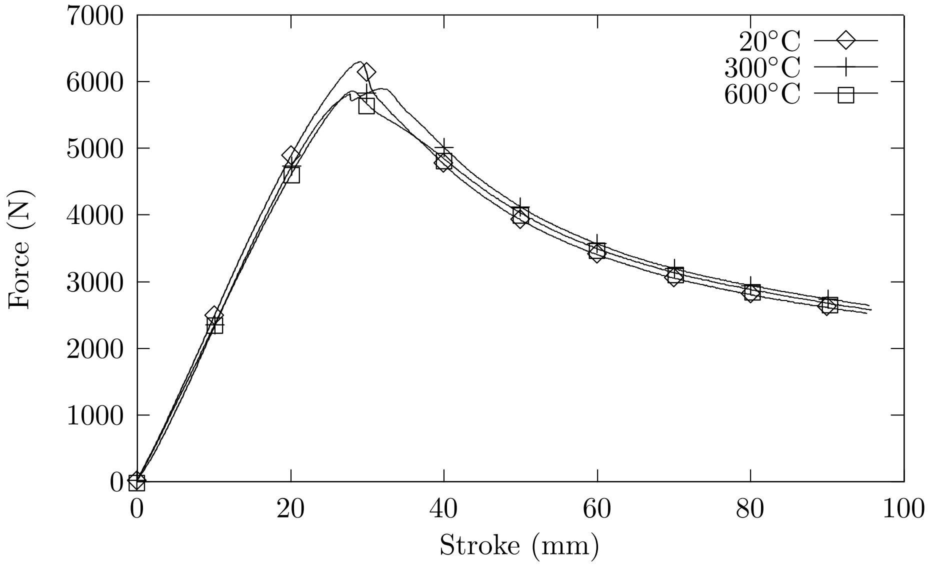

Figure 5.33: Results of the bending tests performed with profiles formed at different temperatures.

No significant differences were observed comparing the bending behavior of heat assisted profiles and profiles formed at room temperature.

Torsion tests

Torsion tests of heat assisted flexible profiles were performed in the laboratories of Centro Ricerche Fiat (CRF) in order to analyze the effect of the temperature in the global behavior of the profile. Three different profiles formed at room temperature, at 300°C and at 600°C were tested.

As explained before, the profiles were closed by 1.2 mm thick CP800 material flat sheet. Additionally, two plates were welded in the extremes of the profile in order to hold the profile in the torsion test machine. A closed profile with additional plates can be seen in Figure 5.34 a.

Torsion tests were performed in a Schenck torsion test machine, Figure 5.34 b. The torsion test machine was provided by a torque cell of 100 Nm and by an angular rotator, that applies the necessary torque.

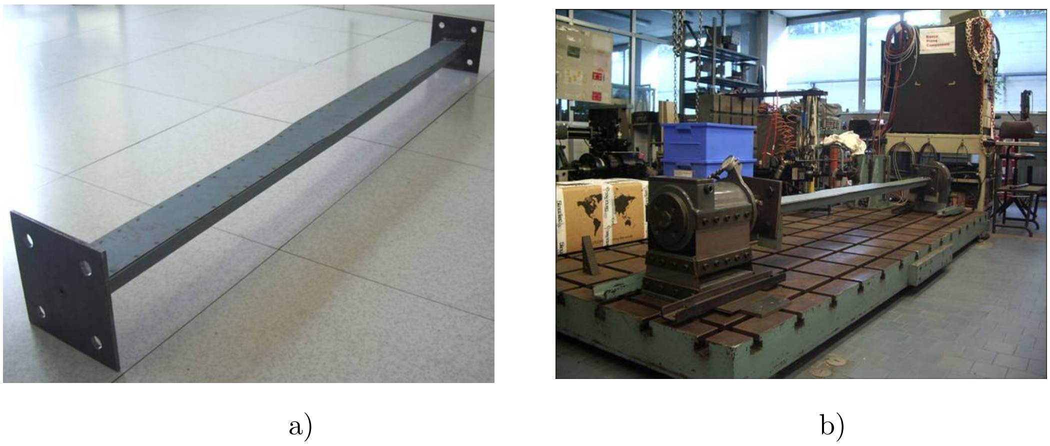
a) b)

Figure 5.34: Closed (a) profile and (b) Schenck torsion test machine used to perform the torsion tests.

The results of the torsion tests are shown in Figure 5.35

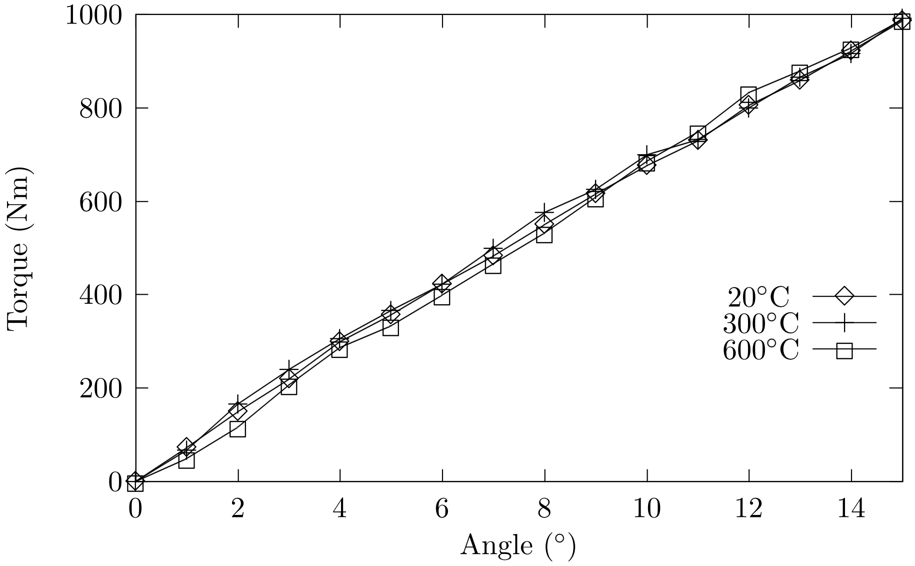

Figure 5.35: Results of the torsion tests performed with profiles formed at different temperatures.

It can be noticed that during the torsion tests, the profiles did not reach the plastic regime. However, no significant differences were observed comparing the torsional behavior of heat assisted profiles and profiles formed at room temperature.

5.4 Conclusions

Conventional roll forming experimental test performed in order to validate the numerical model developed in Chapter 4, show a direct relation between the material strength and the final geometry of the profile. Using high strength materials less longitudinal bow is achieved and the effect of the springback is larger. Comparing the effect of the material strength on the longitudinal and transversal peak strain and on the longitudinal and transversal residual strains, it is shown that the peak strain slightly increases when the material strength decreases and the final residual strains increases when the material strength decreases. Comparing the effect of the material strength on the forming loads and torques, it is shown that when material strength increases both forming forces and torques increase also.

In the second part of the current chapter, heat assisted flexible roll forming experimental tests are shown and the effect of the temperature on the web warping and cross section is analyzed. A reduction of 9% of the total web warping at 300°C it is shown and an increase of 32% of the total web warping at 600°C produced by a local buckling of the web part of the profile. However, analyzing the relative web warping error, a significant decrease of 20.1% at 500°C is shown. On the other hand, analyzing the effect of the temperature in the springback effect, it is shown that when the process temperature increases the sprigback effect decreases. Therefore, it is concluded that heat assisted flexible roll forming is a suitable procedure to reduce the longitudinal web warping of flexible roll formed profiles.

In the final part of the current chapter, results from the microstructure analysis and tensile tests of heat affected areas are shown in order to analyze the effect of the heat assisted areas in the material. Additionally, results of bending and torsion tests with profiles formed at different temperatures are shown in order to analyze the effect of the temperature in the global properties of the profile. Although, local changes on the microstructure and in the mechanical properties of the material are identified in heat affected zones, structural tests do not show any significant differences comparing the bending and torsional behavior of heat assisted profiles and profiles formed at room temperature.

Chapter 6

Conclusions and future work

In seculo seculorum

" Forever and ever "

6.1 Concluding remarks

The main objective of the present dissertation was to develop and analyze the heat assisted flexible roll forming process in order to increase the quality of flexible roll formed profiles made of high strength steels. This general objective was achieved facing the problem from three different point of views: the material mechanical behavior characterization, the numerical modeling of the process and the experimental work.

In the first section of this thesis, Chapter 3, the mechanical characterization of three different AHSS and one mild steel at room temperature is described. Additionally, the mechanical characterization at high temperature of the selected CP800 high strength steel is also considered. The main conclusions drawn from this characterization are:

- The analyzed steels show a wide range of strengths-strains relation:
  MS1200 ($Y_\mathrm{s} \approx 1200$MPa, $\sigma_\mathrm{uts} \approx 1350$MPa and $\varepsilon_\mathrm{f} \approx 0.04$),
  CP800 ($Y_\mathrm{s} \approx 680$MPa, $\sigma_\mathrm{uts} \approx 880$MPa and $\varepsilon_\mathrm{f} \approx 0.15$),
  DP600 ($Y_\mathrm{s} \approx 410$MPa, $\sigma_\mathrm{uts} \approx 740$MPa and $\varepsilon_\mathrm{f} \approx 0.18$) and
  DC01 ($Y_\mathrm{s} \approx 230$MPa, $\sigma_\mathrm{uts} \approx 445$MPa and $\varepsilon_\mathrm{f} \approx 0.3$).
- It is shown that the influence of the strain rate in the flow behavior of the different steels at quasi-static strain rates is very limited.
- Only DP600 and DC01 materials are significantly influenced by the loading direction. Both steels show higher flow stress and lower deformation at fracture in the sample taken at 45° with regard to the rolling direction.

The CP800 material, selected to perform the heat assisted flexible roll forming trials, was mechanically characterized at elevated temperatures and at different strain rates.

- At 300°C an increase of the tensile flow stress is seen with a similar deformation at fracture as the specimen tested at room temperature. This increase of the flow stress is attributed to the increase of the untempered martensite content due to the residual austenite degradation during the heating process.
- At 700°C the flow stress is decreased while the elongation at fracture increases by 139%. In the specimen tested at 700°C, it was observed the degradation of the initial microstructure into ferrite and globular cementite phases which favours the ductility of the material and decreases the flow stress.
- At elevated temperatures, increasing the strain rate in quasi-static strain rates, increases the yield stress and flow stress while decreases the elongation at fracture.
- From a technological point of view, in order to increase the formability of a commercial CP800 steel a minimum temperature of 400°C should be reached in the process.

In the second section of the present dissertation, Chapter 4, once the material plastic behavior was characterized at different conditions, the heat assisted flexible roll forming process was numerically studied. One of the objectives of the present thesis was to develop reliable numerical models that would help to optimize and develop the process of heat assisted flexible roll forming. The following main conclusions are obtained from numerical modeling of roll forming processes:

- The influence of the material strength was numerically analyzed for several roll forming parameters. The results show a decrease of the longitudinal bow and an increase of the springback effect when the material strength increases. On the other hand, the peak strain and the residual plastic strain in longitudinal and transversal directions increase when the material strength decreases. Finally, the forming loads and torques increase when the roll formed material strength increases.
- Numerical and experimental results show similar trends for different material strengths.
- Significant differences are achieved when numerical and experimental values of bent angles and forming torques were compared. The difference on the bent angle

is attributed to the poor representation of the springback effect in the numerical model. The discrepancies found in the torque prediction are attributed to the model's difficulty to accurately represent the frictional interaction between sheet and rolls.

- Although, discrepancies are seen between the numerical and experimental values, the developed numerical models of conventional roll forming describe a similar behavior observed in experimental results. Thus, the developed numerical models are validated knowing the strengths and the weaknesses of the models.

In the same chapter, the modeling of heat assisted flexible roll forming process was carried out in order to optimize the process, obtaining the following conclusions:

- The numerical results show the decrease of the total and relative web warping when process temperature is increased to 600°C.
- The numerical results show the highest improvements when the vertical part of the flexible zone was heated up to 600°C.
- The numerical results show little influence of the temperature on the controlled bent angles in the final profile.
- Comparing numerical and experimental results, similar evolution of the total and relative web warping are achieved increasing the temperature of the process.

In the third section, Chapter 5, heat assisted flexible roll forming experiments were carried out. However, a simplified experimental trials were also performed in order to analyze the effect of the material strength in different roll forming parameters and compare numerical and experimental results, obtaining the following main conclusions:

- The experimental results shows a relation between the material strength and the final geometry of the profile. Using high strength materials less longitudinal bow is achieved and the effect of the springback is larger.
- Comparing the effect of the material strength on the longitudinal and transversal peak strain and on the final residual strains, it is shown that the peak strains and the final residual strains increase when the material strength decreases.
- Comparing the effect of the material strength on the forming loads and torques, it is shown that when material strength increases both forming forces and torques also increase.

In the second part of Chapter 5, heat assisted flexible roll forming experimental test were carried out. The main conclusions extracted from these experiments are:

- The total and relative web warping are temperature dependent.
- The total web warping decreases by 9% at 300°C . However, the total web warping at 600°C increases by 32% produced by a local buckling of the web part of the profile.
- The relative web warping error decreased when the process temperature increased, it is shown a significant decrease of 20.1% at 500°C.
- Analyzing the effect of the temperature in the springback effect, it is shown that when the process temperature increases the sprigback effect decreases, as a consequence of the decreasing of yield stress with the temperature increase.

In the final part of Chapter 5, results from the microstructure analysis and tensile test of heat affected areas were shown in order to analyze the effect of the heat assisted areas in the local and global properties of the profile.

- Local property changes in the microstructure and in the mechanical response of the material are identified in heat affected zones. Analyzing the microestructure it is observed an increase of the ferrite-cementite phase and the degradation of the residual austenite and martensite phases. The mechanical characterization show a decrease of the flow stress and the reduction of the elongation at fracture at higher temperatures than 500°C.
- Global structural property tests do not show any significant differences comparing the bending and torsional behavior of heat assisted profiles and profiles formed at room temperature. Therefore, it is shown that heat assisted roll forming is an interesting process to manufacture high strength steel profiles.

6.2 Future work

The present dissertation has demonstrated the suitability of heat assisted flexible roll forming process in order to increase the quality of high strength steel flexible roll formed profiles. However, further research work is suggested in order to completely optimize and understand some open questions outlined in this thesis.

The understanding of the material behavior at different loading conditions is a key factor to success in the roll forming process design. For this reason, the microstructures of the different high strength steel samples tested at room temperature should be analyzed in order to identify the deformation mechanism that take place.
Regarding the mechanical characterization at high temperatures, it is seen that the tensile strength of the material increases at 300°C. This effect is attributed to the transformation of the retained austenite to untempered martensite during the heating process of the sample. It would also be interesting to verify this statement, performing additional heating tests and tensile test at high temperature, and analyzing these samples not only by optical microscopy and XRD measurements but also with other characterization methods such as SEM or magnetization saturation techniques, in order to analyze the evolution of the different phases of CP800 steel at different loading and temperature conditions.

Regarding the roll forming process modeling it would be interesting to analyze other material characterization methods that better modelize the bending behavior of the material, such as bending methods [Hem11]. In order to improve the springback behavior modeling of numerical models, it would be interesting to analyze other element types (comparison of shell and solid elements), alternative interpolation functions and analyze the effect of bending zone discretization.
Regarding the roll torque modeling, it is seen that the friction modeling and the shaft deflection could play an important role. In order to improve the forming torque modeling, it would be interesting to analyze the implementation of the shaft deflection in the numerical models. Additionally, it would be interesting also to develop a specific methodology to experimentally determinate the friction modelization for the roll forming process.

In the literature review, it has been seen a lack of the basics investigations in the field of flexible and heat assisted roll forming processes. It is known that different authors are facing the problem of the web warping of the flexible roll forming process using different solutions. For instance, some authors used different blank holders to avoid the web warping [Abe08; Sed09; Gro09] and other authors rolled partially [Ona10] or used over bending system [Gro09; Gro10] to achieve the desired longitudinal deformations and avoid the web warping.

Regarding the experimental work, it would be interesting to continue performing a basic research of the heat assisted flexible roll forming process starting with basic geometries, using different materials and heating techniques with the objective of increase the geometrical accuracy of flexible roll formed profiles.

CHAPTER 7

Published work and other submissions

“Scire tuun nihil est,

nisi te scire hoc sciat alter“

“ Your knowledge is nothing when no one else knows that you know it ”

Published work and other submissions

Withing the present thesis different contributions in national and international scientific congresses, publications in international journals and patents were presented:

Patents

- ”Aparato y método de perfilado flexible adaptado para conformar un perfil de sección variable a partir de una chapa metálica” [Gal09a].

International journals

- Development and validation of a numerical model for sheet metal roll forming [Lar10c].
- Tensile characterization of complex phase steel sheets at different temperatures and high strain rates [Lar11]. Manuscript prepared for submission.

International congresses

- International Conference on Technology of Plasticity, (ICTP08), Gyeongju (Korea), 2008 [Lar08a].
- International Congress on Roll Forming,(RollFORM09), Bilbao (Spain), 2009 [Lar09] and [Gal09b].

- International Conference on Advanced Materials and Processing Technologies (AMPT2010), Paris (France), 2010 [Lar10a].

National congresses

- Congreso Nacional de Materiales (CNM2008), San Sebastian (Spain), 2008 [Lar08b].
- Congreso Nacional de Materiales (CNM2010), Zaragoza (Spain), 2010 [Lar10b].

Acknowledgement

Ab imo pectore

“ From the deepest of the heart ”

Tesiaren azken hitzak idazten ari naizen honetan, atzera begira jarri eta igarotako hainbat eta hainbat une eta ezagututako pertsona datozkit burura. Bakarka igarotako une asko, une gogorrak batzuk, atseginak beste batzuk, eta esan daiteke beste batzuetan zoriontsu ere sentitu naizela. Ezagutu ditudan pertsona guztietatik ikasi dut zerbait, eta hitz onak besterik ez zaizkit etortzen gogora beraiekin oroitzean. Bakarrik ezin izango nuen aurkeztera noan lan hau burutu, eta azken urte hauetan lagundu, aholkatu, lan egin edota nire kexuak entzun dituzuen guzti horiei eskerrak eman nahiko nizkizueke.

Lehenik eta behin, lan hau aurrera eramateko ezinbestekoa izan den nire tesi zuzendariari, Lander Galdosi, eskerrak eman nahi nizkioke. Zure doktoretza bukatu berritan jaso zenuen lehen oinordekotza izanik, eskainitako gidaritza, babes, lanerako gogo eta ilusioagatik, eskerrik asko.

Mondragon Goi Eskola Politeknikoko fabrikazio sailari, eta batez ere konformaketa aurreratuko ikerketa lerroari, bere lan taldean hartu eta tesi hau burutzeko aukera eta diru-laguntza emateagatik. Angel Oruna, Carlos Garcia eta Iñaki Hurtadori, eman didazuen konfiantza eta medio guztiengatik, eskerrik asko.

Labein-Tecnalia-ko lantalderi, Marian, Angela, Iñaki, Borja eta Mikeli, tesi honetako zatirik garrantzitsuenean izan duzuen jarrera ona, pazientzia eta eskuzabaltasunagatik, eskerrik asko.

I would also like to acknowledge Albert Sedlmaier, from DataM Sheet Metal solutions, to make it possible to work with him during my stay at his company. Many thanks also to Andreas, Stephan, Claudia, André, Thomas and Bern for all your help and support. Ezin izango nuke eskertu gabe utzi Munichen igarotako 3 hilabete hotzetan

ezagutu nuen Lander Arrupe, emandako laguntza eta igarotako une atsegin guztiengatik, eskerrik asko.

I would like to thank all the people whom I have met all over Europe during this time within the frame of the project ProForm (European project under the Sixth Framework Programme that has supported the present research work). I would like to specially thank Sebastian Berner from the Institute for Production Engineering and Forming Machines of the Technische Universität Darmstadt, for the fruitful collaboration and discussions regarding technical aspects.

Ibai Ulacia eta Andrea Niklas ezin ahaztu eskertze honetan, irakatsi didazuen guztiagatik, eman didazuen laguntza eta izandako pazientziagatik, eskerrik asko.

Urte hauetan zehar nire alboan lanean izan zareten eta beti esker onez erantzun didazuen perfilaketa taldeko guztioi. Leire, Enaitz, Lorena, Hodei eta Andoniri, eskerrik asko, zuen guztion lan eta laguntzarik gabe lan hau ezin izango zen burutu.

”Enbajada” bat nuen bakoitzean ordainetan ezer espero gabe laguntza eman didazuen guztiei: Rafa, Gotzon, Arkaitz, Iñaki, Aitor, Alaitz, Joseba, Ramon, Xabo eta Ainharari, eskerrik asko.

Lau urte hauetan ezagutu ditudan lagun eta lankide guztiei. Elkarbanatu ditugun momentu, janari eta kafe guztietan pasatako une on, irribarre eta elkarrizketengatik. Batez ere, tesi amaiera honetan, pasatako une gogorretan entzuten jakin izan eta eman didazuen laguntza eta bultzadagatik. Andrea, Eneko, Gurutze, Edurne, Jonan, Haritz, Jokin, Jabi, Alaitz, Joanes, Miriam, Ireneo, Nuria, Jon, Nagore, Ainhara, Pablo, Manex, Iñigo eta Axiri, nire eskerrik beroenak.

Koadrilako, lagun, Toulouseko ikaskide ohi eta taldekide guztiei, une zailetan entzun eta askotan emandako erantzun txarrak ulertu, eta animatu nauzuelako, eskerrik asko denei.

Eta azkenik, nire bizitzan gehien maite ditudan pertsonei eskerrak eman gabe ezin dut bukatu eskertza hau. Urteetan zehar ordainetan ezer espero gabe, zenuten dena eman didazue eta zuen laguntza eta babesik gabe, tesi hau ezin izango zatekeen burutu. Nire amari, aitari eta anai Joxeri eta Aingeruri, nire amonari eta iloba Itxasori, Edurneri eta Ainhoari nire eskerrik beroenak bihotz bihotzez.

References

[Abe08] A. Abee, S. Berner, and A. Sedlmaier. Accuracy improvement of roll formed profiles with variable cross sections. In *9th International Conference on Technology of Plasticity, ICTP 2008*, pp. 520–527. Gyeongju, Korea, 2008.

[Abe09] A. Abee and A. Sedlmaier. Development of roll forming applications by means of numerical analysis as a part of quality control. In *1st International Congress on Roll Forming: RollFORM09*, pp. 9–15. Bilbao, Spain, 2009.

[Ada06] J. Adamczyk. Development of the microalloyed constructional steels. *Journal of Achievements in Materials and Manufacturing Engineering*, vol. 14(1-2):pp. 9–20, 2006.

[Akb08] M. R. Akbarpour and A. Ekrami. Effect of temperature on flow and work hardening behavior of high bainite dual phase (HBDP) steels. *Materials Science and Engineering: A*, vol. 475(1-2):pp. 293–298, 2008.

[Ald09] I. Arriola Aldamiz. *Aisi 4140 steel's machinability comprehension analyzing inprocess parameters by advance measurement techniques.* Ph.D. thesis, Mondragon University, 2009.

[Als04] A. Alsamhan, I. Pillinger, and P. Hartely. The development of real time re-meshing technique for simulating cold-roll-forming using FE methods. *Journal of Materials Processing Technology*, vol. 147:pp. 1–9, 2004.

[AST08] ASTM E975-03. Standard practice for X-ray determination of retained austenite in steel with near random crystalographic orientation, 2008.

[Ber08] H. Berns and W. Theisen. *Ferrous Materials: Steels and Cast Iron.* Springer Verlag, 2008.

[Bha84a] D. Bhattacharyya and P. D. Smith. Cold roll forming - engineers' dilemma and artisans' art. *Engineering for Primary Production and Processing*, p. 21, 1984.

[Bha84b] D. Bhattacharyya and P. D. Smith. The development of longitudinal strain in cold roll forming and its influence of product straigthtness. In *1st International Conference on Technology of Plasticity, ICTP 1984*, vol. 1, pp. 181–191. Tokyo, Japan, 1984.

[Bha84c] D. Bhattacharyya, P. D. Smith, C. H. Yee, and I. F. Collins. The prediction of deformation length in cold roll forming. *Journal of Mechanical Working Technology*, vol. 9(2):pp. 181–191, 1984.

[Bha87] D. Bhattacharyya, P.D. Smith, SK Thadakamalla, and I.F. Collins. The prediction of roll load in cold roll-forming. *Journal of Mechanical Working Technology*, vol. 14(3):pp. 363–379, 1987.

[Bla87] T.Z. Blazynski. *Materials at high strain rates.* Springer, 1987.

[Bui08] Q. V. Bui and J. P. Ponthot. Numerical simulation of cold roll-forming processes. *Journal of Materials Processing Technology*, vol. 202(1-3):pp. 275–282, 2008.

[CG07] L. del Campo Gallastegui. *Diseño, construcción y calibración de un radiómetro para medir emisividad espectral direccional. Aplicación a materiales de interés tecnológico.* Ph.D. thesis, The University of the Basque Country, 2007.

[Chi84] K.F. Chiang. *Cold roll forming.* Master's thesis, University of Auckland, 1984.

[Cur09a] S. Curtze. *Characterization of dynamic behavior and microstructure evolution of high strength sheet steels.* Ph.D. thesis, Tampere University of Technology, 2009.

[Cur09b] S. Curtze, V.T. Kuokkala, M. Hokka, and P. Peura. Deformation behavior of TRIP and DP steels in tension at different temperatures over a wide range of strain rates. *Materials Science and Engineering: A*, vol. 507(1-2):pp. 124–131, 2009.

[Dat10] DataM. COPRA ® Roll Forming, DataM sheet metal solution, 2010.

[DeW88] D.P. DeWitt and G.D. Nutter. *Theory and practice of radiation thermometry.* Wiley-Interscience, 1988.

[Dim06] A. Dimatteo, G. Lovicu, M. Desanctis, R. Valentini, and A. Solina. Microstructures and properties of TRansformation Induced Plasticity steels. *Metallurgia Italiana*, vol. 98(11/12):p. 37, 2006.

[Dug95] N. Duggal. *Process simulation of roll forming and roll pass design.* Master's thesis, The Ohio state university, USA, 1995.

[Dug96] N. Duggal, M. A. Ahmetoglu, G. L. Kinzel, and T. Altan. Computer aided simulation of cold roll forming - a computer program for simple section profiles. *Journal of Materials Processing Technology*, vol. 59(1):pp. 41–48, 1996.

[Dut09] T. Dutton, P. Richardson, and G. Duffet. Simulating the complete forming sequence for roll formed automotive component using LS-DYNA. In *1st International Congress on Roll Forming: RollFORM09*, pp. 49–55. Bilbao, Spain, 2009.

[Dyk00] R. J. Dykes, S. J. Mander, and D. Bhattacharyya. Roll forming continuous fibre-reinforced thermoplastic sheets: Experimental analysis. *Composites - Part A: Applied Science and Manufacturing*, vol. 31(12):pp. 1395–1407, 2000.

[Eng01] B. Engl and T.K.S. AG. Cold Rolled HSLA Sheet and Strip Products. In *Internationa symposium niobium, Niobium 2001*, pp. 675–698. Orlando, Florida, USA, 2001.

[Eng06] M. English, M. Castellucci, and D. J. Mynors. Eco-efficiency of the cold roll formed product supply chain. *Journal of Materials Processing Technology*, vol. 177(1-3):pp. 626–629, 2006.

[Eur10] European project PROFORM. An innovative manufacture process concept for a flexible and cost effective production of the vehicle body in white: Profile forming. Tech. rep., 2010.

[Gal09a] L. Galdos, J. Larrañaga, G. Arrizabalaga, L. Uncilla, S. Freitag, A. Sedlmaier, and B. Poks. Pat2009. aparato y método para el perfilado asistido por calor de piezas sección constantes y variables en su longitud., 2009.

[Gal09b] L. Galdos, J. Larrañaga, L. Uncilla, H. Lete, and G. Arrizabalaga. Process simulation and experimental tests of cold roll forming of a U-channel made of different ultra high strength steel. In *1st International Congress on Roll Forming: RollFORM09*, pp. 75–81. Bilbao, Spain, 2009.

[Geh07] A. Gehring and H. Saal. Sensitivity analysis of technological and material parameters in rollforming. In *9th International Conference on Numerical Methods in Industrial Forming Processes, Muniform 07*, pp. 781–796. 2007.

[Gei04] M. Geiger, M. Pitz, M. Merklein, and A. Otto. Laser assisted bending of complex-phase steel. *Production Engineering*, vol. 11/2:pp. 13–16, 2004.

[Gei08] M. Geiger, M. Merklein, and M. Kaupper. Investigation of the mechanical behaviour of advanced high strength steels under various loading conditions. *International Journal of Material Forming*, vol. 1:pp. 225–228, 2008.

[Gir98] E. Girault, P. Jacques, Ph. Harlet, K. Mols, J. Van Humbeeck, E. Aernoudt, and F. Delannay. Metallographic methods for revealing the multiphase microstructure of trip-assisted steels. *Materials characterization*, vol. 40(2):pp. 111–118, 1998.

[Gro03] P. Groche, G. von Breitenbach, M.Jckel, and A. Zettler. New tooling concepts for future roll forming applications. *4th International Conference on Industrial Tools, ICIT Conference*, 2003.

[Gro09] P. Groche, F. Vogler, W. Schmitt, S. Berner, and A. Duschka. Self-ajustment in flexible roll-forming lines. In *1st International Congress on Roll Forming: RollFORM09*, pp. 25–31. Bilbao, Spain, 2009.

[Gro10] P. Groche, A. Zettler, S. Berner, and G. Schneider. Development and verification of a one-step-model for the design offlexible roll formed parts. *International Journal of Material Forming*, pp. 1–7, 2010.

[Gul07] E. Gulceken, A. Abeé, A. Sedlmaier, and H. Livatyali. Finite element simulation of flexible roll forming: A case study on variable width U channel. In *4th International Conference and Exhibition on Desing and Production of MACHINES and DIES/MOLDS, Cesme, TURKEY*, pp. 21–23. 2007.

[Gut10] M. A. Gutierrez, I. Eguia, S. Berner, C. Hennigs, A. Sedlmaier, A. Agnello, and J. Bahillo. PROFORM: Profile forming innovation. In *International Deep-drawing Research Group 2010, IDDRG2010*. Graz, Austria, 2010.

[Hae05] H. J. Haepp and M. Rohleder. Fe simulation of sheet metal forming - state of the art in automotive industry. In *11th International Conference on Sheet Metal 2005, SheMet'05*, vol. 6-8, pp. 13–18. Erlangen, Germany, 2005.

[Hal83a] G. T. Halmos. Roll forming HSLA steels. *HSLA Steels, Technology and Applications*, pp. 515–522, 1983.

[Hal83b] G. T. Halmos. Trends in roll forming. *Sheet Metal Industries*, vol. 60:pp. 38–41, 1983.

[Hal05] G. T. Halmos. *Roll Forming Handbook.* CRC, 2005.

[Han01a] Z.W. Han, C. Liu, W.P. Lu, and L.Q. Ren. The effects of forming parameters in the roll-forming of a channel section with an outer edge. *Journal of Materials Processing Technology*, vol. 116(2-3):pp. 205–210, 2001.

[Han01b] Z.W. Han, L.Q. Ren, C. Liu, and W.P. Lu. Modelling of cold roll forming of steel strip. *Materials Science and Technology*, vol. 17(4):pp. 415–418, 2001.

[Han05] Z.W. Han, C. Liu, W.P. Lu, L.Q. Ren, and J. Tong. Spline finite strip analysis of forming parameters in roll forming a channel section. *Journal of Materials Processing Technology*, vol. 159(3):pp. 383–388, 2005.

[Hei96] F. Heislitz, H. Livatyali, M.A. Ahmetoglu, G.L. Kinzel, and T. Altan. Simulation of roll forming process with the 3-D FEM code PAM-STAMP. *Journal of Materials Processing Technology*, vol. 59(1-2):pp. 59–67, 1996.

[Hel07] S. Hellborg. Finite element simulation of roll forming. *Blech Rohre Profile*, vol. 39:pp. 298–305, 2007.

[Hem11] E. Hemmerich, B. Rolfe, P.D. Hodgson, and M. Weiss. The effect of pre-strain on the material behavior and the Bauschinger effect in the bending of hot rolled and aged steel. *Materials Science and Engineering: A*, vol. 528(9):pp. 3302 – 3309, 2011.

[Hil48] R. Hill. A theory of the yielding and plastic flow of anisotropic metals. *Proceedings of the Royal Society of London Series A, Mathematical and Physical Sciences*, vol. 193(1033):pp. 281–297, 1948.

[Hon01] S. Hong, S. Lee, and N. Kim. A parametric study on forming length in roll forming. In *5th Asia Pacific Conference on Materials processing, APCMP2001*, vol. 113, pp. 774–778. Seoul, Korea, 2001.

[Huh02] H. Huh, W. Kang, and S. Han. A tension split hopkinson bar for investigating the dynamic behavior of sheet metals. *Experimental Mechanics*, vol. 42(1):pp. 8–17, 2002.

[Huh07] H. Huh, S.-B. Kim, J.-H. Song, and J.-H. Lim. Dynamic tensile characteristics of TRIP-type and DP-type steel sheets for an auto-body. *International Journal of Mechanical Sciences*, vol. 50:pp. 918–931, 2007.

[Iml07] K.-P. Imlau and T. Heller. New steel solutions for the worldwide car industry. *Steel research International*, vol. 78(3):pp. 180–184, 2007.

[Int09] International Iron and Steel Institute. *Advanced high strength steel (AHSS) aplication Guidelines*. WorldAutoSteel, June 2009.

[Jac04] P. J. Jacques. Transformation-induced plasticity for high strength formable steels. *Current Opinion in Solid State and Materials Science*, vol. 8(3-4):pp. 259–265, 2004.

[Jeo08] S. H. Jeong, S. H. Lee, G. H. Kim, H. J. Seo, and T. H. Kim. Computer simulation of U-channel for under-rail roll forming using rigid-plastic finite element methods. *Journal of Materials Processing Technology*, vol. 201(1-3):pp. 118–122, 2008.

[Jl05] Y. Ji-long, L. Ying-bing, L. Da-yong, and P. Ying-hong. Simulation of roll forming with dynamic explicit finite element method. In *AIP Conference Proceedings*, vol. 778, p. 197. 2005.

[Kiu84] M. Kiuchi and T. Koudabashi. Automated design systen of optimal roll profiles for cold roll forming. *3rd International conference on rotatory metal working process,*, pp. 423 – 436, 1984.

[Kle03] M. Kleiner, M. Geiger, and A. Klaus. Manufacturing of lightweight components by metal forming. *CIRP Annals - Manufacturing Technology*, vol. 52(2):pp. 521–542, 2003.

[Lar08a] J. Larrañaga, L. Galdos, C. Garcia, R. Ortubay, and G. Arrizabalaga. Flexible roll forming process reliability and optimisation methods. In *9th International Conference on Technology of Plasticity, ICTP 2008*. Gyeongju, Korea, 2008.

[Lar08b] J. Larrañaga, L. Galdos, R. Ortubay, and G. Arrizabalaga. Perfilado asistido láser. Caracterización de material y simulación numerica del proceso. In *X Congreso nacional de Matriales, CNM2008*. San Sebastian, Spain, 2008.

[Lar09] J. Larrañaga and L. Galdos. Geometrical accuracy improvement of flexibly roll formed profiles by means of local heating. In *1st International Congress on Roll Forming: RollFORM09*, pp. 17–19. Bilbao, Spain, 2009.

[Lar10a] J. Larrañaga, S. Berner, L. Galdos, and P. Groche. Geometrical accuracy improvement in flexible roll forming lines. In *Advances in Materials and Processing Technologies conference, AMPT2010*, pp. 557–562. Paris, France, 2010.

[Lar10b] J. Larrañaga, L. Galdos, I. Hurtado, and P. Adeva. Caracterización de cuatro aceros de alta resistencia a temperaturas elevadas. In *XI Congreso nacional de Materiales, CNM2010.* Zaragoza, Spain, 2010.

[Lar10c] J. Larrañaga, L. Galdos, L. Uncilla, and A. Etxaleku. Development and validation of a numerical model for sheet metal roll forming. *International Journal of Material Forming*, vol. 3:pp. 151–154, 2010.

[Lar11] J. Larrañaga, I. Ulacia, A. Niklas, L. Galdos, and I. Hurtado. Tensile characterization of complex phase steel sheets at different temperatures and high strain rates. *Materials Characterization*, 2011. Manuscript prepared for submission.

[Lie87] J.H. Lienhard, R. Eichhorn, and J.H. Lienhard. *A heat transfer textbook.* Prentice-Hall Englewood Cliffs, NJ, 1987.

[Lie02] G. Liedl, A. Kratky, and D. Schuocker. Laser assisted shaping of metallic sheets and wires - a promising new application of high power lasers. In *High-Power Laser Ablation IV*, vol. 4760, pp. 633–44. Taos, NM, USA, 2002.

[Lin05] M. Lindgren. Finite element model of roll forming of a U-channel profile. In *International Conference on Technology of Plasticity, ICTP2005.* Verona, Italy, 2005.

[Lin07a] M. Lindgren. Cold roll forming of a U-channel made of high strength steel. *Journal of Materials Processing Technology*, vol. 186(1):pp. 77–81, 2007.

[Lin07b] M. Lindgren. Experimental investigations of the roll load and roll torque when high strength steel is roll formed. *Journal of Materials Processing Technology*, vol. 191(1-3):pp. 44–47, 2007.

[Lin07c] M. Lindgren. An improved model for the longitudinal peak strain in the flange of a roll formed u-channel developed by fe-analyses. *Steel research international*, vol. 78:pp. 82–87, 2007.

[Lin08] M. Lindgren. Validation of finite element model of roll forming. In *International Deep-drawing Research Group 2008, IDDRG2008*. Olofström, Sweden, 2008.

[Lin09a] M. Lindgren. *Experimental and Computational Investigation of the Roll Forming Process*. Ph.D. thesis, Luleå University of Technology, 2009.

[Lin09b] M. Lindgren, U. Bexell, and L. Wikström. Roll forming of partially heated cold rolled stainless steel. *Journal of materials processing technology*, vol. 209(7):pp. 3117–3124, 2009.

[Lin09c] M. Lindgren and L. Ingmarsson. 3d roll-forming of hat-profile with variable depth and width. In *1st International Congress on Roll Forming: RollFORM09*, pp. 1–8. Bilbao, Spain, 2009.

[Lun08] M. Lundberg and A. Melander. Finite element analysis of roll forming of uhss compared to traditional bending. In *International Deep-drawing Research Group 2008, IDDRG2008*. Olofström, Sweden, 2008.

[Lun09] M. Lundberg, A. Melander, L. Troive, and S. Maulitz. A new test for cracking in roll forming. In *1st International Congress on Roll Forming: RollFORM09*, pp. 125–131. Bilbao, Spain, 2009.

[Mar02] Z. Marciniak, J.L. Duncan, and S.J. Hu. *Mechanics of sheet metal forming*. Butterworth-Heinemann, 2002.

[Mei03] M. Meiler, M. Pfestorf, M. Geiger, and M. Merklein. The use of dry film lubricants in aluminum sheet metal forming. *Wear*, vol. 255(7):pp. 1455–1462, 2003.

[Mer02] M. Merklein and M. Geiger. New materials and production technologies for innovative lightweight constructions. *Journal of Materials Processing Technology*, vol. 125-126:pp. 532–536, 2002.

[Mil02] K.C. Mills. *Recommended values of thermophysical properties for selected commercial alloys*. Woodhead Publishing, 2002.

[Mor07] P. V. Morra, A. J. Böttger, and E. J. Mittemeijer. Decomposition of iron-based martensite. A kinetic analysis by means of differential scanning calorimetry and dilatometry. *Journal of thermal analysis and calorimetry*, vol. 64:pp. 905–914, 2007.

[MSCa] MSC.MARC. *Volume A: Theory and User Information.* Version 2010.

[MSCb] MSC.MARC. *Volume B: Element Library.* Version 2010.

[MSCc] MSC.MARC. *Volume C: Program Input.* Version 2010.

[MV09] M. Maikranz-Valentin, U. Weidig, U. Schoof, H.H. Becker, and K. Steinhoff. Components with optimised properties due to advanced thermo-mechanical process strategies in hot sheet metal forming. *Steel Research International*, vol. 79(2):pp. 92–97, 2009.

[Neu06] R. Neugebauer, T. Altan, M. Geiger, M. Kleiner, and A. Sterzing. Sheet metal forming at elevated temperatures. *CIRP Annals-Manufacturing Technology*, vol. 55(2):pp. 793–816, 2006.

[NN05] S. Nemat-Nasser and W. G. Guo. Thermomechanical response of HSLA-65 steel plates: experiments and modeling. *Mechanics of Materials*, vol. 37(2-3):pp. 379–405, 2005.

[Ona87] H. Ona, T. Jimma, H. K., and T. Nakako. Computer aided design system for forming wide profile section and pipe section. *Bulletin of Research Laboratory of Precision Machinery and Electronics, Tokyo Institute of Technolgy*, (59):pp. 1–9, 1987.

[Ona04] H. Ona. On roll forming of section with different width in longitudinal direction. In *7th Symposium on Engineering*. BeiJing, China, 2004.

[Ona05] H. Ona. Study on development of intelligent roll forming machine. In *International Conference on Technology of Plasticity, ICTP2005*. Verona, Italy, 2005.

[Ona10] H. Ona, R. Sho, T. Nagamachi, and K. Hoshi. Development of Flexible cold roll forming machine controlled by PLC. *Steel research international*, vol. 81:pp. 182–185, 2010.

[Ort01] Ortic. www.ortic.se, 2001.

[Pan92] S.M. Panton, S.D. Zhu, and J.L. Duncan. Geometric constraints on the forming path in roll forming channel sections. *Journal of Engineering Manufacture*, vol. 206(22):pp. 113–118, 1992.

[Pan94] S.M. Panton, S.D. Zhu, and J.L. Duncan. Fundamental deformation types and sectional properties in roll forming. *International Journal of Mechanical Sciences*, vol. 36(8):pp. 725–735, 1994.

[Par09a] J. Paralikas. Investigation of the effects of main roll-forming process parameters on quality for a v-section profile from ahss. *International Journal of Advanced Manufacturing Technology*, vol. 44:p. 223, 2009.

[Par09b] J. Paralikas, K. Salonitis, and G. Chryssolouris. Investigation of the roll forming flower design techniques on main redundant deformations on symmetrical profiles from AHSS. In *1st International Congress on Roll Forming: RollFORM09*, pp. 83–91. 2009.

[Per96] P. Perez. *Caracterización mecánica y comportamiento a la oxidación del Ni3A1 procesado por vía pulmimetalúrgica: influencia del tamaño de partícula y de la implantación iónica.* Ph.D. thesis, Universidad Complutense de Madrid, 1996.

[Pet07] R. Petrov, L. Kestens, A. Wasilkowska, and Y. Houbaert. Microstructure and texture of lightly deformed deformed TRIP-assisted steel characterized by means of EBSD technique. *Material science and engineering A*, (447):pp. 285–297, 2007.

[Pit04] M. Pitz, M. Merklein, A. Giera, and M. Geiger. Laser assisted bending and roll forming. In *4th Laser assisted Net Shape Engineering, LANE 2004*, pp. 1147–1155. Erlangen, Germany, 2004.

[Pit05] M. Pitz and M. Merklein. FE Simulation of Laser Assisted Bending. *Advanced Materials Research*, vol. 6:pp. 745–752, 2005.

[Reb90] N. Rebelo, J. C. Nagtegaal, and H. D. Hibbitt. Finite element analysis of sheet forming processes. *International journal for numerical methods in engineering*, vol. 30(8):pp. 1739–1758, 1990.

[Reb92a] N. Rebelo, J. C. Nagtegaal, L. M. Taylor, and R. Passman. Comparison of implicit and explicit finite element methods in the simulation of metal forming processes. In *4th International Conference on Numerical Methods in*

Industrial Forming Processes - NUMIFORM '92, p. 99. Sophia-Antipolis, France, 1992.

[Reb92b] N. Rebelo, J. C. Nagtegaal, L. M. Taylor, and R. Passman. Industrial application of implicit and explicit finite element methods to forming processes. In *Winter Annual Meeting of the American Society of Mechanical Engineering*, vol. 5, pp. 67–76. Anaheim, CA, USA, 1992.

[Ric73] F. Richter. Die wichtigsten physikalischen Eigenschaften von 52 Eisenwerkstoffen. 1973.

[Rou09] F. Roure, M.M. Pastor, M. Casafont, and J. Bonada. Simulation of the roll-forming process for the determination of relevant residual stresses of cold-formed steel menbers. In *1st International Congress on Roll Forming: RollFORM09*, pp. 41–48. Bilbao, Spain, 2009.

[Sag08] E. Sagström, B. Wadman, R. Moshfegh, M. Lundberg, and A. Melander. The geometrical robustness of roll formed profiles in ultra high strength steels. In *International Deep-drawing Research Group 2008, IDDRG2008*. Olofström, Sweden, 2008.

[Sch04] D. Schuocker. Laser assisted forming - a valuable extension of the limits of metal shaping. In *4th Laser assisted Net Shape Engineering, LANE 2004*. Erlangen, Germany, 2004.

[Sed09] A. Sedlmaier and A. Abee. On the quality improvement of roll formed profiles with variable cross sections. In *International symposium on Plasticity 2009*. St Thomas, US Virgin Islands, 2009.

[Sen01] T. Senuma. Physical metallurgy of modern high strength steel sheets. *Iron and Steel Institute of Japan (ISIJ) international*, vol. 41(6):pp. 520–532, 2001.

[She04] J.-J. Sheu. Simulation and optimization of the cold roll-forming process. In *8th Interantional Conference on Numerical Methods in Industrial Forming Processes, NUMIFORM 2008*, vol. 712, p. 452. Columbus, Ohio, USA, 2004.

[She06] M. A. Sheikh and R. R. Palavilayil. An assessment of finite element software for application to the roll-forming process. *Journal of Materials Processing Technology*, vol. 180(1):pp. 221–232, 2006.

[Spi04] H. Spindler, M. Klein, R. Rauch, A. Pichler, and P. Stiaszny. High strength and ultra high strength hot rolled steel grades - Products for advanced applications. In *1st International Conference on Super-High Strength Steels.* Rome, Italy, 2004.

[Swe03] K. Sweeney and U. Grunewald. The application of roll forming for automotive structural parts. *Journal of Materials Processing Technology*, vol. 132(1):pp. 9–15, 2003.

[Taj02] M. Tajdari and M. Farzin. Numerical analysis of cold roll forming of symmetrical open sections. *Journal of Materials Processing Technology*, vol. 125-126:pp. 633–637, 2002.

[Teh06] M.S. Tehrani, P. Hartley, H.M. Naeini, and H. Khademizadeh. Localised edge buckling in cold roll-forming of symmetric channel section. *Thin-walled structures*, vol. 44(2):pp. 184–196, 2006.

[VDB82] A. Van Den Beukel and U. F. Kocks. The strain dependence of static and dynamic strain-aging. *Acta Metallurgica*, vol. 30:pp. 1027–1034, 1982.

[Vis09] Vishay micro-measurements. High-Elongation Strain Measurements. Application Note TT-605, 2009.

[VS06] J. Van Slycken, P. Verleysen, J. Degrieck, J. Bouquerel, and BC De Cooman. Crashworthiness characterization and modelling of high-strength steels for automotive applications. *Proceedings of the Institution of Mechanical Engineers, Part D: Journal of Automobile Engineering*, vol. 220(4):pp. 391–400, 2006.

[VV05] G.F. Vander Voort and E.P. Manilova. Imaging phases in steels. *Advanced materials & processes*, vol. 163(2):pp. 32–37, 2005.

[Wen05] M. L. Wenner. Overview - simulation of sheet metal forming. In *6th International Conference and Workshop on Numerical Simulation of 3D Sheet Metal Forming Processes, NUMISHEET 2005*, pp. 3–7. Detroit, MI, USA, 2005.

[Wor10] WorldAutoSteel. www.worldautosteel.org, 2010.

[Zen09] G. Zeng, S.H. Li, Z.Q. Yu, and X.M. Lai. Optimization design of roll profiles for cold roll forming based on response surface method. *Materials & Design*, vol. 30(6):pp. 1930–1938, 2009.

[Zhu93] S. Zhu. *Theoretical and experimental analysis of roll forming.* Master's thesis, University of Auckland, 1993.

[Zw02] H. Zhi-wu, L. Cai, and L. Wei-ping. Numerical simulation of roll forming for channel section with outer edge. *Applied Mathematics and Mechanics*, vol. 23(3):pp. 321–328, 2002.

Appendix A

Table A.1: Summary of tensile test results of MS1200 at room temperature.

Direction	$\dot{\varepsilon}$ (s^{-1})	Y_s (MPa)	ς_{Y_s} (MPa)	σ_uts (MPa)	$\varsigma_{\sigma_\mathrm{uts}}$ (MPa)	ε_f (-)	$\varsigma_{\varepsilon_\mathrm{f}}$ (-)
0°	0.001	1182.9	78.3	1328.6	23.7	0.028	0.008
45°	0.001	1135.9	68.3	1321.9	17.9	0.026	0.003
90°	0.001	1153.6	75.1	1350.4	39.6	0.027	0.012
0°	0.01	1255.6	18.9	1355.2	7.9	0.037	0.023
45°	0.01	1251.6	9.3	1357.6	18.3	0.042	0.027
90°	0.01	1278.1	8.5	1366.6	39.3	0.028	0.020
0°	0.1	1207.2	-	1122.3	186.7	0.014	0.015
45°	0.1	-	-	806.1	99.6	0.005	0.001
90°	0.1	1197.7	51.4	1346.7	25.2	0.018	0.008

Table A.2: Summary of tensile test results of CP800 at room temperature.

Direction	$\dot{\varepsilon}$ (s^{-1})	Y_s (MPa)	ς_{Y_s} (MPa)	σ_uts (MPa)	$\varsigma_{\sigma_\mathrm{uts}}$ (MPa)	ε_f (-)	$\varsigma_{\varepsilon_\mathrm{f}}$ (-)
0°	0.001	684.4	5.1	876.1	6.8	0.124	0.010
45°	0.001	670.2	4.3	861.0	4.9	0.118	0.002
90°	0.001	682.9	7.3	874.6	5.5	0.121	0.007
0°	0.01	679.0	2.3	873.5	12.1	0.130	0.007
45°	0.01	666.5	5.2	863.4	13.0	0.123	0.017
90°	0.01	681.6	4.4	877.8	8.8	0.120	0.010
0°	0.1	677.5	0.6	894.4	2.5	0.135	0.002
45°	0.1	671.4	0.6	867.9	17.9	0.113	0.023
90°	0.1	676.6	4.9	895.5	6.5	0.129	0.009

Table A.3: Summary of tensile test results of DP600 at room temperature.

Direction	$\dot{\varepsilon}$ (s^{-1})	Y_s (MPa)	ς_{Y_s} (MPa)	σ_uts (MPa)	$\varsigma_{\sigma_\mathrm{uts}}$ (MPa)	ε_f (-)	$\varsigma_{\varepsilon_\mathrm{f}}$ (-)
0°	0.001	411.3	4.9	725.4	7.0	0.164	0.006
45°	0.001	410.9	6.7	726.7	8.4	0.141	0.010
90°	0.001	390.3	16.6	721.2	11.2	0.147	0.012
0°	0.01	426.7	18.0	730.8	20.0	0.155	0.003
45°	0.01	428.1	4.4	760.9	16.5	0.148	0.013
90°	0.01	384.0	8.2	721.5	9.1	0.135	0.004
0°	0.1	435.8	6.8	764.4	4.2	0.164	0.004
45°	0.1	437.3	4.5	776.2	1.3	0.157	0.033
90°	0.1	382.3	2.2	749.0	4.8	0.156	0.014

Table A.4: Summary of tensile test results of DC01 at room temperature.

Direction	$\dot{\varepsilon}$ (s^{-1})	Y_s (MPa)	ς_{Y_s} (MPa)	σ_uts (MPa)	$\varsigma_{\sigma_\mathrm{uts}}$ (MPa)	ε_f (-)	$\varsigma_{\varepsilon_\mathrm{f}}$ (-)
0°	0.001	202.8	35.1	427.0	34.2	0.306	0.043
45°	0.001	243.4	2.7	457.7	1.8	0.256	0.011
90°	0.001	232.3	2.5	424.6	4.1	0.256	0.005
0°	0.01	211.4	30.4	422.6	29.8	0.279	0.040
45°	0.01	251.5	4.9	461.6	2.1	0.240	0.005
90°	0.01	238.4	0.7	428.9	1.1	0.244	0.002
0°	0.1	222.0	29.5	451.3	31.2	0.312	0.064
45°	0.1	259.5	2.7	482.4	1.0	0.243	0.015
90°	0.1	244.8	5.1	444.9	6.3	0.248	0.014

Table A.5: Mechanical properties of CP800 steel depending on temperature at 0.01 s^{-1}.

Temperature	20°C	100°C	200°C	300°C	400°C	500°C	600°C	700°C
Y_s (MPa)	668.4	643.4	619.4	617.9	547.6	394.0	238.3	138.2
σ_uts (MPa)	852.1	783.4	795.1	902.2	752.8	477.2	284.6	156.7
ε_f (-)	0.28	0.25	0.23	0.31	0.33	0.40	0.54	0.68
K(MPa)	1084.7	946.8	974.0	1136.3	930.1	557.4	326.4	178.3
n(-)	0.09	0.077	0.079	0.117	0.086	0.053	0.031	0.033

Table A.6: Mechanical properties of CP800 steel depending on temperature at 0.1 s^{-1}.

Temperature	20°C	100°C	200°C	300°C	400°C	500°C	600°C	700°C
Y_s (MPa)	682.7	667.3	611.07	621.7	556.8	443.4	286.1	185.0
σ_uts (MPa)	875.9	802.5	789.1	847.1	763.1	544.6	340.8	218.0
ε_f (-)	0.28	0.26	0.23	0.25	0.35	0.38	0.46	0.55
K (MPa)	1084.7	946.8	974.0	1136.3	930.1	557.4	326.4	178.3
n(-)	0.097	0.072	0.076	0.088	0.086	0.052	0.032	0.020

Appendix B

Table B.1: Values of the Hollomon law hardening coefficient (K_{Holl}) and strain hardening exponent (n_{Holl}) at high temperature and at 0.01 s^{-1}.

Temperature	20°C	100°C	200°C	300°C	400°C	500°C	600°C	700°C
K_{Holl}(MPa)	1044.7	923.2	951.4	1123.9	909.2	549.9	315.2	171.4
n_{Holl}(-)	0.092	0.068	0.076	0.119	0.084	0.051	0.031	0.024

Table B.2: Values of the hardening coefficient (K_{Holl}) and is the strain hardening exponent (n_{Holl}) at high temperature and at 0.1 s^{-1}.

Temperature	20°C	100°C	200°C	300°C	400°C	500°C	600°C	700°C
K_{Holl}(MPa)	1075.6	951.7	930.8	1023.4	915.5	619.6	375.2	235.1
n_{Holl} (-)	0.090	0.069	0.070	0.085	0.083	0.047	0.029	0.019

Appendix C

Table C.1: Experimental values of the measured angles and longitudinal bow.

	MS1200	$\varsigma_{\mathrm{MS1200}}$	CP800	$\varsigma_{\mathrm{CP800}}$	DP600	$\varsigma_{\mathrm{DP600}}$	DC01	$\varsigma_{\mathrm{DC01}}$
Long. bow (mm)	0.32	0.04	0.30	0.01	0.81	0.02	1.87	0.10
Angle (°)	12.7	0.46	23.0	0.27	26.2	0.68	33.4	0.34

Table C.2: Experimental values of the peak strain and final residual strain in longitudinal and transversal direction.

	MS1200	CP800	DP600	DC01
Long. peak strain (-)	0.005516	0.005638	0.004697	0.006345
Trans. peak strain (-)	-0.002202	-0.001310	-0.002827	-0.005144
Long. residual strain (-)	-0.000266	-0.000254	-0.000665	0.000504
Trans. residual strain (-)	-0.000013	0.000001	-0.000294	-0.001466

Table C.3: Experimental values of the measured load and torques for different materials.

	MS1200	$\varsigma_{\mathrm{MS1200}}$	CP800	$\varsigma_{\mathrm{CP800}}$	DP600	$\varsigma_{\mathrm{DP600}}$	DC01	$\varsigma_{\mathrm{DC01}}$
Force (KN)	19.2	0.96	8.19	0.29	11.07	0.73	5.18	0.53
Torque (Nm)	27.15	4.0	17.97	0.72	25.86	3.41	19.8	3.52

Table C.4: Experimental values of the measured web warping and relative web warping for different temperatures.

Temperature	20°C	ς_{20°	300°C	ς_{300°	400°C	ς_{400°	500°C	ς_{500°	600°C	ς_{600°
Total	3.34	0.09	3.13	0.16	3.39	0.11	3.31	0.24	4.35	0.27
Relative	2.31	0.05	2.09	0.27	2.07	0.12	1.84	0.28	1.96	0.19

Table C.5: Experimental values of the measured β_1, β_2, β_3 and β_4 angles in the slim section for different temperatures.

Temperature	20°C	ς_{20°	300°C	ς_{300°	400°C	ς_{400°	500°C	ς_{500°	600°C	ς_{600°
β_1	91.4	0.3	91.4	0.2	91.2	0.1	91.1	0.2	91.2	0.2
β_2	93.6	0.6	93.3	0.6	93.8	0.4	92.9	1.1	92.5	0.4
β_3	92.6	1.0	92.4	0.8	91.9	0.7	91.0	0.4	91.0	0.3
β_4	91.6	0.4	91.6	1.5	91.7	0.9	91.4	0.3	91.1	0.6

Table C.6: Experimental values of the measured β_1, β_2, β_3 and β_4 angles in the wide section for different temperatures.

Temperature	20°C	ς_{20°	300°C	ς_{300°	400°C	ς_{400°	500°C	ς_{500°	600°C	ς_{600°
β_1	92.5	0.5	93.1	0.5	92.2	0.4	94.0	0.8	94.7	1.7
β_2	90.3	1.6	89.3	0.2	89.2	0.3	88.3	0.4	87.8	1.3
β_3	90.4	1.0	89.5	0.2	89.6	0.5	88.1	0.5	87.6	1.5
β_4	92.5	0.7	94.0	0.8	93.7	0.7	94.0	1.0	93.8	1.6